

**MODELLING SWEEP FREQUENCY RESPONSE OF
POWER TRANSFORMERS**

Kotagama Lansakara Imiya Mudiyansele Pramod Bandara Jayarathna

(178069V)

Degree of Master of Science

Department of Electrical Engineering

University of Moratuwa

Sri Lanka

October 2018

MODELLING SWEEP FREQUENCY RESPONSE OF POWER TRANSFORMERS

Kotagama Lansakara Imiya Mudiyansele Pramod Bandara Jayarathna

(178069V)

Dissertation submitted in partial fulfilment of the requirements
for the degree Master of Science

Department of Electrical Engineering

University of Moratuwa

Sri Lanka

October 2018

DECLARATION

I declare that this is my own work and this thesis/dissertation does not incorporate without acknowledgement any material previously submitted for a Degree or Diploma in any other University or institute of higher learning and to the best of my knowledge and belief it does not contain any material previously published or written by another person except where the acknowledgement is made in the text.

Also, I hereby grant to University of Moratuwa the non-exclusive right to reproduce and distribute my thesis/dissertation, in whole or in part in print, electronic or other medium. I retain the right to use this content in whole or part in future works (such as articles or books)

Signature:

Date:

K.L.I.M.P.B.Jayarathna

The above candidate has carried out research for the Masters Dissertation under my supervision.

Signatures of the supervisors:

Dr.Rasara Samarasinghe

Date:

Prof. Rohan lucas

Date:

ABSTRACT

Condition monitoring of power system components is crucial in order to supply quality and uninterrupted power supply to its consumers. Among other components, the power transformer is considered to be one of the most expensive and vital components in the power network. Therefore condition assessment and fault diagnosis of power transformers have become main features of the power system's maintenance strategy. Sweep frequency response analysis is a widely used condition monitoring technique to assess mechanical integrity of power transformers. SFRA measures the transformer response to a wide frequency input signal and provides a graphical frequency response of the transformer that needs to be analysed and interpreted afterwards. This thesis presents a novel approach to determine lumped parameter equivalent circuit of transformers using transfer functions estimated from measured SFRA response. Firstly, a novel algorithm based on Levy's and Sanathanan-Koerner method is used to convert the graphical SFRA curves into transfer function in Laplace domain. Once transfer functions estimation is derived, the lumped parameter equivalent circuit model is developed using artificial neural network and genetic algorithm integrated approach. In fact, artificial neural network is used to derive the initial approximation of genetic algorithm where artificial neural network results are optimized by genetic algorithm to find the final estimated parameters. The entire approach has been validated by means of error analysis and actual responses. Furthermore, modelled equivalent circuits by the proposed method have been incorporated to develop reference curves for various power transformer fault types which can be used to assess the severity and fault location of failures. This method can be easily implemented in a digital computer and can be used in on-site fault diagnosis of power transformers.

ACKNOWLEDGEMENT

I would like to express my sincere gratitude to my supervisors, Dr. Rasara samarasinghe and Prof. Rohan Lucas for their guidance and tremendous support given throughout this research. Their instructions and comments immensely helped me to complete this work with success.

I would also like to express my sincere gratitude to the course coordinator, progress review chair and members, and all the lecturers of Department of Electrical Engineering for their valuable feedback and assistance throughout the study.

I would like to thank Mr. W.T.D. Samarasinghe and Mr. M.P.M. Fernando, Electrical Engineers of Asset Management Branch - Transmission division of Ceylon Electricity Board (CEB), for helping me to collect SFRA data from the CEB and for sharing their expertise.

I also thank all my colleagues and friends for giving their fullest cooperation throughout my research and for assisting me to clear my doubts.

Last but not least, I would like to express my deepest gratitude for my parents and family for their understanding, motivation and patience.

TABLE OF CONTENTS

DECLARATION	iii
ABSTRACT	iv
ACKNOWLEDGEMENT	v
TABLE OF CONTENTS	vi
LIST OF FIGURES	ix
LIST OF TABLES	xii
LIST OF APPENDICES	xiii
LIST OF ABBREVIATIONS	xiv
Chapter 1 INTRODUCTION	1
1.1 Background	1
1.2 Objectives	5
1.3 Scope of work	5
1.4 Thesis outline	5
1.5 Publications	6
Chapter 2 BACKGROUND STUDY AND LITERATURE REVIEW	8
2.1 Introduction	8
2.2 Sweep frequency response analysis (SFRA)	8
2.3 Types of SFRA Measurements	13
2.4 Applications of SFRA	14
2.4.1 Fault diagnosis-Reference traces used for comparison	15
2.4.2 Transformer faults identification using SFRA	16
2.5 Existing models of power transformers	16
2.6 Proposed method for transformer modelling	21
Chapter 3 TRANSFER FUNCTION ESTIMATION USING FREQUENCY RESPONSE ANALYSIS	22
3.1 Introduction	22
3.2 Analysis of integer order system in frequency domain	24
3.2.1 Levy's method of identification of transfer function	24
3.2.2 Sanathanan-Koerner iterative method	28
3.3 Routh-Hurwitz stability criterion	29
3.4 Proposed algorithm to derive transfer function from SFRA data	29
3.5 Application of proposed algorithm (Case study for validation of proposed method)	33

3.6	Conclusions	45
Chapter 4	MODELLING TRANSFORMER EQUIVALENT CIRCUIT	47
4.1	Introduction	47
4.2	Lumped parameter network.....	47
4.3	Algorithms and methods used for conversion of transfer function to Lumped parameter network model.....	49
4.3.1	Artificial neural network (ANN).....	49
4.3.2	Genetic algorithm (GA)	51
4.4	Proposed method of parameter estimation of lumped equivalent circuit	53
4.4.1	Initial approximation using ANN (step 1)	55
4.4.2	Secondary approximation –DC gain matching (step 2)	56
4.4.3	Optimization of responses using Genetic algorithm (step 3).....	57
4.5	Case study and method validation	60
4.5.1	Method validation: numerical validation	68
4.5.2	Method validation: comparison with a faulty transformer frequency response.....	69
4.6	Results of other phases and different tests	71
4.6.1	Modelling of side phases (phase R/B for open circuit test)	71
4.6.2	Modelling of windings (phase R, Y & B for short circuit test)	74
4.7	Conclusions	77
Chapter 5	REFERENCE CURVES OF POWER TRANSFORMER FAULTS ..	79
5.1	Introduction	79
5.2	Fault interpreting using frequency ranges of SFRA.....	80
5.2.1	Frequency ranges of SFRA	80
5.2.2	Fault interpretation rules	83
5.3	Generated reference curves	83
5.3.1	Inter-turn faults.....	84
5.3.2	Transformer core faults	86
5.3.3	Earth faults	87
5.3.4	Conductor tilting/ winding buckling	89
5.3.5	Insulation ageing	91
5.4	Conclusions	93
Chapter 6	CONCLUSION AND FUTURE WORK	94
6.1	Conclusions	95
6.2	Future works.....	97

References	99
Appendix A: MATLAB code of Levy method estimation	107
Appendix B: MATLAB code of constraint function used in GA (" <i>constraint_fcn</i> ")	114
Appendix C: MATLAB code of fitness function used in GA (" <i>fit_fcn</i> ")	116
Appendix D: MATLAB code to determine regions.....	119

LIST OF FIGURES

Figure 1.1: Reported failure rates of power transformer [2].....	1
Figure 1.2: Derivation of Bode plots of a power transformers by SFRA [5].....	3
Figure 1.3 Basic structure of the power transformer [1].....	4
Figure 2.1: Test setup of SFRA.....	9
Figure 2.2: Two port model of SFRA test setup	9
Figure 2.3: Simplified SFRA test arrangement.....	10
Figure 2.4: Frequency response of test object.....	12
Figure 2.5: SFRA Signature of Bolawatta TR03 -3phase 31.5MVA, 132/33kV	12
Figure 2.6: Types of SFRA measurements	14
Figure 2.7: Basic steps of modelling transformer using SFRA	21
Figure 3.1: Proposed algorithm to obtain transfer function from SFRA data.....	31
Figure 3.2: Original SFRA of 133/33 kV, 31.5 MVA Pauwels transformer (Phase Y)	34
Figure 3.3: Inverse values of RMS errors for the numerator and denominator combinations of region 1.....	35
Figure 3.4: Estimated response (red) with original response (blue) in 20 Hz – 29.2 kHz (125 rad/s – 184 krad/s).....	36
Figure 3.5: Inverse values of RMS errors for the numerator and denominator combinations of region 2.....	37
Figure 3.6: Estimated response (red) with reshaped response (blue) in 20 Hz to 117 kHz.....	37
Figure 3.7: Inverse values of RMS errors for the numerator and denominator combinations of region 3.....	39
Figure 3.8: Estimated response (red) with Reshaped response (blue) in 20 Hz to 188 kHz.....	40
Figure 3.9: Inverse values of RMS errors for the numerator and denominator combinations of region 4.....	41
Figure 3.10: Estimated response (red) with reshaped response (blue) in 20 Hz to 2 MHz	42
Figure 3.11: Estimated response (red) with original SFRA data (blue) in 20 Hz.....	43
Figure 3.12: Relative error of estimated response with respect to SFRA.....	44
Figure 4.1: Lumped parameter network model.....	48
Figure 4.2: Basic structure of ANN	50

Figure 4.3: Bit-String Crossover followed by bit flipping mutation.....	53
Figure 4.4: Steps of parameter estimation.....	54
Figure 4.5: Pseudo code of constraint function “ <i>constraint_fcn</i> ”.....	58
Figure 4.6: Pseudo code of objective function “ <i>fit_fcn</i> ”.....	58
Figure 4.7: Comparison of responses of order-reduced transfer function (orange) with measured SFRA response (blue).....	62
Figure 4.8: Test setup modelled in Simulink.....	62
Figure 4.9: Six-sectional lumped parameter network used to train ANN.....	63
Figure 4.10: Comparison of bode plots of initial approximation obtained from trained ANN and measured SFRA.....	63
Figure 4.11: Frequency response after DC gain matching.....	65
Figure 4.12: Final Six-sectional lumped parameter network (Used for GA).....	66
Figure 4.13: Frequency response of final synthesized circuit (red) with respect to the response of order reduced transfer function (blue).....	67
Figure 4.14: Magnitude plots of order reduced transfer function and synthesized network with Absolute error graph.....	69
Figure 4.15: pre-fault and post-fault SFRA curves of Biyagama 83.3 MVA 3phase transformer (Phase Y, open circuit response).....	70
Figure 4.16: (a) Altered parameters of lumped parameter network (b) Frequency response before and after alteration.....	71
Figure 4.17: Original open circuit SFRA of 132/33 kV, 31.5 MVA Pauwels transformer (Phase R, Y and B).....	72
Figure 4.18: Frequency response of final synthesized circuit (red) with respect to the response of order reduced transfer function of phase B (blue).....	73
Figure 4.19: Original short circuit SFRA of 132/33kV, 31.5MVA Pauwels transformer (Phase R, Y and B).....	75
Figure 4.20: Frequency response of final synthesized circuit (red) with respect to the response of order reduced transfer function of phase Y (blue).....	76
Figure 5.1: Method of region determination of SFRA.....	82
Figure 5.2: (a) Simulating an inter-turn fault by short circuiting section-3 (b) Pre fault and post fault Frequency response.....	84
Figure 5.3: Frequency response of phase ‘Y’ of the transformers before and after inter-turn fault occurrence on phase ‘Y’ of the HV winding (logarithmic frequency scale from 100 Hz to 1 MHz) [16].....	85
Figure 5.4: Reference frequency responses of inter-turn fault (for each winding section).....	85
Figure 5.5: pre-fault and post-fault (core fault) Frequency response.....	86

Figure 5.6: Comparison of Pre-fault and post-fault, HV, B phase, SFRA [60]	87
Figure 5.7: (a) simulating earth fault by adding parallel resistance (b) pre fault and post fault Frequency response	88
Figure 5.8: Comparison of Pre-fault and post-fault responses of 5 MVA,	89
Figure 5.9: Simulating conductor tilting by increasing the ground capacitances	90
Figure 5.10: Frequency response of 230kV transformer before and after conductor tilting [9]	90
Figure 5.11: Reference frequency responses of tilting/buckling (for different severity levels)	91
Figure 5.12: Simulating insulation ageing by reducing capacitances	92
Figure 5.13: Frequency response of 400MVA transformer with and without insulation oil [67]	92

LIST OF TABLES

Table 2.1: Mechanical and electrical faults identified by SFRA	16
Table 3.1: Selection of best estimation in Sanathanan-Koerner method of proposed algorithm for region 3	39
Table 3.2: Selection of best estimation in Sanathanan-Koerner method of proposed algorithm for region 4	42
Table 4.1: Ranges of randomly generated data for parameters.....	55
Table 4.2: Input parameters of GA	57
Table 4.3: Poles and zeros of the order-reduced transfer function of 132/33kV, 31.5MVA Pauwels transformer (PhaseY).....	61
Table 4.4: Estimated parameter values from ANN (step1).....	64
Table 4.5: Resistance values before and after DC gain matching.....	65
Table 4.6: Final estimated parameter values for lumped parameter network	67
Table 4.7: Final estimated parameter values for lumped parameter network of phase B (open circuit test).....	73
Table 4.8: Final estimated parameter values for Lumped parameter network of phase Y (short circuit test)	76
Table 5.1: Fault interpretation rules	83

LIST OF APPENDICES

Appendix A: MATLAB code of Levy method estimation	107
Appendix B: MATLAB code of constraint function used in GA (“ <i>constraint_fcn</i> ”)	114
Appendix C: MATLAB code of fitness function used in GA (“ <i>fit_fcn</i> ”).....	116
Appendix D: MATLAB code to determine regions.....	119

LIST OF ABBREVIATIONS

DGA	Dissolved gas analysis
DC	Direct current
SFRA	Sweep frequency response analysis
RLC	Resister, inductor and capacitor
ANN	Artificial neural network
GA	Genetic algorithm
Std.	Standard
FRA	Frequency response analysis
R-L-C-M	Resister, inductance, capacitance and mutual inductance
EMTP	Electromagnetic transient program
RMS	Root mean square
H.V	High voltage
L.V	Low voltage
TF	Transfer function
SC	short circuit
freq.	Frequency

Chapter 1

INTRODUCTION

1.1 Background

The power transformer is one of the most important and expensive assets in a power system. A power transformer is subjected to various stresses during its operation caused by different electrical, mechanical and environmental conditions. The condition of power transformers directly affects the reliability and stability of a power system. Various failure modes of these assets have been recorded and some of the major reasons identified over time are ageing of transformer solid insulation, dielectric degradation of oil insulation, increased thermal losses, mechanical faults, latent manufacturing defects, partial discharges and corona discharges in the assets [1]. Figure 1.1 illustrates data from a survey conducted by the international council on large electric systems (CIGRÉ) regarding failures of different transformer parts [2].

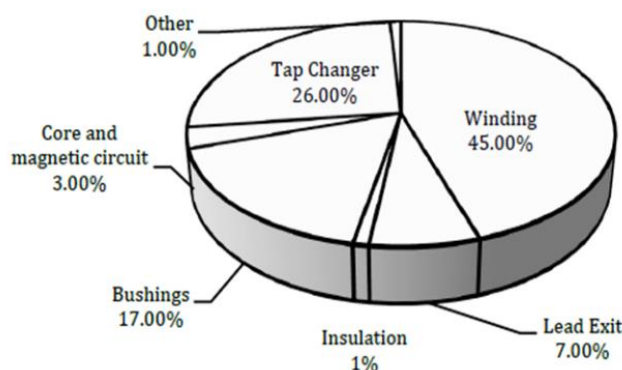


Figure 1.1: Reported failure rates of power transformer [2]

It can be seen that most of the transformer failures are winding failures amounting to 45% share of total failures. Insulation and core (magnetic circuit) are the other internal components of the transformer that accounts for 1% and 3% of failures respectively. Altogether, these three components, that construct the main structure of the transformer, is responsible for almost half of the transformer failures (i.e. 49%). Thus condition monitoring of these components is of great importance to maintain the health of a transformer as well as that of the whole power system. A proper Condition

monitoring regime performed in a regular basis helps in detecting these failures before they develop into catastrophic failures, preventing huge capital losses to the system.

Condition monitoring of power transformers can be divided into two types as online and offline. There are online condition monitoring techniques that can be performed during its normal operation such as transformer winding temperature and internal pressure. Even some of the tests like dissolved gas analysis (DGA) can be done online even though they incur a significant cost. DC winding resistance, winding insulation resistance, excitation current and dielectric dissipation factor measurements are few examples of offline condition monitoring techniques. In the past few decades, with the advancement of power electronics, the area of condition monitoring has revolutionized with the introduction of new techniques. Among those, Sweep frequency response analysis (SFRA) has emerged to be the most effective and sensitive diagnostic method to detect mechanical integrity of power transformers [3].

In simple words, the SFRA compares an output voltage response of the power transformer to a given input response varied within a specific frequency range. Every transformer has its own unique frequency response, which can be referred to as “fingerprint” of the transformer. “Frequency response analysers” based on power electronics are used to obtain the frequency response of a transformer. The generated variable frequency high voltage signal is fed to one terminal of the transformer and measured from another. Final Outcomes of the analysers are a pair of complex graphs called “Bode plot” that depicts amplitude and phase variation of output response with respect to the input response over the frequency range [4, 5]. Figure 1.2 illustrates derivation of bode plots of a power transformer by SFRA.

In contrast to the other methods that give numerical values for its measurements, SFRA provides a graphical output that needs to be interpreted in terms of comparison. Usually, a previously measured SFRA signature of the same transformer is used as the reference curve for this comparison [4]. Variations of the generated curve from the reference curves reveal issues in the power transformer. Currently, an intervention of personal that possess expert knowledge and experience

about this test has become a compulsory factor, as the transformer condition is monitored by analysing (in terms of comparison) and interpreting the graphical responses. Adoption of a transformer model, instead of reference curves, offers a decent solution for all these drawbacks. It will eliminate the presence of industry experts to perform SFRA and eliminate the uncertainty of fault diagnosis.

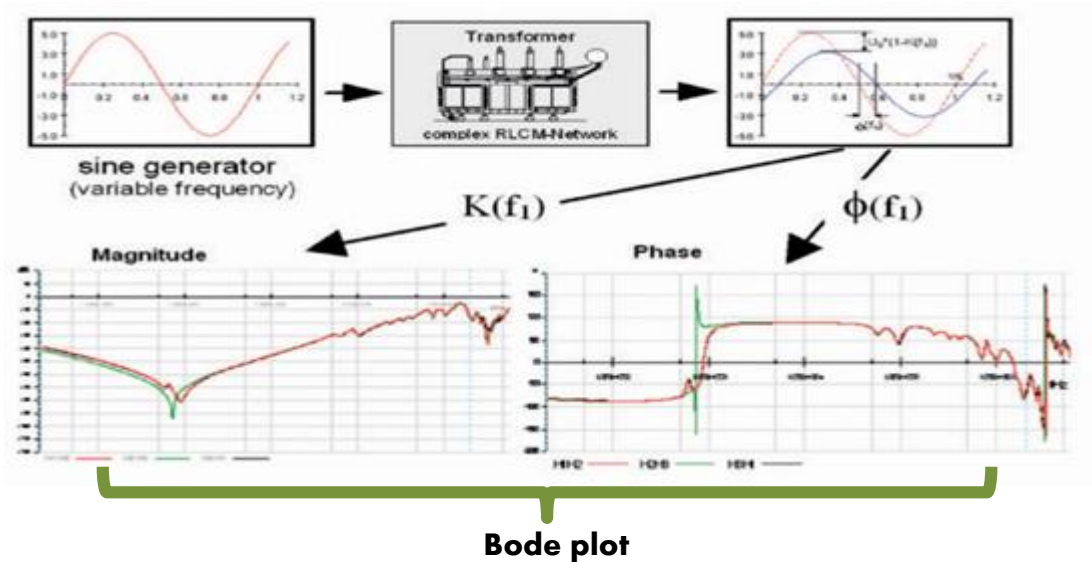


Figure 1.2: Derivation of Bode plots of a power transformers by SFRA [5]

Even though a general equivalent circuit comprised of resistance and inductances gives accurate results at power frequency, the capacitive effect of transformer insulation is not represented by this circuit. Therefore, it cannot be used to interpret its wide frequency response measured from SFRA. Especially in power transformers capable of handling large amounts of power, this effect is predominant. Hence, apart from resistances and inductances, capacitive elements inside power transformers caused by paper/pressboard and oil insulation has to be considered in the analysis as illustrated in Figure 1.3.

In order to model this high frequency behaviour of the transformer, the high frequency response has to be measured at first. Even though SFRA gives its high frequency behaviour, it cannot be used to model the power transformer directly as they are of graphical nature. Deriving the transfer function of frequency response is the

most feasible pathway that links the SFRA curves to the equivalent circuit of the transformer. Once the transfer function is derived, various methods such as synthesis method in circuit theory and algorithms are available to derive the model of a power transformer [6, 7, 8, 9]

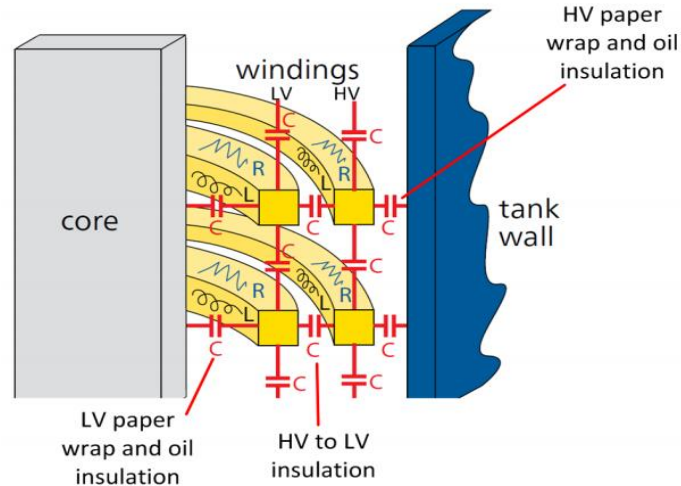


Figure 1.3 Basic structure of the power transformer [1]

Modelling of power transformer can be performed in three ways; Gray-box modelling, Black-box modelling and Hybrid-modelling [10, 11, 12, 13, 14]. The main criteria for deriving the model used in condition assessment of power transformers is that, it should be realised using passive components (resistors, inductors and capacitors) where each and every component represents a specific part or a section of the transformer. The final model of power transformer should be a Gray-box model as it is the type that satisfies the above condition. Using algorithms such as genetic algorithm (GA) and artificial neural networks (ANN), parameter values of model components can be determined efficiently.

As already discussed, these models can be incorporated in condition monitoring to diagnose transformer faults with greater accuracy even without the presence of industry experts. Furthermore using a healthy transformer model, reference curves for possible faults can be simulated by altering various model parameters. Each alteration is attributed to a specific fault type or transformer structural change. Therefore, reference curves for various fault types can be generated by altering parameter values in a scientific and logical manner. These reference figures

can be incorporated into the fault diagnosis process and can be used to localize faults and determine severity levels of the faults.

1.2 Objectives

The main objective of this project is to develop an accurate model for a transformer using its SFRA signature. This accompanies the following specific objectives:

- To formulate an enhanced mathematical model using transfer functions and RLC components to represent the SFRA signature curves for power transformers using available data.
- To provide reference SFRA curves for various fault types of transformers.
- To perform a comprehensive study of SFRA characteristic of transformers according to the factors affecting its response.

1.3 Scope of work

- Perform a comprehensive literature review on transformer modelling using SFRA to identify existing models, limitations and shortcomings.
- Transform SFRA signature waveforms of healthy transformers obtained from power utility to transfer functions and develop practical RLC model to imitate real SFRA signatures
- Verify the proposed model through real SFRA signatures and relative error graphs.
- Comprehensively analyse different SFRA signatures on the parameters affecting its shape.
- Develop reference SFRA signatures for possible transformer fault types.

1.4 Thesis outline

Chapter 2 presents a detailed discussion on sweep frequency response analysis, including method of performance and its applications. This chapter includes a background study on the work carried out by past researchers on modelling the equivalent circuit of a power transformers using its SFRA signature and the approaches proposed in those studies. The advantages and drawbacks of the proposed methods are discussed followed by a brief summary of the proposed method in this thesis to derive

equivalent circuit of a power transformer.

Chapter 3 presents a novel algorithm to convert graphical SFRA signatures to transfer functions. A detailed discussion on the two constituent methods called Levy and Sanathanan-Koerner method with their mathematical derivations are presented in this chapter. Application and validation of the proposed algorithm is illustrated using a sample SFRA response measured from a transformer in operating condition.

Chapter 4 presents the proposed method to synthesize lumped parameter equivalent circuit using estimated transfer functions. First, each step of the proposed method is discussed in detail, including the artificial neural network (ANN) and genetic algorithm (GA) methods. Then the results are validated numerically and with the help of actual responses obtained for power transformers in service, followed by detailed analysis carried out on the variations of resultant lumped parameter equivalent circuit depending on different phases and different test types

Final subsection analyses the variations of resultant lumped parameter equivalent circuit depending on different phases and different test types.

Chapter 5 consists of reference curves generated for possible fault types of power transformers. Resultant reference curves are validated using fault interpretation rules used in industry and actual SFRA responses of power transformers.

Chapter 6 presents the conclusions of this research and highlights the most important discoveries made from the research. It also contains suggestions for future work.

1.5 Publications

- [1] K. L. I. M. Pramod B. Jayarathna, W. E. P. Sampath Ediriweera, J. R. Lucas and R. Samarasinghe, "Modelling Transfer Function of Power Transformers Using Sweep Frequency Response Analysis," *2018 Moratuwa Engineering Research Conference (MERCon)*, Moratuwa, 2018, pp. 500-505.

- [2] K. L. I. M. P. B. Jayarathna, W. E. P. S. Ediriweera, R. Samarasinghe and J. R. Lucas, "An Improved Wide Frequency Model for VFTO of Power Transformers Using Transfer Functions," *2018 2nd International Conference On Electrical Engineering (EECon)*, Colombo, Sri Lanka, 2018, pp. 81-86.

Chapter 2

BACKGROUND STUDY AND LITERATURE REVIEW

2.1 Introduction

Modelling of the power transformer dates back to the invention of power transformer in the nineteenth century. Up to the present, various models have been developed and improved with the development of the engineering field. The basic model widely used by academics and in the industry is the “fundamental equivalent circuit of transformer” that comprise resistance and inductances representing different parts of transformer. However, the high frequency behaviour of power transformer is greatly affected by capacitances created by power transformer insulation system and has been a major research area during the recent past.

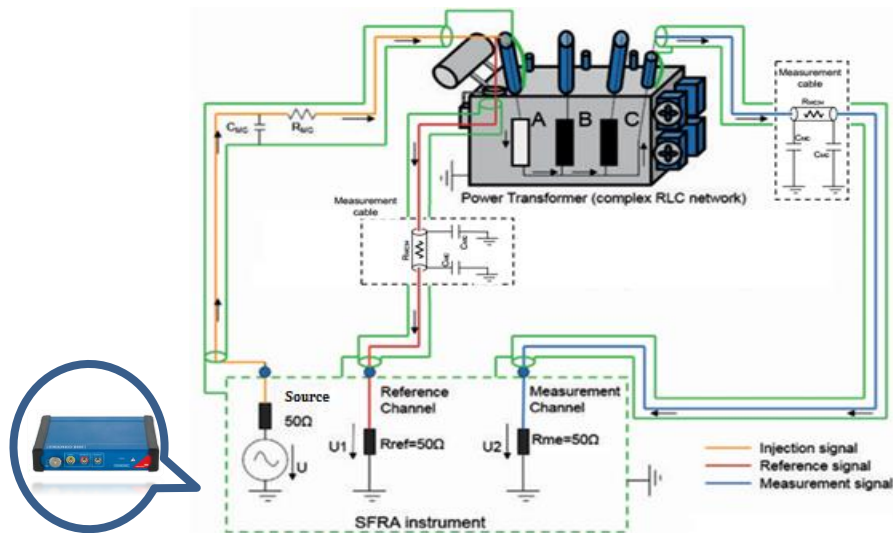
Among other techniques, SFRA is the widely used method to discover this high frequency response of power transformers. Power transformer modelling using SFRA requires thorough knowledge of SFRA technique itself, in addition to numerical and analytical methods needed in modelling. This thesis provides a comprehensive study of sweep frequency response analysis, transformer modelling, and a novel algorithm to obtain the equivalent RLC circuit of a power transformer. This chapter will provide a detailed review of the sweep frequency response analysis, currently proposed methods of transformer modelling, and their advantages and disadvantages.

2.2 Sweep frequency response analysis (SFRA)

Sweep frequency response measurements are taken from industrial frequency analyser, (E.g. “**Omicron FRA analyser- FRANEO 800**”) according to **IEEE Std C57.149** standard or **IEC 60076-18** standard [4, 15]. The test setup arrangement is illustrated in Figure 2.1.

The test device basically consists of three ports, namely “Source”, “Reference Channel” and “Measurement Channel”. A sweep frequency generator which can vary

its generation frequency within 20 Hz -2 MHz is connected to the port named *Source*. Measurement cables from *Source* port and *Reference Channel* port are connected to the same terminal of the power transformer through standard 50 Ω resistors where the *Reference Channel* is used to measure the input given by source to the transformer terminals. *Measurement Channel* is used to measure output response of the transformer (across a standard 50 Ω resistor).



Omicron FRA
analyser
- **FRANEO 800**

Figure 2.1: Test setup of SFRA

The power transformer connected for SFRA testing can be considered as a two port network [16]. Figure 2.2 shows the two port model of the SFRA test setup where Z_S represent standard 50 Ω resistors, Z_{11} & Z_{22} represent input and output impedances and Z_{12} & Z_{21} represent transfer impedances.

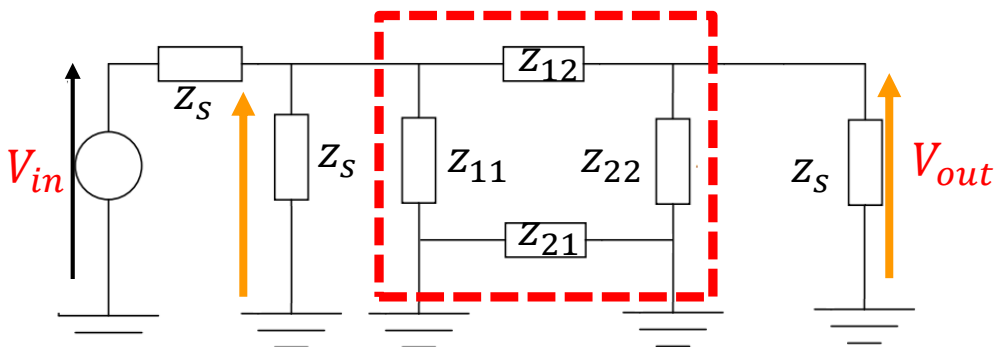


Figure 2.2: Two port model of SFRA test setup

Each Z_{ij} parameter is formed by distributed passive components and corresponds to components inside the transformer. Z_{11} and Z_{22} represent ground impedances while Z_{21} represents the impedance between two grounding points. The effect of this Z_{21} to the final output response is nullified as two sides are short circuited through the transformer casing (Tank). Z_{12} is the most important quantity which represents the equivalent impedances caused by windings and bushings of transformer.

Moreover, when frequency analysis is performed in the field, one of the winding ends are solidly grounded. Therefore, the input impedance (V_{in}/I_{in}) becomes the impedance of the transformer winding [16]. Thus final model of the test setup arrangement can be simplified into a one port network as shown in Figure 2.3, with Z_T representing the transformer with windings under test, same as Z_{12} [16, 17].

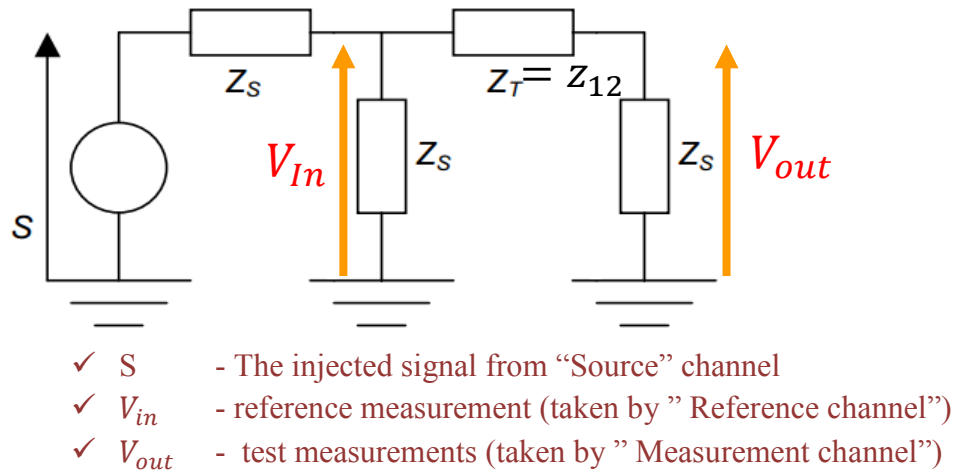


Figure 2.3: Simplified SFRA test arrangement

The prime objective of sweep frequency response analysis is the measurement of the impedance distributed over a wide frequency range of the power transformer. In the case of a power transformer, a resultant variation of impedance is a complex function of frequency due to its complex internal arrangement. Hence Transfer function, a representation in the frequency domain is used in the test to present results.

Transfer function is the ratio of output voltage to input voltage shown by (2.1),

which can be represented either in the time domain or frequency domain, but preferred one is the frequency domain.

$$G(s) = \frac{V_{out}(s)}{V_{in}(s)} \quad (2.1)$$

where $s = j\omega$ is the Laplace operator

The Voltage measured using *Reference Channel* corresponds to $V_{out}(s)$ and the voltage measured using “Measurement Channel” corresponds to $V_{in}(s)$. In case of a study of impedances (with the 50 Ω standard resistance as explained earlier), the impedance equation (2.2) can be used to derive the impedance of the transformer (Z_T).

$$G(s) = \frac{V_{out}(s)}{V_{in}(s)} = \frac{50}{50 + Z_T} \quad (2.2)$$

Like any other complex number, this transfer function can be decomposed into magnitude and phase as (2.3) and (2.4).

$$|G(s)| = 20 \log_{10} \left(\frac{V_{out}}{V_{in}} \right) \quad (2.3)$$

$$\angle G(s) = \tan^{-1} \left(\frac{V_{out}}{V_{in}} \right) \quad (2.4)$$

SFRA test analysers are not capable of calculating this transfer function numerically, as they have been designed to present this measured transfer function in graphical form, referred as bode plots. The concept behind this approach to generate bode plots can be described as follows.

Consider, an applied sinusoidal signal in which the frequency is varied between 20Hz and 2MHz, of the form;

$$x(t) = A \sin(\omega t) \quad (2.5)$$

And the output response, of the form;

$$y(t) = B \sin(\omega t + \emptyset) \quad (2.6)$$

When the input signal passes through the transformer, its amplitude and phase get altered, but not the output frequency for a given input frequency. Phase angle difference (\emptyset) can be inductive or capacitive, when respective output signal lags or leads the input signal. Figure 2.4 shows the input and output signals measured at a frequency(ω) where output lags the input as the system impedance is inductive.

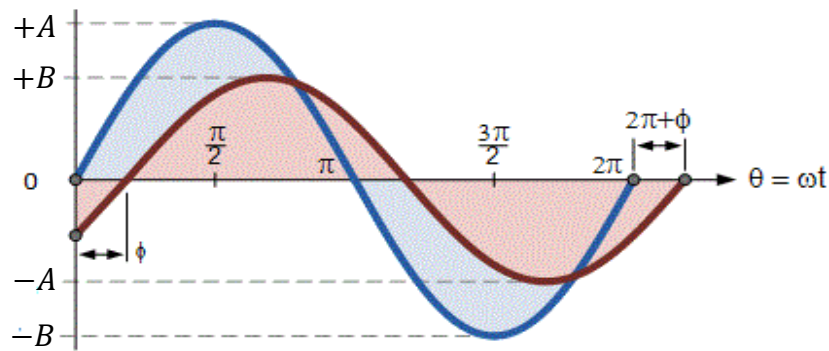


Figure 2.4: Frequency response of test object

The frequency of the input signal (ω) is varied within the range in predefined time intervals and respective output signals are measured. Magnitude ratio ($20\log_{10}(V_{out}/V_{in})$ i. e. ($20\log_{10}(A/B)$) and phase difference ($\tan^{-1}(V_{out}/V_{in})$ i. e. $\tan^{-1}(\phi)$) are calculated at each frequency and measured results are plotted as two graphs, magnitude and phase plots (referred as bode plots). Comparing with (2.3) and (2.4) equations, it is clear that resultant bode plot is the graphical representation of transfer function. Figure 2.5 illustrates a sample bode plot taken from Omicron FRA analyser (FRANEO 800) for transformer installed in Bolawatta area in Sri Lanka.

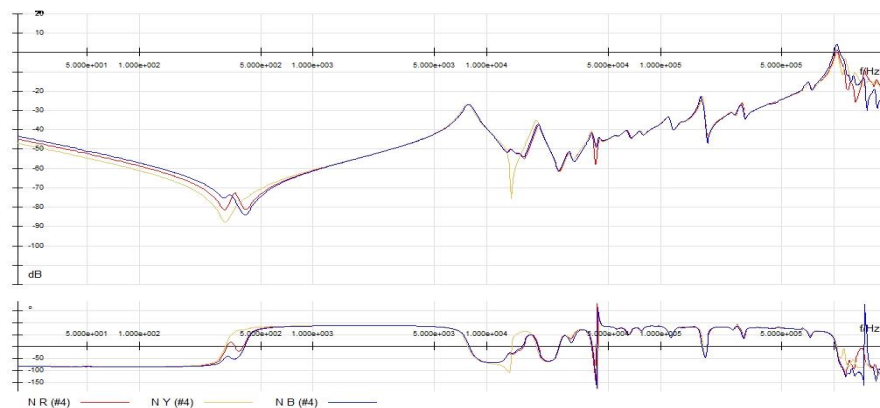


Figure 2.5: SFRA Signature of Bolawatta TR03 -3phase 31.5MVA, 132/33kV

As depicted in Figure 2.5, the final outcome of the test is in graphical nature. Usually, logarithmic scale is preferred as it gives an overall description of resonances of plots where linear scale can be used when detailed picture of high frequency ranges is required. Currently, these graphs are analysed and interpreted by industry experts in transformer fault diagnosis [18].

2.3 Types of SFRA Measurements

Basically, there are four types of tests that can be identified from the literature [4]. They are,

- Open-circuit measurement
- Short-circuit measurement
- Capacitive inter-winding measurement
- Inductive inter-winding measurement

Open-circuit and short-circuit tests are performed at the two ends of a single winding. In other words, sinusoidal signal with variable frequency is applied to one end of the winding and response is measured from the other end. All the unused windings are floating in the open-circuit measurements, whereas they are shorted in short-circuit measurements. The response produced by these two are dissimilar in initial ranges of SFRA. The reason is, due to this short-circuiting, core effects are nullified in the short circuit test and results in different curve shapes in low frequency region that depict influences of transformer core. Both these tests are performed at primary, secondary and tertiary windings (if available).

Unlike open-circuit and short-circuit tests, the capacitive inter-winding test is performed at the ends of two isolated windings, with all other terminals kept open. The inductive inter-winding test is performed in the same way, but with one end of each winding are grounded.

Responses obtained from each test have distinct features and adopted in different scenarios for different purposes [4]. However, amongst the other types, open circuit measurement and short circuit measurements are the most commonly used test types in the industry as responses of a single winding given by these two are suitable in isolating faulty sections or windings directly. Circuit configurations of each type of test are illustrated in Figure 2.6.

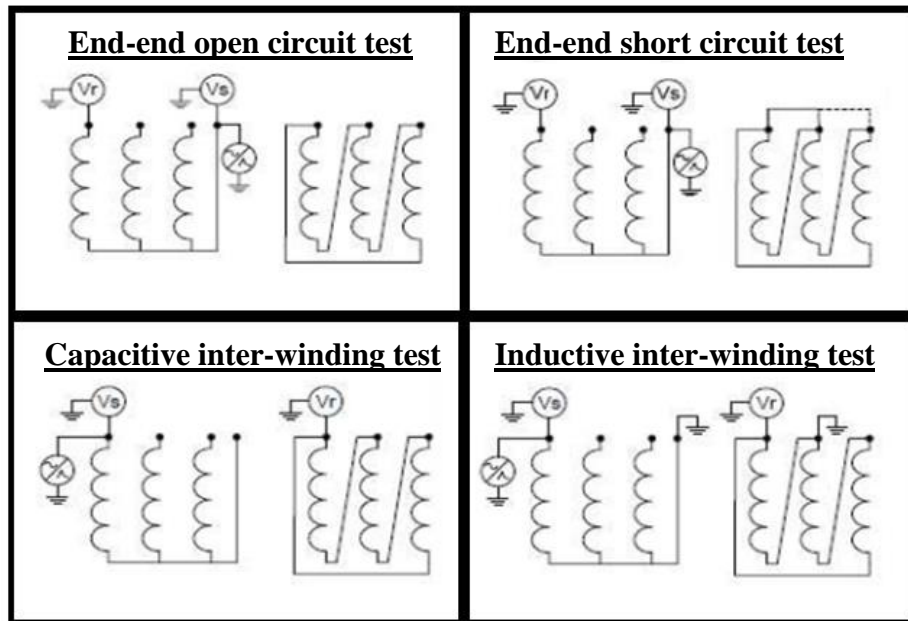


Figure 2.6: Types of SFRA measurements

2.4 Applications of SFRA

Basically, SFRA measurements are entirely governed by the mechanical structure of the transformer [19]. Therefore, any event (electrical or mechanical) that alters the existing structure can be identified using this analysis. Applications of SFRA can be categorized into two considering whether they performed in the factory or in the field, as explained below [4, 19].

In the factory

- Quality assurance
- preparation of transformers for re-location
- generation of baseline curves for diagnosis

In the field,

- Commissioning or re-location validation:- once transformer being brought to the premises or change in the location has happened, an SFRA is performed to ensure that the mechanical integrity of the transformer hasn't been compromised by the transportation
- Routine diagnostic purposes
- Fault diagnosis:- After a significant fault event or change in electrical test

condition (e.g. change of insulation resistance) or after transformer Alarm (e.g. Buchholz)

2.4.1 Fault diagnosis-Reference traces used for comparison

Three types of baseline traces are used for the comparison, especially in fault detection. Faults are diagnosed by comparing its post-fault frequency response with one of these types of reference curves.

1. Time based comparison - This is the comparison of traces of the same transformer. A previously obtained response curve when the transformer operates in a healthy condition is taken as the reference and compared with the faulty response, in order to detect faults. This is the most reliable way of doing fault diagnosis of power transformers using SFRA.
2. Type based comparison - This is the comparison of different transformers of same design. When pre-fault response curve is not available, the frequency response trace of a transformer with the same design is used as the reference for the comparison.
3. Design based comparison -This is the comparison based on different phases of same transformer. In a transformer, the response of identical design components (identical winding legs, bushings) are used as the reference trace, for an instance, comparing two side phases (phase R and B).

Recommended cabling practices indicated in aforementioned standards (**IEEE Std C57.149** standard and **IEC 60076-18** standard [4, 15]) should be used during these measurements to ensure correct diagnosis of faults. Time based comparison is always recommended as it delivers the highest accuracy in the detection process. But the rest of the methods have to be used when pre-fault, healthy transformer response curves are unavailable.

2.4.2 Transformer faults identification using SFRA

Failure modes of transformers can be categorized into two viz. electrical and mechanical failures [20]. Numerous conventional methods are available to detect electrical faults such as short circuited windings, open circuited windings, grounding issues etc. But for the mechanical faults, fault detection methods are limited in number. In that sense, sweep frequency response analysis can be regarded as the best option to detect both these failures, especially as a highly accurate method to diagnose faults caused by mechanical issues. This is really important to avoid catastrophic failure of the power transformer which will not only impact the system adversely but also economically. Some of the Faults types that can be identified are summarized in Table 2.1.

Table 2.1: Mechanical and electrical faults identified by SFRA

Mechanical faults	Electrical faults
core displacements	Short circuit of turns
Winding deformation(buckling)	Ground connection issues
Winding movements(axial and radial)	Open circuited windings
Clamping structure issues	
Partial collapse of windings	

Apart from these applications, SFRA can be used in power transformer modelling [4]. A model with proper mathematical formulation will improve the accuracy of fault diagnosis using SFRA.

2.5 Existing models of power transformers

Most basic model of the power transformer is the fundamental equivalent circuit of transformer which has been used by professionals, researchers and undergraduates throughout many decades. Winding resistances/inductances referred to primary or secondary, resistance and inductance values to represent core loss and magnetizing components are the elements of this basic circuit which is used in various instances such as estimation of losses and power system fault diagnosis. Even though

this model provides acceptable results at power frequency, it fails to represent the behaviour of actual transformer over a wide frequency range owing to the absence of capacitive elements that characterize the effect of transformer insulation.

For the first time, in 1978, diagnosis of power transformer using frequency response analysis (FRA) was proposed Dick and Erven [21]. Since then, it inspired so many researchers to improve its capabilities in fault diagnosis. As a result, various indexes [22] and algorithms [6, 7, 8, 9] has been developed to analyse these faults numerically. These numerical indicators and algorithms can be incorporated in the analysis process, yet some of the features like localization of faults are not straightforward. As a solution, approaches based on transformer models have been developed.

It is vital to have an accurate circuit model of a power transformer in order to study its actual behaviour. In this regard, different approaches have been used to represent the behaviour of transformers which can be divided into Black-box models [10, 11]; Gray-box models [12, 13]; and hybrid models [14].

Black-box models usually consist of RLC components with no real physical correlation with actual values of transformer parameters. Both [10, 11] followed the same approach where measured admittance or impedance corresponding to nodes of the circuit is presented in matrix form and parameter values have been approximated using a fitting process. One disadvantage of these black box modelling approach is, it requires an in-depth knowledge about circuit synthesis in circuit realization as resultant admittance or impedance matrices can be dissimilar depending on the transformer structure. Nevertheless, rendering a physical interpretation for these realized circuits is challenging and inappropriate to model inner-physical phenomena and deformation of the winding.

Gray box models, also referred to as physical models, are the preferred method to model power transformers that offer the convenience of physical interpretation. Basically, these are based on physical configuration of power tranforemer and valid

even at a wide frequency range. Furthermore, Gray box modelling enables to use network analysing tools such as MATLAB and PSpice which facilitate calculating currents/voltages in case of intricate transformer circuit designs. Investigation reveals that physical models are of two types; Transmission line models and detailed models based on lumped parameter networks.

Transmission line models given in [23] can be used to model transformer windings with few number of coils and are not suitable when the number of coils is substantial. Because the size of the resultant matrices increases with the increment of components in the transmission line model, extending the computation time significantly. Compared with multi-conductor transmission line models, detailed modelling based on lumped parameter networks offer more benefits. Also, there are various methods of modelling to choose from. These models not only capture physical lengths of windings, but also represent wide frequency response including lightning impulse, transient behaviours. Quite obviously, ladder network helps to accomplish the objective of localization of faults.

Ladder network can be realized using transfer function or impedance/admittance function. Transfer functions for model estimation has been used in past research work [10, 11, 24, 25]. D. M. Sofian and others [26] used admittance function to model power transformer as series/parallel arrangement of passive components. But this method results in negative resistance values in the realized circuit. The reason behind this is that the estimated transfer function that derive its admittance function does not satisfy the rules of circuit synthesis. Owing to this reason, usage of transfer functions that satisfy Hurwitz criterion is essential [25]. Ragavan et al. [12, 24] presented a method to construct a physically realizable driving point impedance function which is based on pole/ zero locations (anti-resonances and resonances) of frequency response analysis. One drawback of these models is that it realizes the parameter values of lumped parameter network as equal values. The test object with non-interleaved double disk winging has been used to represent high voltage winding of a distribution transformer in [13]. S.P Ang et al. Used duality principle in modelling where dimension and insulation properties of the transformer

components are used to calculate values of model elements [27]. This model has been used to represent core behaviour that has very few resonance points. This is not suitable to represent the power transformer with winding and core together. Modelling based on finite element analysis (FEA) was proposed in [28]. Prior knowledge of the structure and material properties of the transformer is a necessary requirement in modelling using FEM, despite the fact that FEA can simulate models with almost being identical to the actual situation. A transformer was represented as a coupled ladder network where driving point impedance is used in the model derivation in [24, 29]. It is found that the number of sections of power transformer directly affects the measured response. Therefore, researchers have used different strategies to decide this number correctly, for instance an algorithm is used to detect this number using the measured equivalent capacitance value [24]. Since this model estimates similar capacitances for each section, number of estimated sections can deliver values than that of the actual transformer. At the same time, these models require measured capacitance, inductance and resistance values at different transformer components which are not available at most of the times together with frequency response analysis data. Therefore simple and robust method that doesn't depend on implementing circuit is crucial for modelling of power transformers.

Hybrid models are combinations of black-box and Gray-box models. So inevitably inherits the disadvantages of black-box models.

Some of the above-mentioned models require calculated parameters of the transformer in modelling, so measurement must be precise. Some of the information can be calculated using manufacturer data sheets, but there are tolerances attached with them that can have a significant impact on the final model. Most importantly, as transformer ages and due to its operation, actual values of the components can possess different values than its data sheets. Considering these facts and the complexity of the power transformer circuit, it is important to abstain from methods using analytical calculations. Thus, researchers made the use of evolutionary approaches based on new algorithms such as Genetic algorithm [13, 30], artificial bee-colony algorithm [29], Bat Algorithm [31], Bacterial swarming algorithm [32] and techniques such as Neural

networks [33, 34], Vector fitting [35].

The estimation of model parameters is a nonlinear optimization problem as a large number of elements are involved in the problem. Among these algorithms, genetic algorithm (GA) is the mostly used emerging method to solve nonlinear, highly dimensional problems [36]. Compared with the other numerical methods, intrinsic parallel nature of stochastic search is very effective to arrive at global optimum [30]. Rashtchi et al. have used Genetic algorithm based parameter estimation for R-L-C-M model [13]. The objective of the optimization has been taken as minimization of difference between measured and estimated response. A model without mutual inductances has been considered to reduce the complexity. Hence estimated model does not represent actual windings.

Major criticism regarding GA is the long-time duration for its computation. However, integration of GA with other techniques such as neural networks (NN) has been well accepted and used in the industry in the past [36]. This gives a well-guided solution to reduce its computation time. Currently, numerous software tools are available to perform these complex calculations with an interactive environment such as neural network tools and genetic algorithm tools of MATLAB [37]. Approaches based on the integration of new techniques has become increasingly popular in modelling transformers.

As a conclusion, an appropriate model to represent power transformer frequency response must have the following conditions

- Corresponding transfer function must be realizable i.e. it should satisfy Hurwitz criterion.
- All the component value of the lumped paramour network must be real positive.
- It should represent the actual behaviour of power transformer with reasonable accuracy.

Also, simplicity of model would be an added advantage, if the model is to be

implemented in an electromagnetic transient program (EMTP) where the complexity of the model decides its execution time.

2.6 Proposed method for transformer modelling

Comparing all the approaches, lumped parameter network modelling approach, one of a Gray-box modelling methods that provides reasonable accuracy with the ability of physically interpreting the model was chosen as the desirable approach in this thesis. The proposed methodology of modelling the equivalent circuit is a two-step approach as shown in Figure 2.7. In this study, the transfer function based approach has been used to synthesize transformer equivalent circuit where model parameter estimation is achieved by a Genetic algorithm (GA) and artificial neural network (ANN) integrated method

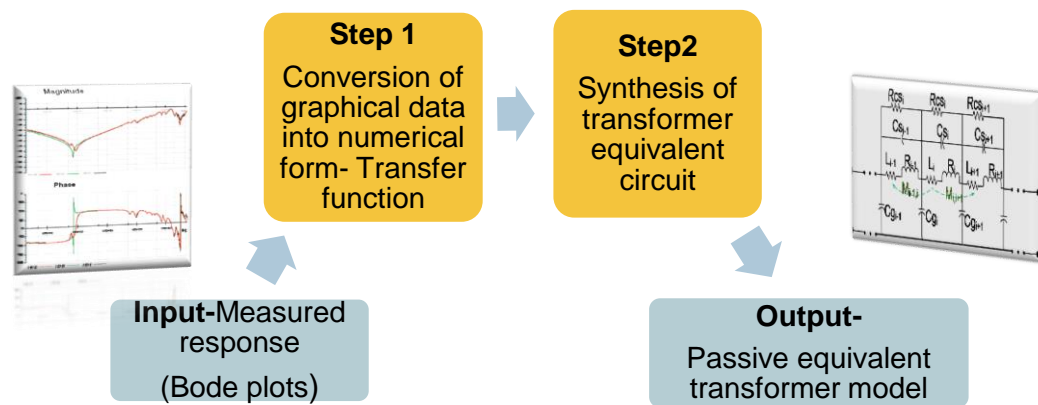


Figure 2.7: Basic steps of modelling transformer using SFRA

Chapter 3

TRANSFER FUNCTION ESTIMATION USING FREQUENCY RESPONSE ANALYSIS

3.1 Introduction

Bode plot, the output of SFRA given by frequency response analyser is a pair of graphs that need to be analysed and interpreted by industry experts during fault diagnosis. An accurate model of power transformer derived from SFRA would be useful in diagnosing faults with a greater accuracy as faults can be interpreted by changes in parameter values rather than comparing with reference curves. In order to obtain an accurate circuit model, each step of modelling should be performed with high accuracy. Therefore, the first step of modelling, the estimation of transfer function is vital as any bias caused in this step propagates over the subsequent steps. Sometimes, synthesizing of ladder network may not even be feasible due to erroneous transfer function estimation. This chapter presents a novel algorithm to convert the measured frequency response data, the bode plots, into the transfer function. This algorithm can be used to estimate the transfer function of power transformers for the entire region of SFRA with a high accuracy.

There are several methods to represent measured results of SFRA. These can be categorized into two: frequency domain and time domain. Due to the simplicity of analysing the results, frequency domain representations are used in general. Some of those are;

- Bode plots (magnitude and phase plots)
- Impedance/admittance function (Graph contains Magnitude/admittance values over the frequency range)
- State space representation
- Transfer function

Each type of these representation can be converted to any of the others.

However, while some of the conversions are very simple and straightforward, some are not. For an example, state space representation, transfer function and impedance/admittance functions can be easily plotted as bode plots, but the opposite is really challenging as bode plots are not a numerical property. In fact, this difficult conversion is the one that has to be executed in the process of transformer modelling as the final outcome produced by the industrial sweep frequency response analysers are these bode plots.

Transfer function is the most appropriate numerical methodology to convert bode plots. The main reason for this is, bode plots are the graphical representation of the transfer function. Therefore any other method like state space etc. has to be derived through this transfer function.

Various techniques have been proposed to estimate the transfer function using frequency response data. Levy presented a least square based approach to linearize the regression problem [38]. Numerator and denominator coefficients have been determined by minimizing error function (error between estimated and actual data) defined over the frequency range. One shortcoming of this method is that the error function has inherent weighing, owing to multiplication by denominator during calculations [39]. As a solution, to minimize this resultant error, Sanathanan and Koerner proposed an iterative method in which resulted bias of Levy method is gradually minimized through an iterative process [40]. When this two methods were applied to some of the systems, resultant poles and zeros might not be stable in nature [41]. But, this issue does not arise in case of power transformers as numerator and denominator orders are almost similar values. Simply, this fact can be validated by means of frequency response i.e. bode plot of power transformers contains resonance and anti-resonance alternatively, giving rise to a similar range of poles and zeros that make the estimated transfer function to be a quantity with same ordered numerator and denominator. A.K. Kamath et al. has developed Sanathanan-Koerner method to estimate transfer function with fractional orders in reference [42]. However, the usage of fractional order transfer function is unacceptable, since the physical configuration of a power transformer cannot result in such fractional order relation. In other words,

resistive, inductive and capacitive elements that build the transformer equivalent circuit have integer order terms once represented in Laplace domain, making actual transfer function of the power transformer to be an integer order.

The transfer function of power transformer contains high ordered numerator and denominator due to its complex nature of the circuitry [42, 43]. Usually, this is more than 50 order. Hence, researchers have sectionalized the whole bandwidth into few regions and modelled them separately [25, 42]. The major drawback of this technique is that there would be a several numbers of equivalent circuits for the same transformer corresponding to its derived multiple sections. Also, it can result in the exclusion of essential poles or zeros, or repetition of poles or zeros, when these separate sections are combined to get the entire response.

The algorithm presented in this chapter can be used to estimate the transfer function of power transformers eliminating the aforementioned issues. First few sections consist the derived equations together with theory behind Levy, Sanathanan-Koerner method that are used to convert graphical frequency response into a transfer function. The Routh-Hurwitz criterion is also presented, followed by a detailed description of the algorithm to estimate transfer function with a case study.

3.2 Analysis of integer order system in frequency domain

Transfer function, the ratio of output response to input response of an integer order system can be defined in the Laplace domain as follows.

$$G(s) = \frac{A_0 + A_1(s) + A_2(s)^2 + A_3(s)^3 + \dots + A_m(s)^m}{B_0 + B_1(s) + B_2(s)^2 + B_3(s)^3 + \dots + B_n(s)^n} \quad (3.1)$$

Where A_i, B_i, m and n are real numbers. At any instance, this relation can be evaluated in the frequency domain by substituting Laplace operator s with $(j\omega)$.

3.2.1 Levy's method of identification of transfer function

This method presents least square based approach to estimate numerator and denominator coefficients by linearizing quadric error function [38]. This well-

established method can be used for any plant where frequency behaviour is known in advance [44].

Without loss of generality, constant value B_0 can be assumed to be one. Hence (3.1) can be represented in the frequency domain by substituting Laplace operator with $(j\omega)$ shown as follows.

$$G(s) = \frac{\sum_{x=0}^m A_x (j\omega)^x}{1 + \sum_{x=0}^n B_x (j\omega)^x} \quad (3.2)$$

$$= \frac{\alpha(\omega) + j\beta(\omega)}{\sigma(\omega) + j\tau(\omega)} \quad (3.3)$$

$$= \frac{N(\omega)}{D(\omega)} \quad (3.4)$$

where

$$\alpha(\omega) = \sum_{x=0}^m A_x \text{Re}[(j\omega)^x] \quad (3.5a)$$

$$\beta(\omega) = \sum_{x=0}^m A_x \text{Im}[(j\omega)^x] \quad (3.5b)$$

$$\sigma(\omega) = 1 + \sum_{x=1}^n B_x \text{Re}[(j\omega)^x] \quad (3.5c)$$

$$\tau(\omega) = \sum_{x=0}^n B_x \text{Im}[(j\omega)^x] \quad (3.5d)$$

where N , D are complex valued terms and α , β , σ , τ are real values that represent real and imaginary components of numerator (N) and denominator (D). Consider, precise transfer function $F(j\omega)$ that represent actual response of the system is available. Then it can be written using complex notation as follows.

$$F(j\omega) = R(\omega) + jI(\omega) \quad (3.6)$$

Error attributed to the fitting process (ε) can be represented by the difference of ideal and current responses as

$$\varepsilon(\omega) = F(j\omega) - G(j\omega) = F(j\omega) - \frac{N(\omega)}{D(\omega)} \quad (3.7)$$

Multiplying above equation (3.7) by denominator $D(\omega)$ and substituting with (3.3), (3.4) and (3.6), weighted error at a known frequency ω_k can be found as,

$$D_k(\omega_k)\varepsilon_k(\omega_k) = D_k(\omega_k)F_k(j\omega_k) - N_k(\omega_k) \quad (3.8)$$

$$= [\sigma_k(\omega_k) + j\tau_k(\omega_k)][R_k(j\omega_k) + jI_k(j\omega_k)] - (\alpha_k(\omega_k) + j\beta_k(\omega_k)) \quad (3.9)$$

For convenience, equations that come next are alleviated by omitting frequency dependence term. Thus equation (3.8) is written as

$$D_k\varepsilon_k = [R_k\sigma_k - \tau_kI_k - \alpha_k] + j[R_k\tau_k + I_k\sigma_k - \beta_k] \quad (3.10)$$

If total weighted error evaluated over the sampling frequencies is E , then

$$E = \sum_{k=1}^f \{ [R_k\sigma_k - \tau_kI_k - \alpha_k]^2 + [R_k\tau_k + I_k\sigma_k - \beta_k]^2 \} \quad (3.11)$$

Unknown coefficients of numerator (A_k) and denominator (B_k) can be determined based on minimization of total weighted error E . Accordingly, $(m + n + 1)$ number of equation can be found by calculating partial derivatives for every individual. Substituting x value with a coefficient number, partial derivative with respect to x^{th} coefficient can be easily determined by (3.12), (3.13)

$$\frac{\partial |E|^2}{\partial A_x} = \sum_{k=1}^f \{ -2[R_k\sigma_k - \tau_kI_k - \alpha_k][Re[(j\omega_k)^x] - 2[R_k\tau_k + I_k\sigma_k - \beta_k][Im[(j\omega_k)^x]] \} \quad (3.12)$$

$$\frac{\partial |E|^2}{\partial B_x} = \sum_{k=1}^f \{ 2R_k[R_k\sigma_k - \tau_kI_k - \alpha_k][Re[(j\omega_k)^x] + 2I_k[R_k\tau_k + I_k\sigma_k - \beta_k][Re[(j\omega_k)^x] - 2I_k[R_k\sigma_k - \tau_kI_k - \alpha_k][Im[(j\omega_k)^x] + 2R_k[R_k\tau_k + I_k\sigma_k - \beta_k][Im[(j\omega_k)^x]] \} \quad (3.13)$$

Solution to these equations are derived by setting partial derivative values to zero. Since it is fairly difficult to manipulate plentiful equations individually, resultant equations are converted into matrix form.

$$\begin{bmatrix} M1 & M2 \\ M3 & M4 \end{bmatrix} \begin{bmatrix} A \\ B \end{bmatrix} = \begin{bmatrix} C1 \\ C2 \end{bmatrix} \quad (3.14)$$

Where $M1, M2, M3, M4, A, B, C1$ and $C2$ are sub matrices as shown below.

$$M1_{l,c} = \sum_{k=1}^f \{-Re[(j\omega_k)^l]Re[(j\omega_k)^c] - Im[(j\omega_k)^l]Im[(j\omega_k)^c]\} \quad (3.15)$$

$$l = 0,1 \dots m \text{ \& } c = 0,1 \dots m$$

$$M2_{l,c} = \sum_{k=1}^f \{R_k Re[(j\omega_k)^l]Re[(j\omega_k)^c] + I_k Im[(j\omega_k)^l]Re[(j\omega_k)^c]$$

$$- I_k Re[(j\omega_k)^l]Im[(j\omega_k)^c] + R_k Im[(j\omega_k)^l]Im[(j\omega_k)^c]\} \quad (3.16)$$

$$l = 0,1 \dots m \text{ \& } c = 0,1 \dots n$$

$$M3_{l,c} = \sum_{k=1}^f -R_k Re[(j\omega_k)^l]Re[(j\omega_k)^c] + I_k Im[(j\omega_k)^l]Re[(j\omega_k)^c]$$

$$- I_k Re[(j\omega_k)^l]Im[(j\omega_k)^c] - R_k Im[(j\omega_k)^l]Im[(j\omega_k)^c] \quad (3.17)$$

$$l = 0,1 \dots n \text{ \& } c = 0,1 \dots m$$

$$M4_{l,c} = \sum_{k=1}^f (R_k^2 + I_k^2)(Re[(j\omega_k)^l]Re[(j\omega_k)^c] + Im[(j\omega_k)^l]Im[(j\omega_k)^c]) \quad (3.18)$$

$$l = 0,1 \dots n \text{ \& } c = 0,1 \dots n$$

$$C1_{l,1} = \sum_{k=1}^f (-R_k Re[(j\omega_k)^l] - I_k Im[(j\omega_k)^l]) \quad (3.19)$$

$$l = 0,1 \dots m$$

$$C2_{l,1} = \sum_{k=1}^f (-Re[(j\omega_k)^l](R_k^2 + I_k^2)) \quad (3.20)$$

$$l = 0,1 \dots n$$

$$A = \begin{bmatrix} A_0 \\ \vdots \\ A_m \end{bmatrix} \quad B = \begin{bmatrix} B_1 \\ \vdots \\ B_n \end{bmatrix} \quad (3.21)$$

When both sides of Equation (3.14) are multiplied by Matrix inverse of M (This is the single matrix constructed by combining $M1$, $M2$, $M3$ and $M4$ sub-matrices in (3.14)), matrix A and B can be determined. These are the two matrices that represents numerator and denominator coefficients of the estimated transfer function.

3.2.2 Sanathanan-Koerner iterative method

One drawback of levy method is, elements of matrix M has less influence to lower frequency values compared to its high frequency values [40]. Error function values are clearly dominated by larger values since small variation of a large value has a greater impact to any output. Hence, the estimated transfer function of Levy's method prominently represents high frequency behaviour i.e. sometimes, low frequency resonances are not accurately estimated. For this reason, Levy's method alone does not provide a way to estimate the transfer function from measured SFRA response.

A method to improve results obtained from Levy's method is proposed by Sanathanan and Koerner, which incorporate an iterative process to reduce bias caused by the multiplication of denominator during the process [40]. Weighted error E can be replaced by

$$E_L = \frac{F(j\omega)D_L(\omega) - N_L(\omega)}{D_{L-1}(\omega)} \quad (3.22)$$

Where L is the number of iterations from beginning and $D_{L-1}(\omega)$ is the denominator found in the previous iteration. It should be noted that in the initial iteration $D_{L-1}(\omega)$ is set to 1 and the results are that of Levy's method. If convergence exists, E_L converge to ε as $D_{L-1}(\omega)$ reach to $D_L(\omega)$. This modification will minimize the influence of weighing by a factor of W_k .

$$W_k = \frac{1}{|D_{L-1}(\omega_k)|^2} \quad (3.23)$$

Simply, the numerator and denominator matrices (A and B) can be generated by doing a simple adjustment to equations (3.15) - (3.20). Multiplying each side by a factor W_k prior to summation will implement Sanathanan and Koerner iterative method in the matrix form and resultant A, B matrices offer improved results for numerator and denominator, respectively. At each iteration calculated denominator(D_{L-1}) has to be fed back to the system to compute revised W_k that will be used in the following iteration. This iterative process has to be terminated by a

stopping criteria i.e. iterations are stopped, once relative error between adjacent terms becomes less than a pre-specified value. This assignment will ensure an acceptable output result as iteration process would diverge the process otherwise.

3.3 Routh-Hurwitz stability criterion

Derived transfer function of any physical circuit must satisfy necessary and sufficient conditions of Routh-Hurwitz criterion with positive realness in order to be able to realize into a physical circuit with passive components.

Any transfer function that gives positive real value for any real value of Laplace operator (s) is called a positive real function [25, 43]. When such function is drawn in the z plane (complex plane), every pole and zero should be outlined in left half real axis i.e. they should be negative real values. This condition can be easily tested by "Routh-Hurwitz stability criterion" performing a "Routh-Hurwitz test" which is explained as follows [45].

When the transfer function is written as (3.4), with $D(s)$ being denominator

- All the coefficients of $D(s)$ should be non-zero.
- All the coefficients of $D(s)$ must have no sign change (i.e. all coefficients must be positive, or equivalently all must be negative)
- All the terms in the first column of Routh's array must have the same sign

The transfer function of a power transformer should satisfy above criterions as SFRA data that used to derive transfer function relate to a physically existing circuit. Consequently, numerator and denominator of power transformer's derived transfer function should contain positive real values for each coefficient A_i and B_i that will satisfy Routh-Hurwitz stability criterion.

3.4 Proposed algorithm to derive transfer function from SFRA data

To interpret every resonance of SFRA, four options can be found which satisfy Routh-Hurwitz stability criterion. Those are

- Real pole (single pole)

- Real zero (single zero)
- Underdamped pole (double pole)
- Underdamped zero (double zero)

In simple terms, “Poles” of a transfer function are frequencies for which denominator of transfer function becomes zero and “Zeros” are the frequency values for which numerator value become zero. The reason to evaluate transfer function using these four combinations of integer order is, any component of a physical circuit like power transformer must be an integer order as explained in the previous chapter. Thus, the proposed algorithm estimates the transfer function as a product of these components which results in a transfer function as given in (3.1). The proposed algorithm is shown in Figure 3.1.

Initially, frequency analysis data has to be entered into the system (magnitude and phase values over the measured frequency range(20 HZ to 2 MHz)), where they were separated to few bandwidths depending on the variations. Maximum number of resonances are limited to specific value. Otherwise, the size of the resultant transfer function would be larger than a standard processor can handle. Since there are relatively few variations in the lower frequencies compared to higher frequencies in the bode plots, preceding bandwidths are widespread than subsequent bandwidths. However, accuracy can be improved by reducing the size of bandwidth, but it will extend computational time. As a compromise, the default number of bandwidths are taken as four.

Regions (R_i) defined in this method refers to the frequency range from 20Hz to the end frequency of the considered bandwidth (BW_i), or in other words region R_i of i^{th} iteration is the summation of bandwidths (BW_i) shown in (3.24).

$$R_i = \{BW_1 + BW_2 + \dots + BW_i\} \quad (3.24)$$

Defining regions in this manner is useful in case any pole or zero hasn't been recognized during the estimation process. Algorithm retrieves any missed pole or zero in its subsequent regions.

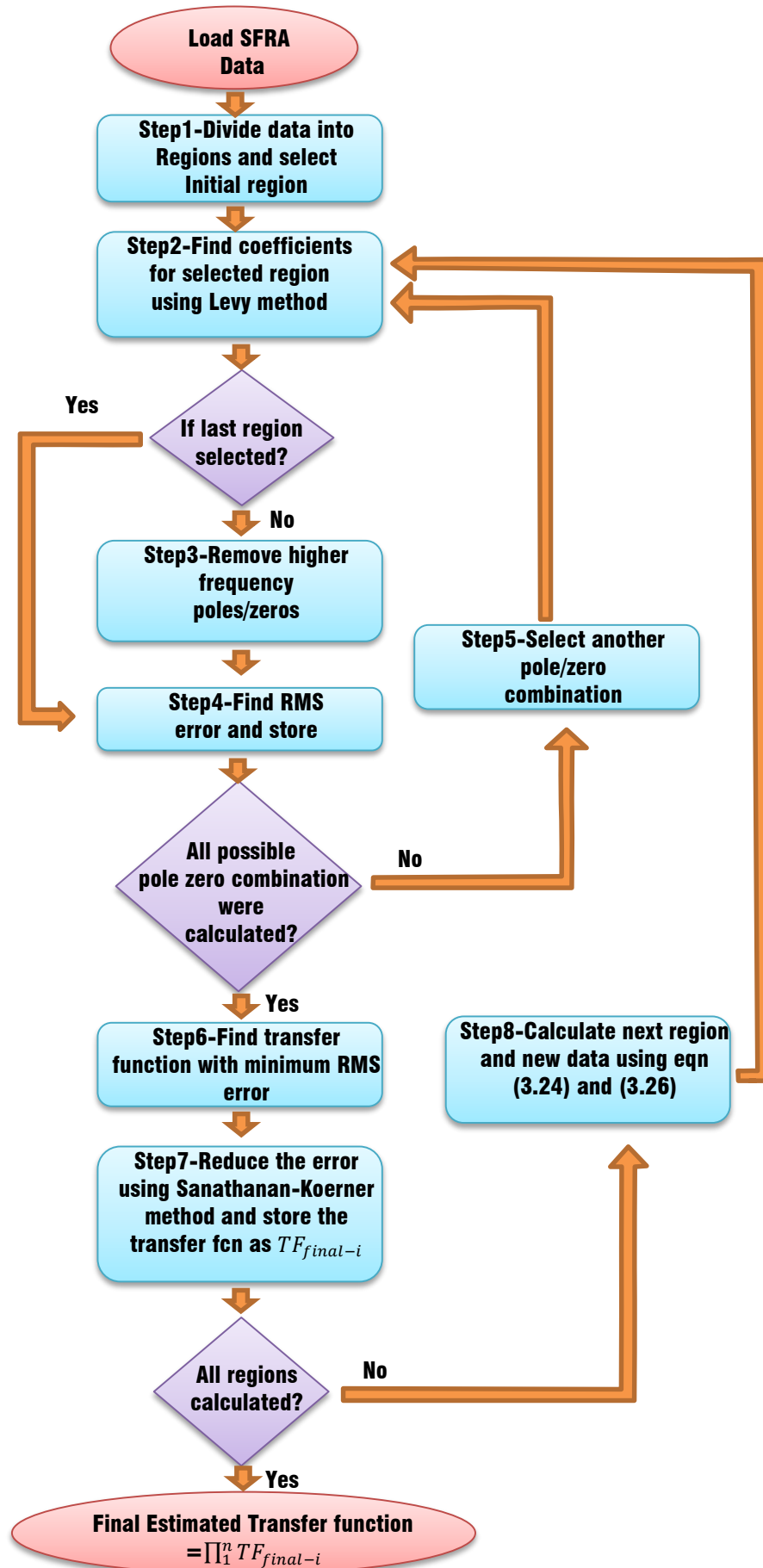


Figure 3.1: Proposed algorithm to obtain transfer function from SFRA data

In the step two, the initial transfer function is estimated using the derived equations based on Levy's method. Intrinsically, this method estimates poles and zeros that aren't inside the considered region. As the estimation of resonances without real data is incorrect, resonance points outside the considered region are removed in the next step. If they actually exist, any excluded pole or zero will be recovered in the subsequent region. This process is repeated for every numerator and denominator combination and respective transfer functions are calculated. Depending on the order of numerator and denominator, selected pole zero combination will be different. At each combination, RMS error between measured and estimated plots are calculated using (3.25) and stored in the computer.

$$Rms_{error} = \sqrt{\sum_1^{(end\ freq\ of\ R_i)} \frac{1}{size(R_i)} |(N - E)|} \quad (3.25)$$

where E is the evaluated transfer function $TF_{final-i}$ at frequency f and N is the magnitude value of considered frequency. Note that N is not identical for all regions. As the algorithm suggested in Figure 3.1, input frequency response data for each iteration is recalculated in step 8 by dividing original SFRA data from the product of transfer functions found up to $(i - 1)^{th}$ iteration using (3.26).

$$Newdata_i = \frac{Original\ SFRA\ data}{\prod_1^{i-1} TF_{final-i}} \quad (3.26)$$

where N which mentioned in the above paragraph is the magnitude value of this $Newdata_i$ at frequency f .

Once all combinations were assessed, the best possible combination that gives minimum RMS value is selected in the step 6. This is the transfer function fed into the Sanathanan-Koerner iterative method that will reduce the bias of Levy's method as it proceeds through its iterations.

This cycle is repeated for all the other regions where data fed into the system at each region to generate regional transfer function is calculated using (3.24) and

(3.26). The outcome of this whole process is i number of transfer functions corresponding to i numbers of divided regions. Final estimated transfer function is the product of these individual transfer functions obtained for each region.

The rationale behind estimation of transfer function by sectionalizing frequency region can be explained as follows. The circuitry inside the transformer is a combination of many different components such as individual winding, insulation and mechanical structure including parts like tap changer, bushings etc. Even though these parts can be seen as quantities that continues physically, arrangement inside the transformer forms sections where each section has own individual transfer function characteristics. Therefore transfer function for the complete assembly is a combination of individual transfer functions i.e., the product of transfer functions.

3.5 Application of proposed algorithm (Case study for validation of proposed method)

The proposed algorithm in this thesis is illustrated using actual SFRA data of power transformer in operation. Selected transformer is 31.5 MVA, 132/33 kV, 3phase, YNd1 transformer manufactured by Pauwels in 2012. Modelled frequency response is H.V middle phase (usually refer as phase Y) With L.V side being opened. Figure 3.2 shows obtained bode plots for corresponding SFRA test.

According to the algorithm, the frequency response is separated into four bandwidths as shown below.

- Bandwidth 1: 20 Hz – 29.2 kHz -(i.e. 125 rad/s-184 krad/s)
- Bandwidth 2: 29.2 kHz – 117 kHz -(i.e. 1.84 krad/s -735 krad/s)
- Bandwidth 3: 117 kHz – 188 kHz -(i.e. 735 krad/s -1.18 Mrad/s)
- Bandwidth 4: 188 kHz – 2 MHz -(i.e. 1.18 Mrad/s -12.5 Mrad/s)

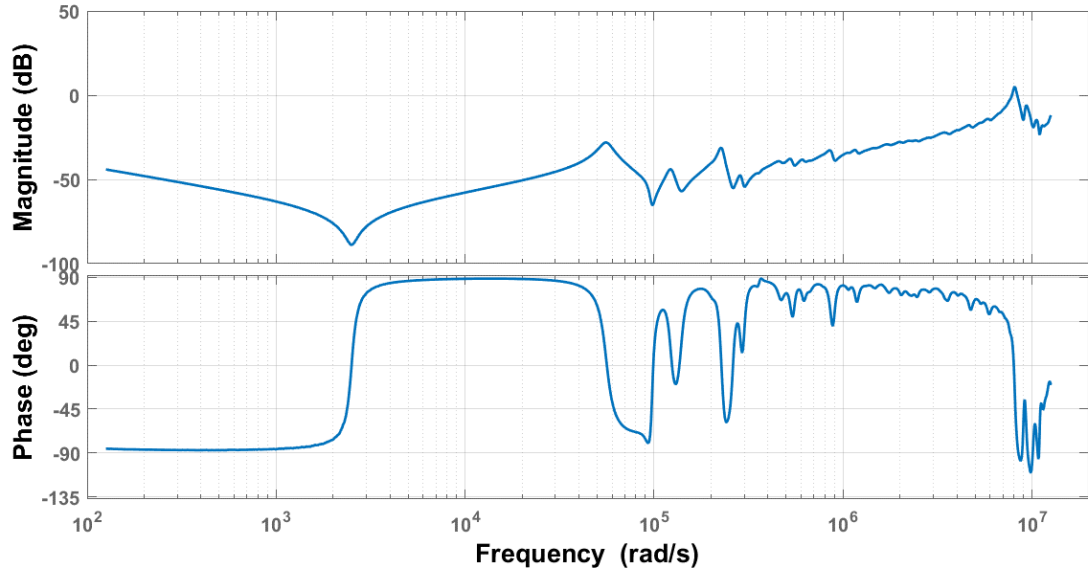


Figure 3.2: Original SFRA of 133/33 kV, 31.5 MVA Pauwels transformer (Phase Y)

The algorithm was implemented using commercially available software MATLAB 2016. This software provides a user friendly platform to perform complex mathematical computations required by the proposed algorithm.

As the algorithm suggests, transfer function for the first iteration in the region of 20 Hz – 29.2 kHz is estimated using Levy method. Figure 3.3 Shows numerator and denominator combinations considered in the Levy’s method. Usually, RMS error varies in large range with the error of best combination being the smallest. Hence, for the sake of clarity, the inverse of RMS errors are drawn in the figure for the each combination. As it depicts, Maximum inverse of RMS error 5101.7 (Corresponds to minimum RMS error of 1.960×10^{-4}) is resulted when the order of both numerator and denominator is 17. Since this is not the final region, resonances outside the considered frequency region are eliminated according to the proposed algorithm that will result in an order reduction of numerator and denominator to 14 and 15 respectively (To be precise, a double zero at 2.642×10^5 rad/s is eliminated from numerator and a single pole at 1.6771×10^6 rad/s with a double pole at 2.2001×10^5 rad/s is eliminated from denominator resulting an order reduction by a value of 2 and 3 respectively). Corresponding transfer function produced by this step is shown in (3.27), (3.28) and (3.29).

$$TF_{final-1} = \frac{NumTF_{final-1}}{DenTF_{final-1}} \quad (3.27)$$

where

$$\begin{aligned} Num - TF_{final-1} &= 2.742 \times 10^{-75} s^{15} + 2.454 \times 10^{-70} s^{14} \\ &+ 3.084 \times 10^{-64} s^{13} + 2.525 \times 10^{-59} s^{12} \\ &+ 1.387 \times 10^{-53} s^{11} + 1.024 \times 10^{-48} s^{10} \\ &+ 3.189 \times 10^{-43} s^9 + 2.088 \times 10^{-38} s^8 \\ &+ 3.953 \times 10^{-33} s^7 + 2.248 \times 10^{-28} s^6 \\ &+ 2.507 \times 10^{-23} s^5 + 1.206 \times 10^{-18} s^4 \\ &+ 6.38 \times 10^{-14} s^3 \\ &+ 2.497 \times 10^{-09} s^2 \\ &+ 1.066 \times 10^{-06} s + 0.0156 \end{aligned} \quad (3.28)$$

$$\begin{aligned} DenTF_{final-1} &= 8.021 \times 10^{-68} s^{14} + 6.96 \times 10^{-63} s^{13} \\ &+ 8.094 \times 10^{-57} s^{12} + 6.515e \times 10^{-52} s^{11} \\ &+ 3.175 \times 10^{-46} s^{10} + 2.333e \times 10^{-41} s^9 \\ &+ 6.14e \times 10^{-36} s^8 + 4.039e^{-31} s^7 \\ &+ 6.093e \times 10^{-26} s^6 + 3.503 \times 10^{-21} s^5 \\ &+ 2.867 \times 10^{-16} s^4 + 1.392 \times 10^{-11} s^3 \\ &+ 4.721 \times 10^{-07} s^2 + 0.01841 s + 1 \end{aligned} \quad (3.29)$$

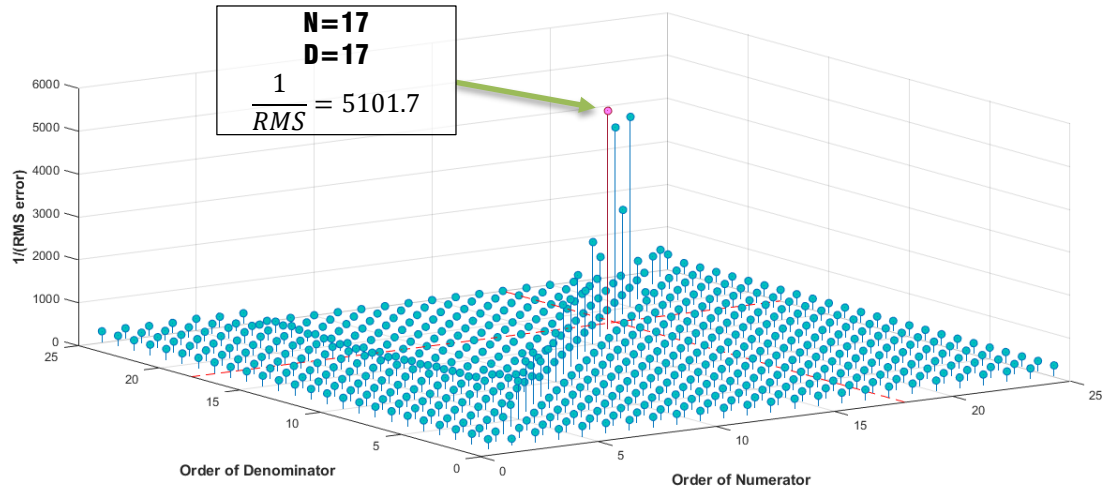


Figure 3.3: Inverse values of RMS errors for the numerator and denominator combinations of region 1

Bode plot of the transfer function after removal of higher frequency poles and zeros is shown in Figure 3.4 with respect to measured SFRA response. Note that the

transfer function obtained from Levy method is taken as the final transfer function for the region 1 as resulting RMS error of Sanathanan-Koerner method does not converge. This situation mainly arises due to the small size coefficients of estimated transfer function. Highest order coefficient is a power of -75 in the numerator and it is -68 for the denominator. Therefore even a tiny variation of estimated value will alter the RMS in a great extent that will result in a non-converging iteration scenario.

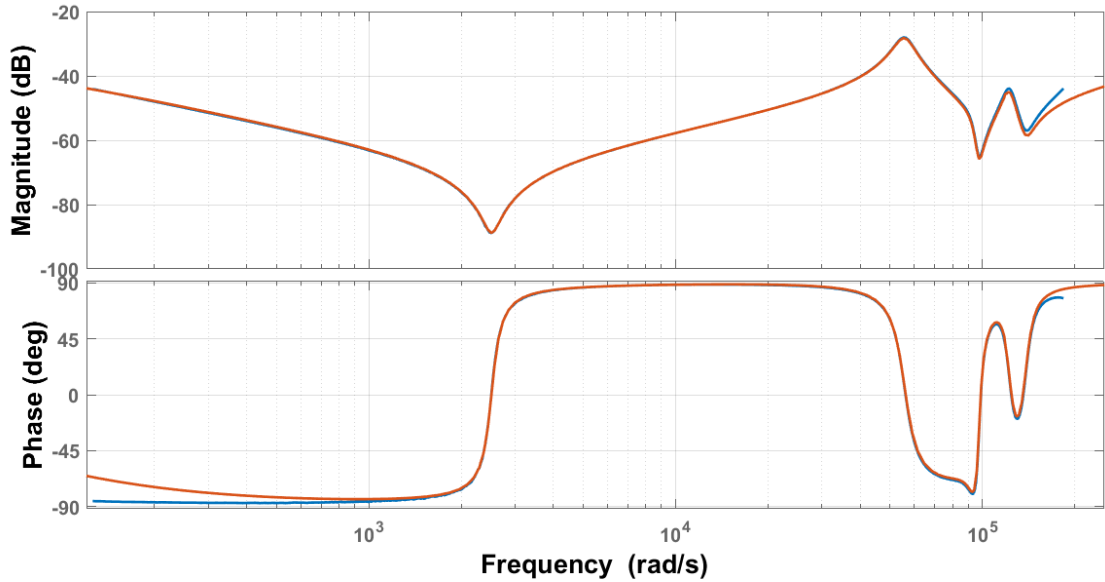


Figure 3.4: Estimated response (red) with original response (blue) in $20 \text{ Hz} - 29.2 \text{ kHz}$ ($125 \text{ rad/s} - 184 \text{ krad/s}$)

The range of consideration for the next iteration is obtained by adding first two bandwidths (20 Hz to 117 kHz). Original SFRA data of the power transformer were divided by $TF_{final-1}$ at the beginning of the iteration, as described in (3.26). Estimated transfer function after levy method is 22 order (both numerator and denominator) with RMS error of 0.0309. Inverse of RMS values for considered combinations were shown in .

After removing resonances outside the region, a transfer function of 18 order is obtained. (Two single zeros (at $2.1157 \times 10^7 \text{ rad/s}$ and $4.7804 \times 10^5 \text{ rad/s}$) with a double zero at $8.6944 \times 10^5 \text{ rad/s}$ are removed from the numerator and two single poles (at $1.2084 \times 10^7 \text{ rad/s}$ and $4.7669 \times 10^5 \text{ rad/s}$) with a double pole at $8.4649 \times 10^5 \text{ rad/s}$ are removed from the denominator results in decreasing the order

by a value of 4). As the previous occasion, this is taken as the final estimated transfer function as Sanathanan-Koerner method does not converge. Recalculated data for the second region with estimated transfer function for the region is shown in Figure 3.6. The transfer function in Laplace domain is shown in (3.26),(3.27) and (3.28) .

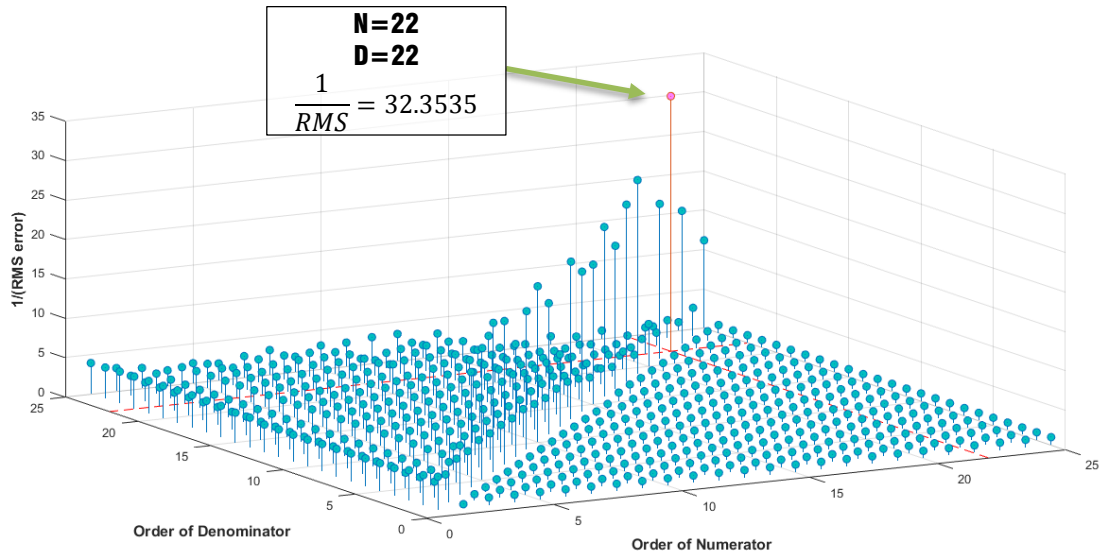


Figure 3.5: Inverse values of RMS errors for the numerator and denominator combinations of region 2

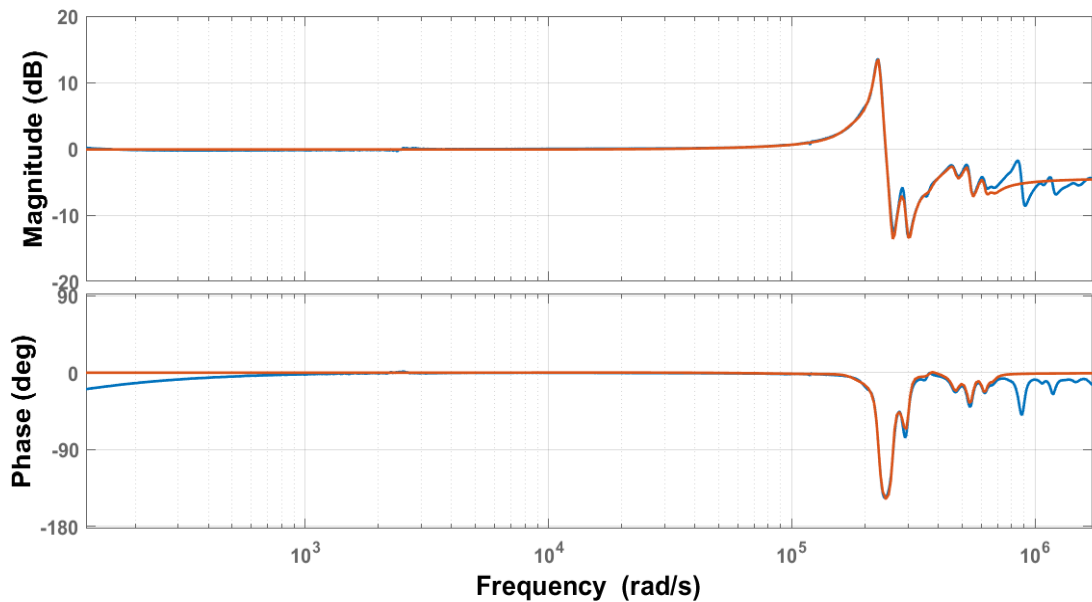


Figure 3.6: Estimated response (red) with reshaped response (blue) in 20 Hz to 117 kHz

$$TF_{final-2} = \frac{NumTF_{final-2}}{DenTF_{final-2}} \quad (3.30)$$

Where

$$\begin{aligned} NumTF_{final-2} &= 1.886 \times 10^{-100} s^{18} + 1.278 \times 10^{-94} s^{17} \\ &+ 3.494 \times 10^{-88} s^{16} + 2.068 \times 10^{-82} s^{15} \\ &+ 2.637 \times 10^{-76} s^{14} + 1.361 \times 10^{-70} s^{13} \\ &+ 1.054 \times 10^{-64} s^{12} + 4.711 \times 10^{-59} s^{11} \\ &+ 2.425 \times 10^{-53} s^{10} + 9.289 \times 10^{-48} s^9 \\ &+ 3.284 \times 10^{-42} s^8 + 1.057 \times 10^{-36} s^7 \\ &+ 2.566 \times 10^{-31} s^6 + 6.706 \times 10^{-26} s^5 \\ &+ 1.08 \times 10^{-20} s^4 + 2.134 \times 10^{-15} s^3 \\ &+ 2.056 \times 10^{-10} s^2 + 2.524 \times 10^{-05} s \\ &+ 0.9881 \end{aligned} \quad (3.31)$$

$$\begin{aligned} DenTF_{final-2} &= 3.159 \times 10^{-100} s^{18} + 2.074 \times 10^{-94} s^{17} \\ &+ 5.674 \times 10^{-88} s^{16} + 3.244 \times 10^{-82} s^{15} \\ &+ 4.137 \times 10^{-76} s^{14} + 2.053 \times 10^{-70} s^{13} \\ &+ 1.588 \times 10^{-64} s^{12} + 6.792 \times 10^{-59} s^{11} \\ &+ 3.485 \times 10^{-53} s^{10} + 1.269 \times 10^{-47} s^9 \\ &+ 4.454 \times 10^{-42} s^8 + 1.353 \times 10^{-36} s^7 \\ &+ 3.243 \times 10^{-31} s^6 + 7.938 \times 10^{-26} s^5 \\ &+ 1.256 \times 10^{-20} s^4 + 2.317e^{-15} s^3 \\ &+ 2.192 \times 10^{-10} s^2 + 2.539e^{-05} s + 1 \end{aligned} \quad (3.32)$$

To generate the next region's data for 117 kHz – 188 kHz range, original data were divided by product of transfer function, $TF_{final-1} \times TF_{final-2}$. Among the other combinations, a numerator of 11 order and a denominator of 11 order offers the minimum RMS error for Levy's method (RMS error is 0.03575). Considered combinations together with inverse RMS error values are shown in Figure 3.7.

By removing resonance points outside the region 3, a 10th order transfer function is resulted (Order reduction process eliminates a single zero at 1.7908×10^6 rad/s and a single pole at 2.0968×10^6 rad/s which decrease the order of estimated transfer function by one, in both numerator and denominator). In the next step, Sanathanan-Koerner method minimizes the error of the above result. Table 3.1 shows variation of error throughout the iterations where relative error in the considered

iteration compared to the previous iteration is calculated using the equation (3.33)

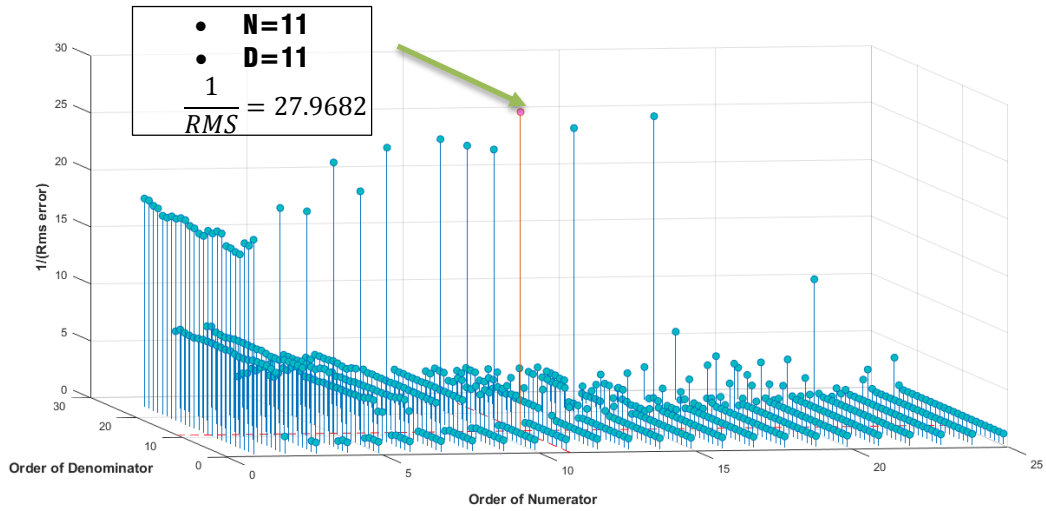


Figure 3.7: Inverse values of RMS errors for the numerator and denominator combinations of region 3

Relative error is used to depict stopping criteria, since RMS error variations are too small to be illustrated in a diagram.

$$Relative\ Rms_{error} = (Rms_{error})_i - (Rms_{error})_{i-1} \quad (3.33)$$

where $(Rms_{error})_i$ is the Rms error of i^{th} iteration

Table 3.1: Selection of best estimation in Sanathanan-Koerner method of proposed algorithm for region 3

	RMS error	Relative RMS error
<i>Initial approx. by Levy method</i>	0.03575485	
1	0.03411355	-1.64E-03
2	0.03360125	-5.12E-04
3	0.03354917	-5.21E-05
4	0.03353906	-1.01E-05
5	0.03353742	-1.64E-06
6	0.03353638	-1.04E-06
7	0.03353588	-4.96E-07
8	0.03353552	-3.63E-07
9	0.03353551	-7.53E-09
10	0.03353537	-1.38E-07
11	0.03353535	-2.23E-08
12	0.03353521	-1.39E-07
13	0.03353528	6.96E-08

14	0.03353524	-4.40E-08
15	0.03353522	-1.79E-08
16	0.03353527	5.08E-08
17	0.03353528	1.19E-08
18	0.03353521	-7.26E-08
19	0.03353523	1.97E-08
20	0.03353518	-4.96E-08

The negative coefficient of relative RMS error implies the error in the considered iteration is smaller compared to the previous one. Therefore iteration process in Sanathanan-Koerner has to be stopped at 12th iteration as error begins to diverge the results afterwards. Recalculated data for the third region with estimated transfer function for the region is shown in Figure 3.8. The transfer function in Laplace domain is shown in (3.34),(3.35) and (3.36).

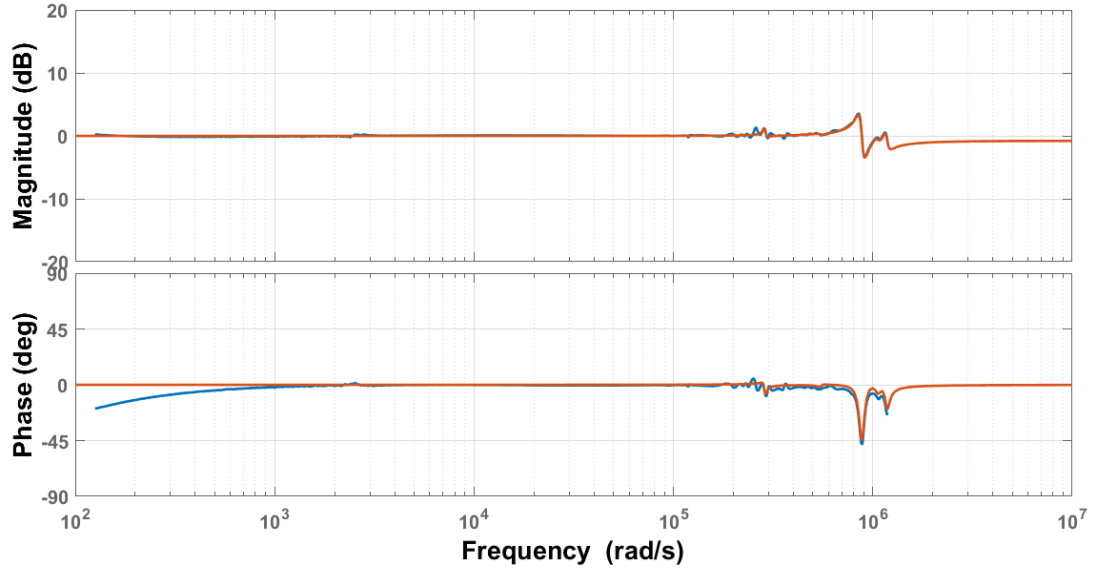


Figure 3.8: Estimated response (red) with Reshaped response (blue) in 20 Hz to 188 kHz

$$TF_{final-3} = \frac{NumTF_{final-3}}{DenTF_{final-3}} \quad (3.34)$$

Where

$$\begin{aligned} NumTF_{final-3} = & 3.283 \times 10^{-59} s^{10} + 8.877 \times 10^{-54} s^9 \\ & + 1.218 \times 10^{-46} s^8 + 2.369 \times 10^{-41} s^7 \\ & + 1.601 \times 10^{-34} s^6 + 2 \times 10^{-29} s^5 \\ & + 8.834 \times 10^{-23} s^4 + 5.746 \times 10^{-18} s^3 \\ & + 1.842 \times 10^{-11} s^2 + 4.186 \times 10^{-07} s + 1 \end{aligned} \quad (3.35)$$

$$\begin{aligned}
DenTF_{final-3} = & 3.593 \times 10^{-59} s^{10} + 9.065 \times 10^{-54} s^9 \\
& + 1.303 \times 10^{-46} s^8 + 2.382 \times 10^{-41} s^7 \\
& + 1.673 \times 10^{-34} s^6 + 1.979 \times 10^{-29} s^5 \\
& + 9.028 \times 10^{-23} s^4 + 5.609 \times 10^{-18} s^3 \\
& + 1.855 \times 10^{-11} s^2 + 3.993 \times 10^{-07} s + 1
\end{aligned} \tag{3.36}$$

The corresponding transfer function for the final region (20 Hz to 2 MHz) is generated by means of dividing actual measured SFRA response data by $TF_{final-1} \times TF_{final-2} \times TF_{final-3}$. Considered combinations for numerator and denominator orders are shown in Figure 3.9. The minimum RMS error is resulted as 0.0437 (corresponding inverse RMS error is 22.8833), when the orders of numerator and denominator are both are 15. But the results does not agree with the Routh-Hurwitz stability criterion (Explained in 3.3) as all coefficients of the denominator are not in the same sign. Best possible combination that gives the minimum RMS error while satisfying Routh-Hurwitz criterion is the transfer function of 11th order numerator and denominator.

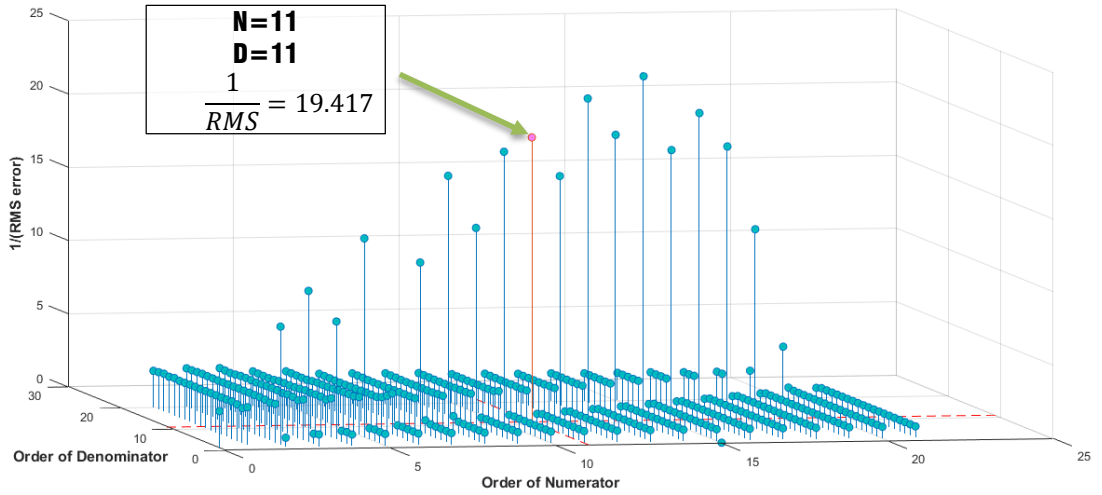


Figure 3.9: Inverse values of RMS errors for the numerator and denominator combinations of region 4

As the algorithm suggests, transfer function obtained from the above step is directly fed to the next step in this final region. In this next step, Sanathanan-Koerner method is used to improve the results where RMS error is minimized to 35.2268 from 4

iterations as shown in Table 3.2. Same stopping criterion as the previous region is used to select the best estimation (Relative error become positive in 5th iteration and start to diverge the results. Hence Sanathanan-Koerner method is terminated after 4 iterations)

Table 3.2: Selection of best estimation in Sanathanan-Koerner method of proposed algorithm for region 4

	RMS error	Relative RMS error
<i>Initial approx. by Levy method</i>	0.05150547	
1	0.04766983	-3.84E-03
2	0.04737200	-2.98E-04
3	0.04584650	-1.53E-03
4	0.04438072	-1.47E-03
5	0.04515372	7.73E-04
6	0.04590020	7.46E-04
7	0.04574370	-1.57E-04
8	0.04500583	-7.38E-04
9	0.04491769	-8.81E-05
10	0.04528567	3.68E-04

Recalculated data for the final region with estimated transfer function for the region is shown in Figure 3.10. The transfer function in Laplace domain is shown in (3.37), (3.38) and (3.39).

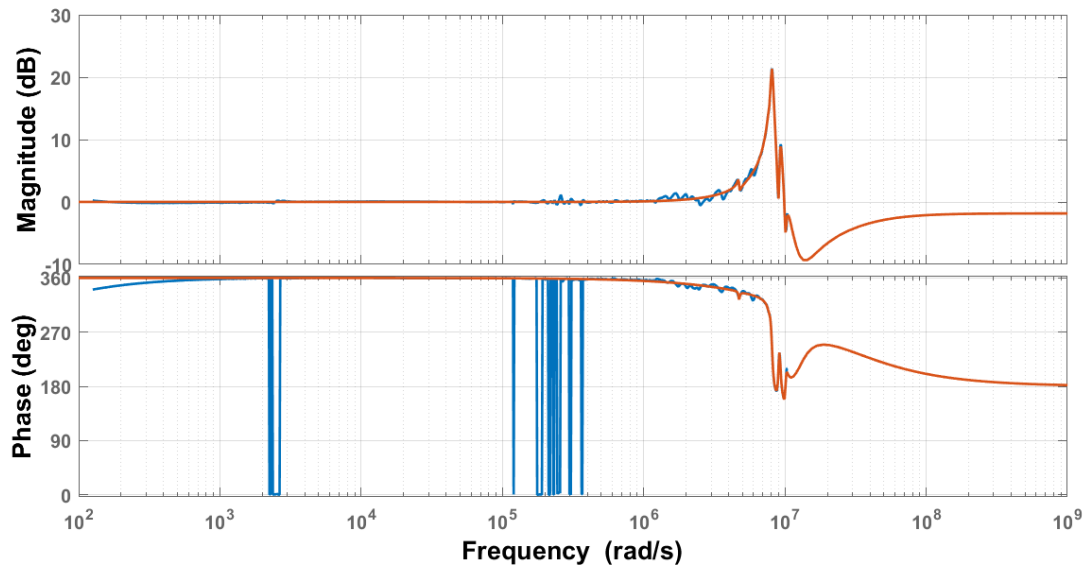


Figure 3.10: Estimated response (red) with reshaped response (blue) in 20 Hz to 2 MHz

$$TF_{final-4} = \frac{NumTF_{final-4}}{DenTF_{final-4}} \quad (3.37)$$

Where

$$\begin{aligned} NumTF_{final-4} = & -1.38 \times 10^{-76} s^{11} + 1.194 \times 10^{-69} s^{10} \\ & - 4.798 \times 10^{-62} s^9 + 5.153 \times 10^{-55} s^8 \\ & - 6.059 \times 10^{-48} s^7 + 7.697 \times 10^{-41} s^6 \\ & - 3.359 \times 10^{-34} s^5 + 4.904 \times 10^{-27} s^4 \\ & - 7.714 \times 10^{-21} s^3 + 1.27 \times 10^{-13} s^2 \\ & - 5.385 \times 10^{-08} s + 1.003 \end{aligned} \quad (3.38)$$

$$\begin{aligned} DenTF_{final-4} = & 4.997 \times 10^{-77} s^{11} + 3.479 \times 10^{-69} s^{10} \\ & + 2.032 \times 10^{-62} s^9 + 1.059 \times 10^{-54} s^8 \\ & + 2.888 \times 10^{-48} s^7 + 1.197 \times 10^{-40} s^6 \\ & + 1.793 \times 10^{-34} s^5 + 6.133 \times 10^{-27} s^4 \\ & + 4.748 \times 10^{-21} s^3 + 1.371 \times 10^{-13} s^2 \\ & + 4.113 \times 10^{-08} s + 1 \end{aligned} \quad (3.39)$$

Even though estimated transfer function for the final region ($TF_{final-4}$) satisfies Routh-Hurwitz stability criterion, estimated numerator has negative coefficients. This is because, influences of the measurement system such as interaction between measurement connections and grounding leads effect the frequency response other than the power transformer itself [4, 18]. Final estimated transfer function of the power transformer is the product of each individual transfer functions i.e. $TF_{final-1} \times TF_{final-2} \times TF_{final-3} \times TF_{final-4}$. Measured SFRA response and final estimated transfer function are shown in Figure 3.11.

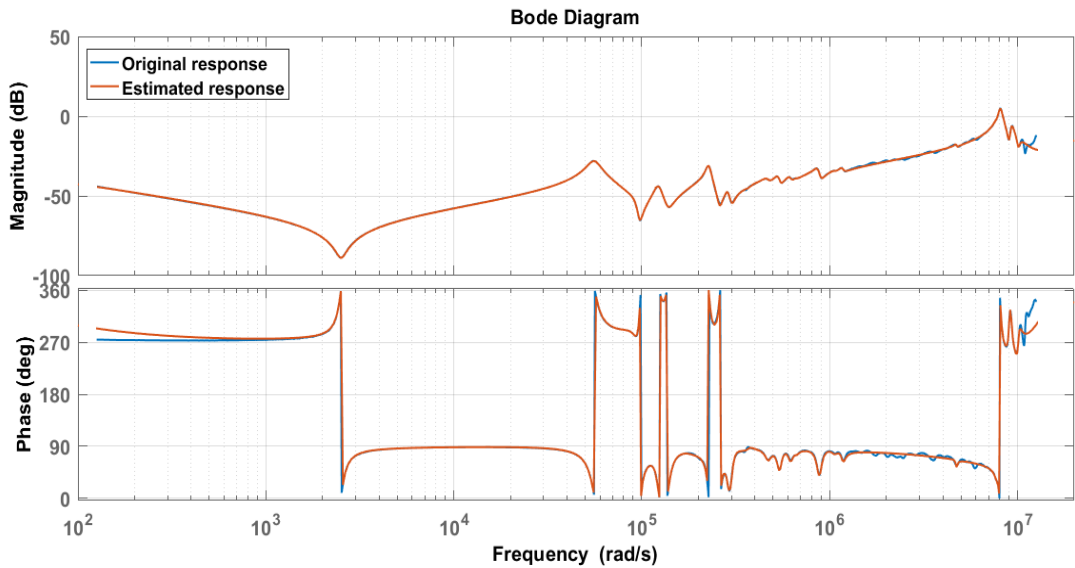


Figure 3.11: Estimated response (red) with original SFRA data (blue) in 20 Hz to 2 MHz

To validate the results, error graphs can be used as follows. Figure 3.12 shows the relative error (%) with respect to original and evaluated responses (relative error is the percentage ratio of the estimated and original response differences to its original response i.e. $\frac{\text{estimated transfer fcn}-\text{original response}}{\text{original response}} \times 100\%$)

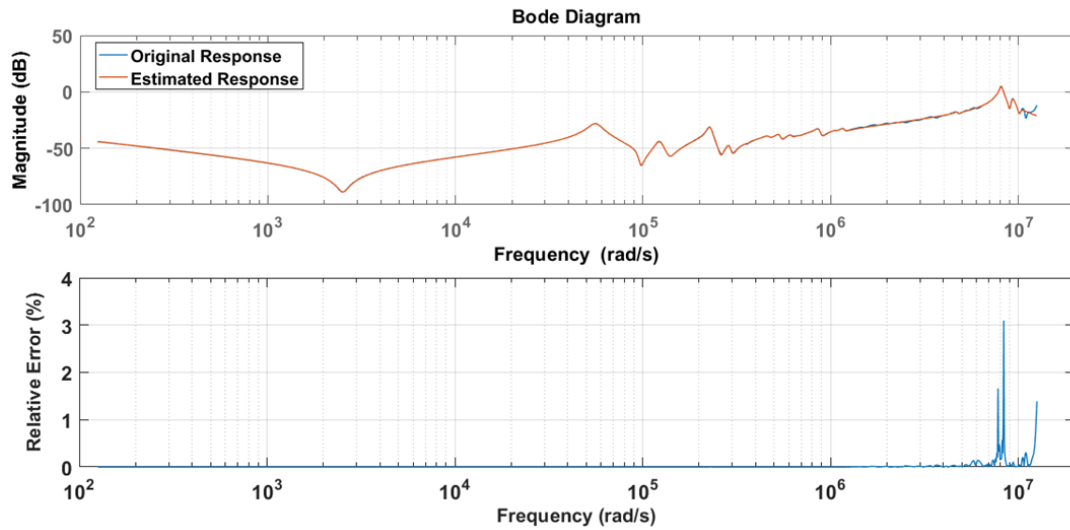


Figure 3.12: Relative error of estimated response with respect to SFRA

Comparing the estimated and measured SFRA response results, it can be seen that the accuracy of the model at lower frequencies is much higher than higher frequencies (Error throughout all frequencies, except in the final frequency range is almost zero. Maximum error is 3% recorded at near 10Mrad/s). Resultant error is caused by two reasons.

Measured SFRA data used for the modelling are in logarithmic scale which makes the error in high frequency range larger than low frequencies (because, in the logarithmic scale, the number of data points in the high frequency range is lesser compared to the lower frequencies). This is an inherent error of this kind of estimation where response varies more than six decades (decade is a 10-times increase in frequency). This can be minimized by using SFRA data measured in linear scale, especially in the high frequency range.

The Second reason is unavailability of data outside the considered region. Note

that available range of the frequency response data is determined by the frequency generator of the SFRA device ($20\text{ Hz} - 2\text{ MHz}$ or $1.25\text{ rad/s} - 12.5\text{ Mrad/s}$). Poles and zeroes which might exist outside the measured region effect its nearby regions resulting a higher error in the end frequencies. To overcome this issue, a SFRA device with a wider frequency range can be used. However, the current range can be considered as the optimum range for the measurement of power transformer. Because if the frequency is increased above 2 MHz , the effect of the transformer is repressed by the external factors such as grounding and measurement connections.

Corresponding MATLAB codes for Levy estimation is shown in the APPENDIX A. For Sanathanan-Koerner method, the same code is iteratively used by substituting denominator from the previous iteration, explained under subsection 3.2.2.

3.6 Conclusions

This chapter presents a novel algorithm to convert SFRA data into the transfer function in Laplace domain, based on Levy and Sanathanan-Koerner methods. All the steps are described in detail, together with the equations derived using the Levy and Sanathanan-Koerner methods.

RMS error between measured and actual responses are used to ascertain the best combination of poles and zeros at each iteration. However, the combination that gives minimum RMS error is not always realizable. The realisability can be determined by Routh-Hurwitz test. Usually, in the low frequency region where few resonance points are present, the combination that gives minimum RMS error will always be realisable. But in high frequencies, the combination that gives minimum RMS error is not always realizable due to the effect of external factors such as grounding and measurement connections. Therefore, performing Routh-Hurwitz test is not compulsory for the transfer functions corresponding to low frequencies of SFRA.

It can be deduced that the proposed method can be incorporated to estimate the transfer function of power transformer as a single quantity with more accuracy whereas

Levy's and Sanathanan-Koerner methods alone fail to implement. As an estimation for the whole bandwidth is derived using this proposed algorithm, results can be used in synthesizing the lumped parameter equivalent circuit model of the power transformer to represent its complete SFRA region.

Chapter 4

MODELLING TRANSFORMER EQUIVALENT CIRCUIT

4.1 Introduction

Simple and analytical methods available in the literature of circuit theory for the circuit realization of power transformer have been utilized for decades by researchers. Their limitations and existing problems have been discussed in detail in Chapter 2 section 2.5. It is noteworthy that some of these methods give better approximations for transformer equivalent circuit, but still they cannot be incorporated into online condition monitoring as they require additional measured parameters that are unavailable at hand. The proposed method in this chapter for circuit realization that uses a transfer function to implement the lumped circuit model offers a solution for this problem with reasonable accuracy.

After the transfer function estimation of a transformer is derived, it can be used to synthesise the equivalent circuit using passive components, as explained in the step 2 in Figure 2.7. Among the other methods of circuit realization, Lumped parameter network modelling is selected in this study. This is one of the Gray-box modelling types that gives reasonable accuracy with other advantages such as localization of faults. In this chapter, component values of lumped parameter network are calculated using genetic algorithm (GA) and artificial neural network (ANN) based approach. These models enable to study various types of deformations and analyse the sensitivity of SFRA for different fault types.

4.2 Lumped parameter network

Lumping several turns into a single element reduces the complexity of the final model [46]. Transformer modelling as individual turn to turn requires excessive computation as it is unnecessarily complex. In reality, this is not a requirement as parameters of a transformer are distributed in nature. Even though each turn has its own electric/magnetic characteristics such as resistances, inductances/ capacitances

and losses, effects of the individual parameters merge when the final output response is generated. Therefore equivalent circuit can be approximated as a lumped circuit model that gives an intrinsic combined response of adjacent turns. Figure 4.1 shows the lumped parameter circuit model used for the modelling of a power transformer.

According to the illustration, the section containing passive elements shown in the highlighted area represents a basic section. These basic sections are connected in series to form the lumped equivalent circuit. At lower frequencies, resistance and inductance dominate the frequency response while effects of the capacitances are significant at high frequencies.

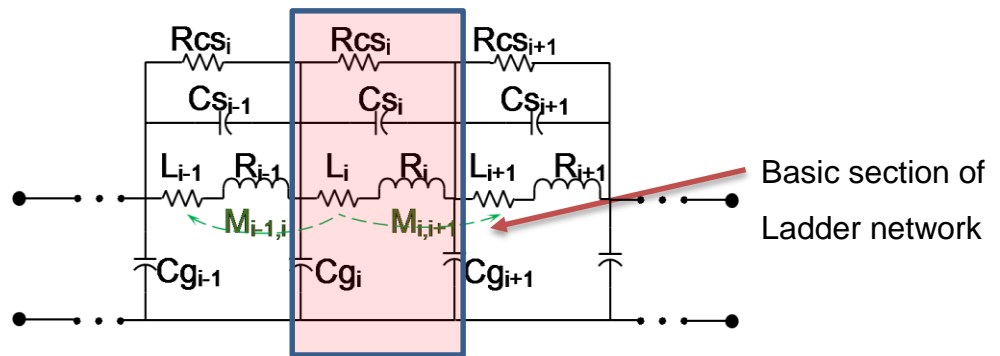


Figure 4.1: Lumped parameter network model

Where

- R_i - Winding resistance of section
- L_i - Winding self-inductance of section
- C_s_i - Winding series capacitance of section
- C_g_i - Ground capacitance of section
- $R_c s_i$ - Parallel insulation resistance of section
- $M_{i,j}$ - Mutual inductance between i^{th} and j^{th} section

R_i represents the internal resistance of i^{th} section that causes the copper losses of the winding section. $R_c s_i$ represents resistance of the insulation between two sections i.e. it gives the equivalent resistance of surrounding oil and pressboard/ paper insulation system. Self-inductance (L_i) that represents flux leakage is considered to be linear. M_{ij} is the mutual inductance which represents flux linkage between i^{th} and j^{th} winding segments. Usually, in power transformers, resistance values are larger compared to the inductances while the self-inductances always being the larger one

than mutual inductance values. Capacitances of a lumped section are two types: Winding series capacitances (Cs_i) and ground capacitances (Cg_i). Series capacitance of winding is a combination of capacitances due to inter disk and inter winding turns whereas Shunt capacitance is the equivalent resultant capacitance caused by insulation between ground to disk sections.

4.3 Algorithms and methods used for conversion of transfer function to Lumped parameter network model

Analytical methods cannot be employed to estimate parameter values of the lumped equivalent circuit. For an instant, if transfer function equations are written in Laplace domain, number of equations obtained by comparing derived transfer function would be insufficient to find all the unknowns. Hence, alternative method/s that allows an easy and efficient computation should be used in circuit modelling. A unified approach that incorporates artificial neural network (ANN) and Genetic algorithm (GA) methods has been used to determine unknown parameter values of the lumped equivalent circuit.

4.3.1 Artificial neural network (ANN)

An artificial neural network (ANN) is a computational model with information processing structure which is inspired by the brain's biological nervous system [47]. Every information passes through ANN define its structure as ANN learns or in other words it changes its behaviour according to inputs and outputs like a human brain. This is used as a modelling tool that discovers complex relationships or patterns between inputs and outputs of nonlinear statistical data.

Among various advantages of ANN, the ability to learn from input data has made this technique very promising in the modern world. Therefore ANN can be used as a tool to estimate random functions while providing an easy and effective way to estimate its solutions. ANN process data samples instead of the whole data set that helps in saving computational time.

Structure of ANN can be explained as follows. The basic Structure of ANN has three layers namely input layer, output layer and hidden layer. In the hidden layer, a large number of highly interconnected nodes exist that work together to relate elements of the input layer to the output layer called “neurons”. Figure 4.2 shows the basic structure of a simple multilayer feed-forward ANN.

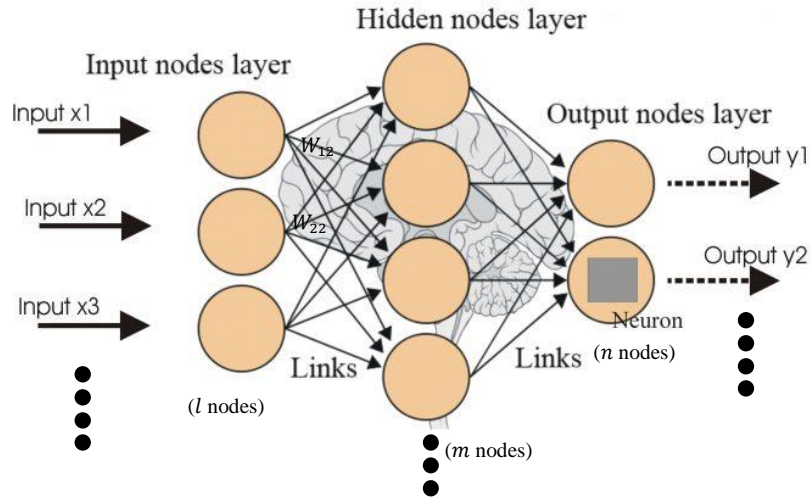


Figure 4.2: Basic structure of ANN

The training process of ANN involves use of a known data set. As illustrated by the figure above, input layer (consisting l nodes) is mapped to the output layer (consisting n nodes) via hidden layer (consisting m nodes). As suggested in the research, numerator and denominator coefficients of the transfer function obtained using novel algorithm proposed in Chapter 3, are used as input neurons of ANN whereas output neurons of ANN are parameter values of the lumped equivalent circuit.

The relationship of output variables (y_i) represented using input variables (x_i) with weightings are shown by (4.1) and (4.2). Here, w_{ij} represent weight or the extent of influence of i^{th} input neuron and j^{th} hidden layer neuron whereas w_{jk} represent weight of j^{th} hidden layer neuron and k^{th} input neuron.

$$Hidden\ layer\ node\ h_i = \sum_{i=1}^{l+1} w_{ij} x_i \quad (4.1)$$

where $i = 1, 2, \dots, l$ & $j = 1, 2, \dots, m$

$$\text{Output layer node } y_k = \sum_{j=1}^{m+1} w_{jk} h_j \quad (4.2)$$

where $k = 1, 2, \dots, n$ & $j = 1, 2, \dots, m$

To train ANN, several model types can be used that associate different algorithms such as back-propagation algorithm, Levenberg-Marquardt etc. [48]. Considering the type of problem, pattern recognition (discriminant analysis) has to be used instead of function approximation (regression). User needs to change the number of hidden layer nodes for a given set of input and output data and select the number of neurons that gives the minimum error for its estimation.

Several attempts can be seen to identify parameters of transformer circuit using neural network method. For example, M. A. Eldery et al. [33] have used ANN to estimate sectionalized parameters of single winding transformer and G. M. V. Zambrano et al. [34] have used ANN to estimate the transfer function of power transformer. For all these attempts, a supervised training is necessary to update weights of ANN and in [33] even an initial guess of parameters are required. This is one of the shortcomings of neural networks in parameter estimation of power transformers where the process become complex due to large number of outputs (Values of model elements are the outputs of ANN that becomes larger in number when the number of sections are high). Another drawback of this method is, a large set of data samples are required to obtain an accurate estimation of parameters which will increase the estimation time significantly. As a solution, integration of neural networks with genetic algorithm is proposed under this research.

4.3.2 Genetic algorithm (GA)

Genetic algorithm is a technique used in solving nonlinear systems and complex optimizing problems [30, 36]. This is inspired by the biological process called natural selection where stronger individuals among a group of species survive in a competing environment [36]. Compared with other traditional numerical methods, genetic algorithm is more attractive as it is very effective in reaching the global optimum owing to the stochastic nature of the process.

GA Presumes that the solution is a single element represented by a set of parameters which are called “genes” of a chromosome. These can be represented by binary or string form. These chromosomes are evaluated using “fitness function” that shows the degree of “goodness” of the considered chromosome in solving problem. Throughout its evolution, the fitting chromosome tends to produce a better offspring i.e. better solution as the output.

In the considered problem of parameter estimation of power transformer, population pool of chromosomes has to be defined within the possible range of values. For example winding resistances should be within the ohm range. In every cycle, the current population chromosomes called “parents” produce next-generation called “offspring”. The process called as “evolution” where genes of parent chromosome mixed and recombined to give offspring. In fact, chromosomes that give a better result will produce a large number of offspring which has more chance of surviving in the subsequent regions. In the case power transformer, combination that gives a better solution for the parameters of equivalent circuit will produce more estimations in the subsequent generations. As a result, the solution converges to the optimum parameter estimation (global minimum).

Two operators can be identified that facilitate the evolution of GA: Crossover operator and Mutation operator. Crossover operator produces offspring by exchanging information of parent individual chromosomes [30]. crossover point can be set by the user where two chromosomes beyond a cut-off point will be exchanged producing an offspring. The default value for the probability of crossover is 0.8. Mutation process is exercised after crossover operation is performed. Mutation operator changes a randomly select bit of resulted offspring of crossover. The way of generating offspring during crossover and mutation is shown in following Figure 4.3, using an example.

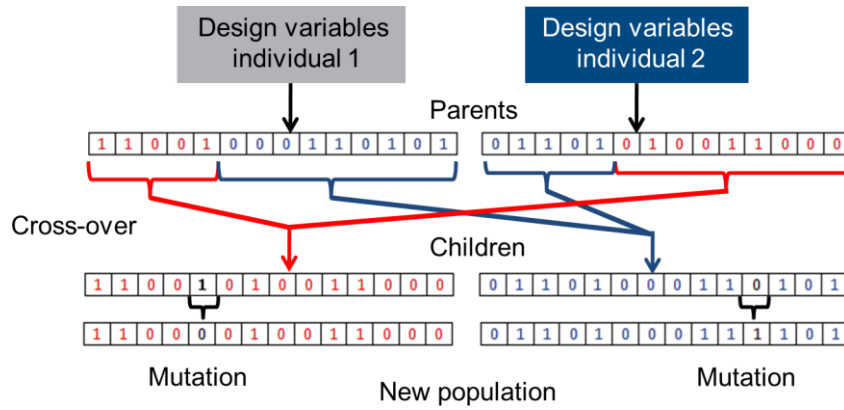


Figure 4.3: Bit-String Crossover followed by bit flipping mutation

Apart from these two operators, selection strategy chooses individuals from the pool of parents that contribute to the population in the next generation [49]. This cycle of crossover, mutation and selection is repeated until one of stopping criteria is reached or optimization objective is achieved.

4.4 Proposed method of parameter estimation of lumped equivalent circuit

An integrated approach of ANN and GA to estimate parameter values of the elements in lumped equivalent circuit is presented in Figure 4.4. However, Transfer function derived using the novel algorithm proposed under Chapter 3 cannot be used directly in this process. This is because, even though the algorithm can be used to estimate the transfer function with whole SFRA range, the frequency response of power transformer does not replicate power transformer over its entire measured frequency range. Especially, the high frequency range ($> 1 \text{ MHz}$), measurement setup influences such as interaction between measurement connection and ground leads dominate the frequency response [4, 18]. Hence order reduction of transfer function has to be done by eliminating high frequency resonances. Steps of parameter estimation of lumped parameter network is shown in Figure 4.4 as a flow chart.

At high frequencies, an increasing trend of amplitude can be observed without major resonance points in SFRA response. This is resulted by the domination of capacitances of power transformer at high frequencies (as shown in Figure 3.2 in which positive slope exists in magnitude plot after 1MHz). Moreover, zero crossing points in

the phase plot cannot be observed after this range implying the key resonance points do not exist afterwards. Therefore during the modelling of power transformer, usage of major frequencies which have zero crossing points in the phase plot will give a reasonably accurate transformer model while reducing the its complexity. Therefore order reduction of transfer function can be achieved by estimating resonances up to 1MHz, not whole SFRA response. In case, if the algorithm has already employed in transfer function estimation, eliminating poles and zeros higher than 1MHz will give order reduced transfer function. It should be noted that the gain of magnitude plot should settle at 0 dB after order reduction due to the capacitive behaviour of lumped network (Order reduction process is explained further in case study of the latter part of this chapter).

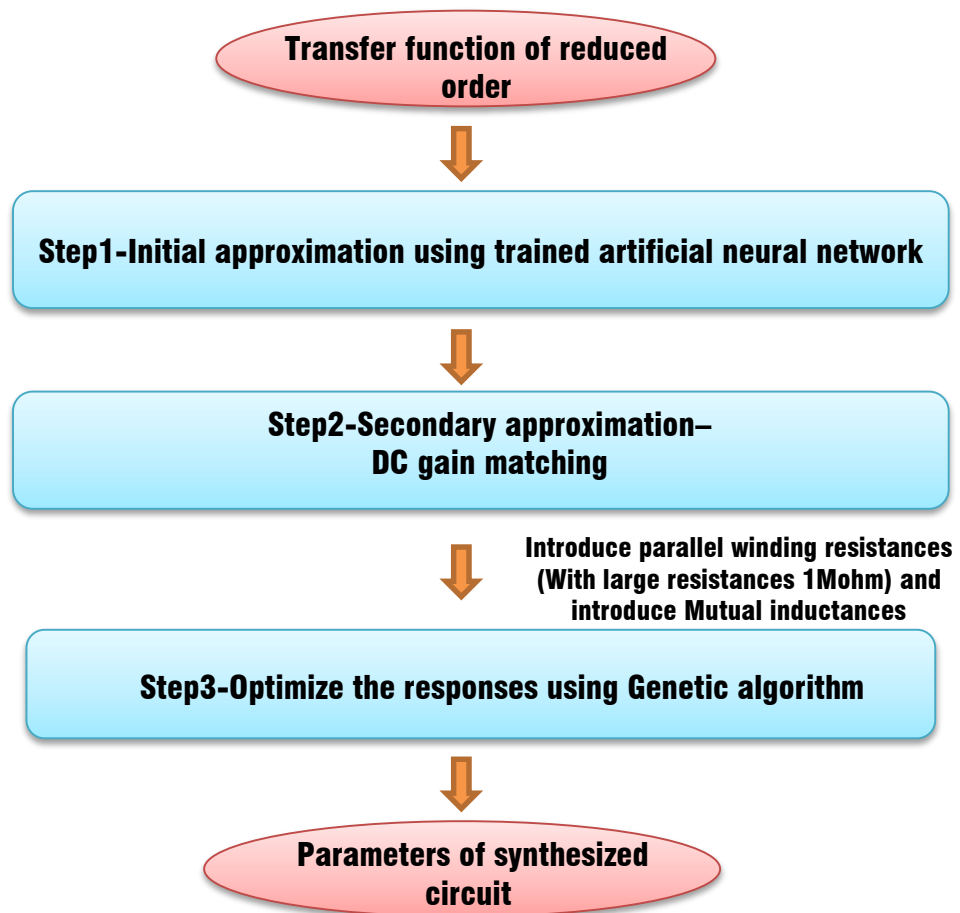


Figure 4.4: Steps of parameter estimation

As above figure depicts, order reduced transfer function has to be inserted to the system which will be used by the trained ANN to find an initial approximation for the parameter values. Details of each step are given in the following subsections.

4.4.1 Initial approximation using ANN (step 1)

DC gain (i.e. gain at zero frequency) of the SFRA response is dominated by the resistance values. Because at zero frequency, the impedance of inductors which are connected in series becomes zero and impedance of capacitances connected in parallel becomes infinite (see Figure 4.1). Furthermore, as Winding resistance of sections (R_i) is smaller compared to Parallel insulation resistance of sections (Rcs_i), winding resistance of sections (R_i) has more impact on DC gain of the frequency response (This is because, during SFRA, output response is measured across 50Ω resistance which is effectively connected in parallel with insulation resistance of sections (Rcs_i), usually mega ohm range. Therefore, equivalent value of DC gain resistance is dominated by 50Ω [50]. More importantly, resistances do not define resonance frequency, whereas they decides the magnitude of resonances [24]. Therefore ANN network which has been trained using 10000 data samples (excluding parallel resistances (Rcs_i) and mutual inductances (M_{ij})) is used to generate the initial approximation for the genetic algorithm. The reason to exclude these parameters in the initial approximation is to reduce the complexity of ANN being modelled. Since the estimation error increases with the number of outputs, least possible components are used to derive initial approximation.

MATLAB Simulink model is used to derive samples for the training process. Firstly, random values for each parameter are generated using computer within their specific ranges which were based on actual parameter ranges according to [50, 51].

Table 4.1: Ranges of randomly generated data for parameters

Component name	Min value	Max value
Resistance	1Ω	1000Ω
Inductance	$1 mH$	$100 H$
Capacitances	$1 pF$	$1 \mu F$

Each sample includes all resistor, capacitor and inductance values for corresponding n section equivalent circuit. By feeding this randomly generated parameter values to the modelled equivalent circuit in MATLAB, corresponding 10000 transfer functions are obtained. It should be noted that the number of sections are determined by the order of the transfer function to be synthesized. In fact, the number of sections should be equal to half of the order of transfer function. As a result, several ANN networks has to be trained in advanced, depending on the order of resultant order-reduced transfer function. (Generally, the order of the power transformer's transfer function in healthy condition would be 12 to 16. Hence the number of sections to be used is a value between 6 to 8).

Inputs of the trained ANN should be the numerator and denominator coefficients whereas outputs being the corresponding parameter values. Hence, the initial approximation can be obtained by giving the numerator and denominator coefficients of actual order reduced-transfer function to the trained ANN. There can be slight variations in resonance locations as mutual inductances (M_{ij}) are not included in the model in this stage. Due to the exclusion of parallel resistances, DC gain is not matched with the actual response even magnitudes at the responses are properly modelled.

4.4.2 Secondary approximation –DC gain matching (step 2)

In this step, DC gain (gain at zero frequency) is rectified by changing the winding resistance of sections (R_i) of resultant output. Equivalent resistance value ($\sum R_i$) that gives corresponding actual DC gain is obtained by the following equation.

$$DC\ gain = 20\log\left(\frac{50}{\sum R_i + 50}\right) \quad (4.3)$$

DC gain should be calculated by substituting Laplace operator (s) of order-reduced transfer function with zero. Using this DC gain and (4.3), the equivalent series resistance ($\sum R_i$) is derived afterwards. Then, the resistance values obtained from the previous step is altered proportionally to match this DC gain. The output of this step is a response that has a DC gain identical to the actual response with variations in

resonance amplitudes.

4.4.3 Optimization of responses using Genetic algorithm (step 3)

After DC gain is matched, estimated parameters are applied as the initial approximation of genetic algorithm (GA). The excluded parameters (parallel resistances(Rcs_i) and mutual inductances(M_{ij})) are also included in the modelled circuit used in the optimization. MATLAB Simulink and MATLAB GA tool integrated method is used where in each iteration of GA, MATLAB Simulink model is executed which returns corresponding response of the parameters to GA. Input parameters of GA are selected as follows.

Table 4.2: Input parameters of GA

Options	Value/function name
Population	Double vector
Initial population	Results of ANN
Fitness function	(@fit_fcn)
Constraint function	(@constraint_fcn)
Selection	Tournament
reproduction	0.8
Crossover	Intermediate
Mutation	Constraint dependent
Stopping criteria	Generations:100*number of variables Function tolerance:1e-4 Constraint tolerance:1e-3

“Tournament function” is used as the selection function that selects two parents at random and choose the best individual out of those to be a parent. Reproduction term determines, how GA creates offspring in the next generation. The factor 0.8 is the crossover factor which is the fraction of parents used for the crossover operation and the rest is used by mutation function. As explained earlier in this chapter, crossover function combines two individuals where the selected “intermediate” option creates offspring by a random weighted average of the parents. For the mutation, a function

called “Constraint dependent” is used. This randomly generates directions that are adaptive with respect to the last successful or unsuccessful generation [52].

The most important subject of implementation of GA is its objective and constraints which have to be defined by the user as two separate scripts (MATLAB codes) for the algorithm. The objective function is denoted as “*fit_fcn*” and constraint function is denoted as “*constraint_fcn*”. The pseudo codes of these functions are expressed in Figure 4.5 and Figure 4.6.

```

Load Tf_ori;           //Load Transfer function (order reduced)
Convert chromosome to parameters;
Load Li;           // Li is ith section self inductance
Load Mp,q;       // Mp,q is mutual inductance b/w pth and qth sections
C(x) = Mi,i+1 - min(Li, Li+1); // mutual inductance < self-inductance
C(x) = Mp,q - min(Mp,q-1 - Mp+1,q); // Condition :Mutual inductance
                                         reduces with distance

Run Simulink model;
Tf_model;             //calculate model transfer function
Ceq(x) = order(numerator of Tf_ori) - order(numerator of Tf_model);

```

Figure 4.5: Pseudo code of constraint function “*constraint_fcn*”.

```

Load Tf_ori;           //Load Transfer function (order reduced)
Convert chromosome to parameters;
Run Simulink model;
Tf_model;             //calculate model transfer function
IF constraints satisfy
    Fitt_val = abs(20log(Tf_ori) - 20log(Tf_model)); // calculate
                                                    fitness value
ELSE
    Fitt_val = 1e12;
ENDIF

```

Figure 4.6: Pseudo code of objective function “*fit_fcn*”

Figure 4.5 illustrates the way of evaluating constraints of GA. Once crossover and mutation operators generate an offspring, it has to be checked by “*constraint_fcn*”. In each occasion, order-reduced transfer function is loaded to the function (Because in MATLAB, any variable used by a function should have been

defined inside the function).

Once chromosome is converted to parameters, constraint values have to be calculated. Two types of constraints are used inside the “*constraint_fcn*”, named as linear and non-linear constraints.

- Nonlinear constraint $c(x)$:

The Nonlinear constraint has the form of $c(x) \leq 0$, where $c(x)$ is the vector containing all the individual nonlinear constraints. Two types of nonlinear inequalities are defined inside the pseudo code:

- (i) mutual inductances between any couple of winding sections should be smaller than their self-inductances ($M_{i,i+1} - \min(L_i, L_{i+1}) \leq 0$)
- (ii) mutual inductance value should become smaller with the distance along the winding ($M_{p,q} - \min(M_{p,q-1}, M_{p+1,q}) \leq 0$)

- Linear constraint $C_{eq}(x)$:

The Nonlinear equality constraints are of the form $c_{eq}(x) = 0$, where $c_{eq}(x)$ is the vector containing all the individual linear constraints. “Order of the transfer function estimated by GA being equal to order of the order-reduced transfer function” is the linear constraint applied here.

As Figure 4.6, order-reduced transfer function has to be recalled again in the “*fit_fcn*”. Thereafter, by executing the n -sectional Simulink model of power transformer, the frequency response is obtained. If resulted transfer function satisfy the conditions given by “*constraint_fcn*”, the fitness value is calculated as gain difference of the resultant and order-reduced transfer function (this is the logarithmic difference shown in the Pseudo code). If constraints are not satisfied, the fitness value is replaced by a large number, in this case, $1e12$. Objective of the whole process is to reduce the estimated error i.e. reduce the value of fitness function. To ensure the fact that GA optimize while satisfying its conditions, a very large value is assigned for the fitness value whenever conditions are not satisfied. Corresponding MATLAB codes of “*constraint_fcn*” and “*fit_fcn*” are shown in the APPENDIX B and C, respectively.

4.5 Case study and method validation

The proposed method to estimate parameters of lumped equivalent circuit is illustrated using same SFRA response used in section 3.5 where the open-circuit response of H.V middle phase (usually referred as phase Y) has been selected. Already, this graphical information has been converted into the transfer function in Laplace domain using the novel algorithm proposed under the previous chapter.

As the first step of parameter estimation, the estimated transfer function in section 3.5 is simplified by removing high frequency resonances retaining the resonances with zero crossings in the phase response. The estimated transfer function ($TF_{final-1} \times TF_{final-2} \times TF_{final-3} \times TF_{final-4}$) had a numerator of 54 order and a denominator of 53 order. Removal of high frequency poles and zeros has reduced it to 12th order numerator and 11th order denominator. By adding a zero at very high frequency ($4.35e07 \text{ rad/s}$), the magnitude at high frequencies are made to approach 0 DB, which increase order of denominator by one (resultant order-reduced transfer function has of 12th order numerator and denominator).

Transfer function after order-reduction is shown in (4.4). Corresponding poles and zeros are shown in Table 4.3. Note that resultant poles and zeros have negative real coefficients. Therefore the order-reduced transfer function is regarded as realizable since it complies with Routh-Hurwitz stability criterion (see subsection 3.3)

$$\begin{aligned}
 & \text{Transfer function after order reduction} = \\
 & \left(\begin{array}{l}
 2.293 \times 10^{46} s^{12} + 1.671 \times 10^{51} s^{11} + 4.532 \times 10^{57} s^{10} \\
 + 2.539 \times 10^{62} s^9 + 2.93 \times 10^{68} s^8 + 1.175 \times 10^{73} s^7 \\
 + 7.164 \times 10^{78} s^6 + 1.857 \times 10^{83} s^5 + 7.09 \times 10^{88} s^4 \\
 + 9.143 \times 10^{92} s^3 + 2.432 \times 10^{98} s^2 \\
 + 7.104 \times 10^{100} s + 1.53 \times 10^{105} \\
 \hline
 2.293 \times 10^{46} s^{12} + 9.995 \times 10^{53} s^{11} + 6.412 \times 10^{58} s^{10} \\
 + 1.621 \times 10^{65} s^9 + 7.623 \times 10^{69} s^8 + 8.161 \times 10^{75} s^7 \\
 + 2.711 \times 10^{80} s^6 + 1.446 \times 10^{86} s^5 + 3.043 \times 10^{90} s^4 + \\
 + 9.404 \times 10^{95} s^3 + 9.236 \times 10^{99} s^2 \\
 + 1.732 \times 10^{105} s + 9.418 \times 10^{106}
 \end{array} \right) \quad (4.4)
 \end{aligned}$$

Table 4.3: Poles and zeros of the order-reduced transfer function of 132/33kV, 31.5MVA Pauwels transformer (PhaseY)

Pole value	Pole type	Resonant frequency
-5.4388e+01	Single pole	5.4388e+01
-4.2032e+03 ± 5.5612e+04i	Double pole	5.5771e+04
-6.0561e+03 ± 9.3345e+04i	Double pole	9.3541e+04
-5.7721e+03 ± 1.2258e+05i	Double pole	1.2272e+05
-5.6572e+03 ± 2.2622e+05i	Double pole	2.2629e+05
-8.5402e+03 ± 2.8739e+05i	Double pole	2.8752e+05
-4.3526e+07	Single pole	4.3526e+07
Zero value	Zero Type	Resonant frequency
-1.3485e+02 ± 2.5080e+03i	Double pole	2.5116e+03
-2.2521e+03 ± 9.7584e+04i	Double pole	9.7610e+04
-9.6260e+03 ± 9.7165e+04i	Double pole	9.7641e+04
-7.1253e+03 ± 1.3809e+05i	Double pole	1.3827e+05
-8.9192e+03 ± 2.6146e+05i	Double pole	2.6162e+05
-8.3808e+03 ± 2.9816e+05i	Double pole	2.9828e+05

Corresponding bode plot is shown in Figure 4.7, where all the zero crossing points of actual SFRA is included in estimated order-reduced transfer function (shown in the orange coloured graph) and gain become zero (0 DB) at $4.35e07 \text{ rad/s}$ due to the addition of “Zero”. If two graphs are compared, after the final zero at $2.9828e05 \text{ rad/s}$, the same trend is preserved with smaller variations. In brief, all the important resonances within 20Hz to 1MHz range where the effects of external connections have no impact over SFRA, is reflected by the order-reduced transfer function.

Since the resultant transfer function is 12th order, the number of sections of the circuit modelled in MATLAB Simulink is 6 (i.e. equivalent to half of the order). Modelled test setup configuration (according to the standards) is shown in Figure 4.8. A variable frequency Power Supply of 1kV rms is used to energize the power transformer through 50 Ω resistance. Input and output voltages are measured across 50 Ω resistances as the test is conducted. The power transformer is modelled inside the

block named “subsystem”.

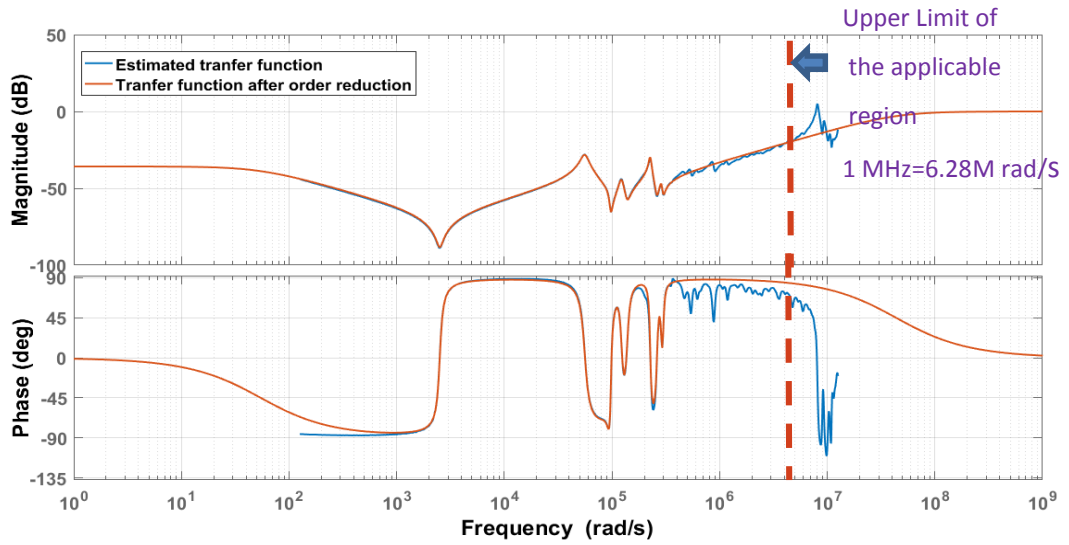


Figure 4.7: Comparison of responses of order-reduced transfer function (orange) with measured SFRA response (blue)

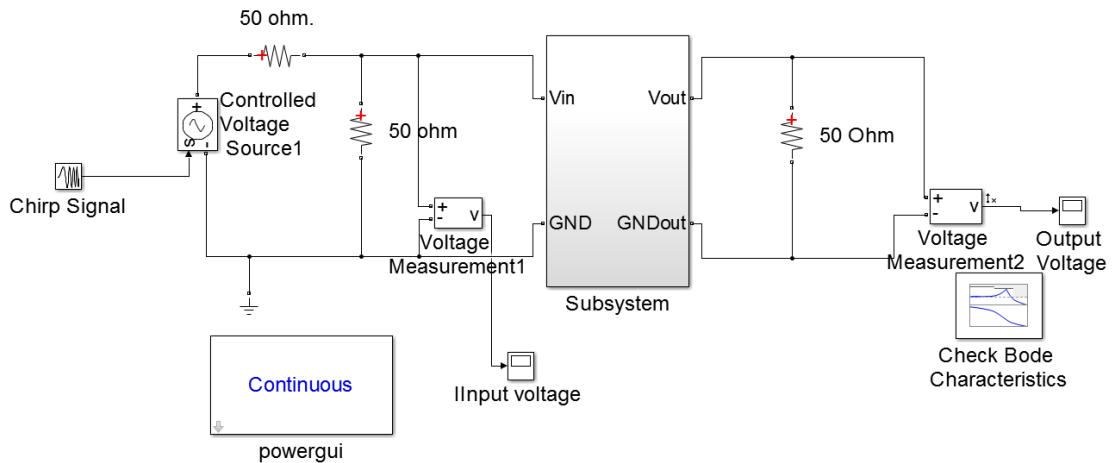


Figure 4.8: Test setup modelled in Simulink

The first step of the proposed method in Figure 4.4 is derivation of initial approximation (using trained ANN). To train the neural network, neural network fitting application (“nftool”) available in MATLAB software is used. Out of 10000 samples generated, 15% of them are used for the validation and 15% are used for the testing. Rest of 70% are used for the training process. Coefficients of numerator and denominator are given as inputs (26 inputs) and parameters of 6 sections are given as outputs (24 parameters). Number of hidden layers is 50. ANN trained for 6 section is

used to derive the initial approximation since this is a 6-sectional lumped parameter equivalent circuit. Figure 4.9 depicts the transformer model used in ANN where parallel resistances (R_{cs_i}) and mutual inductances (M_{ij}) are absent as described in the previous subsection.

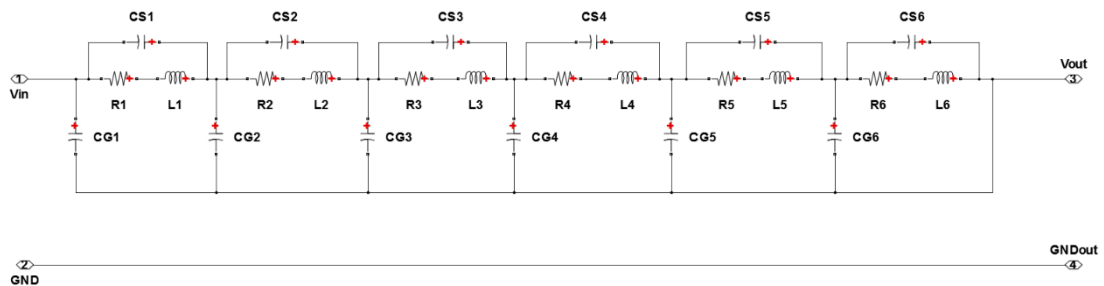


Figure 4.9: Six-sectional lumped parameter network used to train ANN

When the coefficients of order reduced transfer function in (4.4) are given to the trained network, ANN provides initial parameter estimations as shown in Table 4.4. Corresponding bode plot is shown in Figure 4.10, where DC gain hasn't modelled due to exclusion of parallel winding resistances.

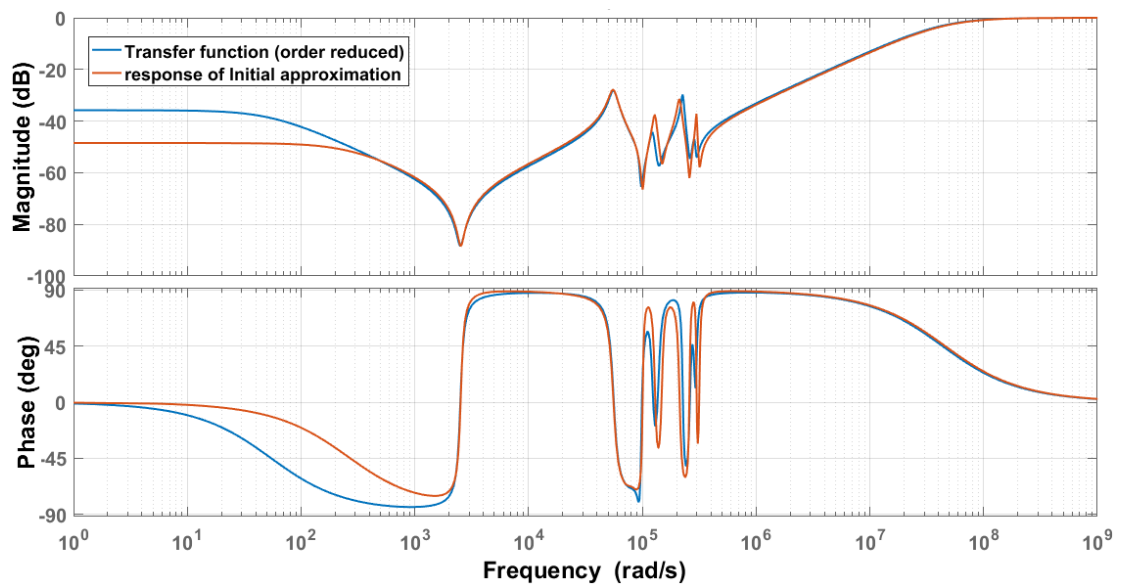


Figure 4.10: Comparison of bode plots of initial approximation obtained from trained ANN and measured SFRA

Table 4.4: Estimated parameter values from ANN (step1)

	$R_i(\Omega)$	$L_i(H)$	$CS_i(F)$	$CG_i(F)$
Section 1	165.7227	0.0407	2.53E-09	1.38E-10
Section 2	432.9302	0.0250	2.68E-10	1.68E-10
Section 3	83.8425	0.0270	1.24E-10	7.53E-10
Section 4	300.8222	0.0201	1.42E-09	2.78E-10
Section 5	12000	49.9996	1.10E-09	5.05E-10
Section 6	273	0.1100	1.68E-09	1.23E-08

In the next step, DC gain matching process is performed by changing resistances. Actual DC gain that should be represented by the estimated curves can be found by (4.4), Substituting Laplace operator $s = 0$.

$$DC \text{ gain} = 20 \log_{10}(\text{order reduced transfer function @ } s = 0) \quad (4.5a)$$

$$= 20 \log_{10} \left(\frac{1.53 \times 10^{105}}{9.418 \times 10^{106}} \right) \text{ dB} \quad (4.5b)$$

$$= -35.7869 \text{ dB} \quad (4.5c)$$

(See Figure 4.10, where blue coloured line settles at -35.7869 dB)

Corresponding total resistance value can be found using (2.2) and (2.3) as follows.

$$-35.7869 = 20 \log_{10} \left(\frac{50}{50 + \sum R_i} \right) \quad (4.6)$$

Therefore

$$\sum R_i = 3028.3287 \Omega \quad (4.7)$$

As explained under subsection 4.4.2, resistances obtained in the previous estimation were proportionally altered to match the DC gain of estimation as Table 4.5.

Table 4.5: Resistance values before and after DC gain matching

	<i>Previous $R_i(\Omega)$</i>	<i>Ratio</i>	<i>New $R_i(\Omega)$</i>
Section 1	165.7227	$\frac{165.7227}{13256.32}$	$\frac{165.7227}{13256.32} \times 3028.3287 = 37.8584$
Section 2	432.9302	$\frac{432.9302}{13256.32}$	$\frac{432.9302}{13256.32} \times 3028.3287 = 98.9004$
Section 3	83.8425	$\frac{83.8425}{13256.32}$	$\frac{83.8425}{13256.32} \times 3028.3287 = 19.1533$
Section 4	300.8222	$\frac{300.8222}{13256.32}$	$\frac{300.8222}{13256.32} \times 3028.3287 = 68.7211$
Section 5	12000	$\frac{12000}{13256.32}$	$\frac{12000}{13256.32} \times 3028.3287 = 2741.3298$
Section 6	273	$\frac{273}{13256.32}$	$\frac{273}{13256.32} \times 3028.3287 = 62.3653$
	$\sum R_{i-old} = 13256.32$		$\sum R_{i-new} = 3028.3287$

The estimated transfer function for the equivalent circuit after this alteration is depicted in Figure 4.11. Note that low frequency response of the order-reduced transfer function (blue) and estimated response (red) coincides in the low frequency region (in other words, DC gain has been matched).

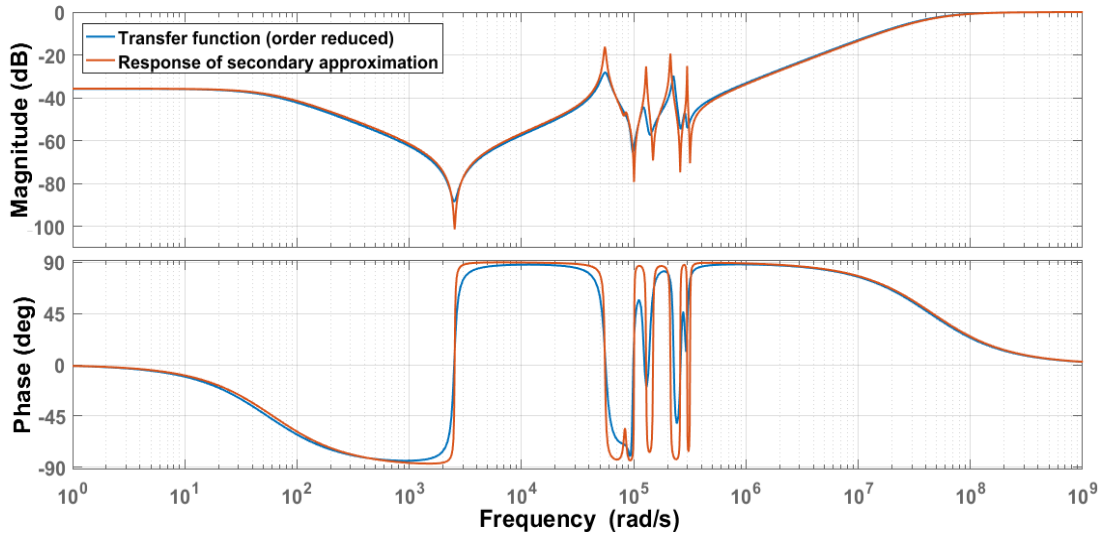


Figure 4.11: Frequency response after DC gain matching

Next step is the optimization of results using genetic algorithm as explained under subsection 4.4.3. Since the excluded parameters (parallel resistances(Rc_s_i) and

mutual inductances(M_{ij}) are also included in the modelled circuit, MATLAB Simulink model in Figure 4.9 has to be modified as shown by Figure 4.12 where all self and Mutual inductance values are represented by a single Simulink block (using matrix form).

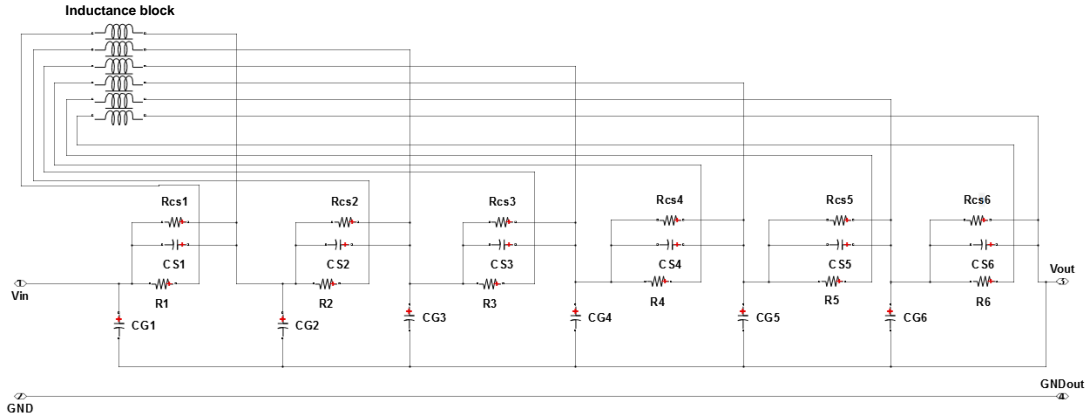


Figure 4.12: Final Six-sectional lumped parameter network (Used for GA)

Multi-objective optimization using genetic algorithm (“gamultiobj solver”) available in MATLAB Optimization tool is used to minimize the error between measured and estimated responses. Constraint function (“*constraint_fcn*”) and Fitness (“*fit_fcn*”) are coded as APPENDIX B and C.

All the inputs options for GA are specified as per Table 4.2. GA reduces “**Fitt_val**” value from 808.1632 to 557.3758 after 203 iterations, exiting after constraint tolerance value $1e-4$ is reached. The entire process took approximately 12 hours to complete (Intel® i5 1.80GHz processor with 8.00 GB RAM was used). The frequency response of final synthesized circuit with the estimated transfer function (Order-reduced transfer function) is illustrated in Figure 4.13 where both DC gain and magnitudes at resonances are modelled to the fullest extent.

Final optimized values are shown in Table 4.6. Matrix M is the inductance matrix corresponds to inductance block in Simulink where main diagonal (M_{ii}) corresponds to sectional winding inductances and the rest corresponds to mutual inductances between sections (M_{ij}).

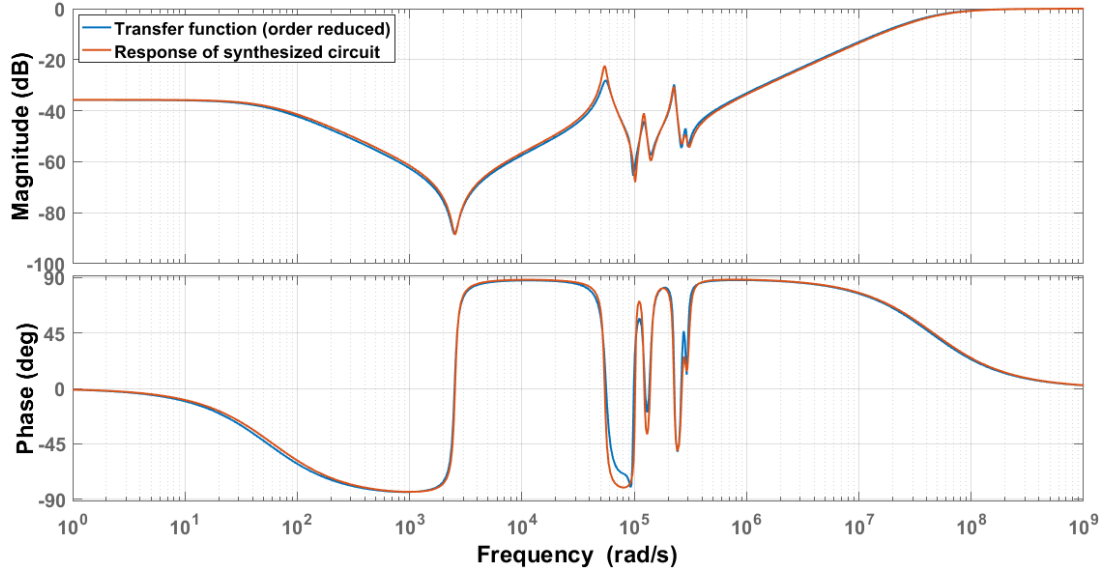


Figure 4.13: Frequency response of final synthesized circuit (red) with respect to the response of order reduced transfer function (blue)

Table 4.6: Final estimated parameter values for lumped parameter network

	$R_i(\Omega)$	$L_i(H)$	$CS_i(F)$	$CG_i(F)$	$RCS_i(\Omega)$
Section 1	37.6295	0.0397	2.29E-09	1.32E-10	1.45E+05
Section 2	95.98029	0.0275	2.32E-10	1.68E-10	1.45E+05
Section 3	19.02851	0.0350	1.42E-10	7.27E-10	6.31E+04
Section 4	68.27348	0.0176	1.07E-09	2.21E-10	8.96E+04
Section 5	2723.457	50.0014	1.37E-09	5.00E-10	1.74E+06
Section 6	61.95872	0.2285	1.84E-09	1.00E-08	1.00E+03

$$M = \begin{bmatrix} 3.97E-02 & 1.38E-04 & 3.03E-05 & 1.25E-06 & 3.61E-07 & 4.00E-08 \\ 1.38E-04 & 2.75E-02 & 1.84E-03 & 1.62E-03 & 1.80E-04 & 7.87E-05 \\ 3.03E-05 & 1.84E-03 & 3.50E-02 & 2.37E-03 & 9.61E-04 & 7.29E-04 \\ 1.25E-06 & 1.62E-03 & 2.37E-03 & 1.76E-02 & 1.42E-02 & 7.59E-03 \\ 3.61E-07 & 1.80E-04 & 9.61E-04 & 1.42E-02 & 5.00E+01 & 1.13E-02 \\ 4.00E-08 & 7.87E-05 & 7.29E-04 & 7.59E-03 & 1.13E-02 & 2.28E-01 \end{bmatrix}$$

Analysing the results, it can be observed that the sections of lumped parameter network directly correspond to the resonance locations of SFRA signature (locations are decided by inductor and capacitor values like any other RLC circuit). In fact,

resonances in the left half correspond to the right half sections of lumped parameter network and vice versa. Therefore, it can be deduced that the rightmost sections of lumped parameter network correspond to transformer core and the leftmost sections correspond to transformer winding since the low frequency region corresponds to transformer core and mid and high frequency regions correspond to transformer winding [4, 18, 53, 54]. Resultant lumped equivalent circuit ratify this statement as parameters of the 5th section (from left) are comparatively large from others, especially R_5 and L_5 are in *kiloOhms* and *Henries* than being *Ohms* and *miliHenries*. This implies that the rightmost sections characterise the power transformer's core losses and magnetizing inductances rather than windings parameters.

Resistance values decide the damping at resonance points. Lower the resistance, lower the damping or in other words, a high amplitude can be expected. Among the two types of resistance values contain here, winding resistances are relatively small compared to the parallel resistances. This agrees with the actual power transformer configuration. Because Winding resistances are in *Ohms* whereas parallel resistances which denote insulation resistances are very large, usually in *megaOhms*. As per the constraints, mutual inductance values are getting smaller with the distance between sections and result in insignificant values after three or four sections. Hence, when simplicity and immediate results are necessary, mutual inductances after three/four sections can be neglected.

4.5.1 Method validation: numerical validation

To validate the proposed method numerically, absolute error graphs are shown in Figure 4.14. Absolute error is calculated using the following equation (4.8).

$$\begin{aligned}
 & \text{Absolute error}(dB)_{@f} \\
 & = 20\log|(Transfer\ function\ of\ synthesized\ circuit)_{@f}| \quad (4.8) \\
 & - 20\log|(Order\ reduced\ transfer\ function)_{@f}|
 \end{aligned}$$

Calculated error at frequency f over the frequency range is illustrated in the absolute error graph. Maximum error recorded as 6dB whereas error at non-resonance points averages 2dB. Reason for high relative error at the resonance points is, the

magnitude of resonances (damping at the resonance) are influenced by the resistance values which vary in a large range. Especially, as parallel insulation resistances (RCS_i) vary within a large range, even a smaller error is magnified.

Generally, the response of actual power transformer, hence the response of equivalent lumped parameter network is governed by RLC values. Usually, L and C values are very small and parallel resistance values are very large. (Inductor values are in *miliHenries*, capacitor value are in *picoFarads* and parallel insulation values are in *megaOhms*). These values result in very large coefficients in transfer functions, for example, the numerator and denominator constants of order reduced transfer function are 1.53×10^{105} and 9.418×10^{106} respectively. Therefore Calculation of these transfer functions has a certain inherent error due to its large-sized numbers (rounding error is high during the each calculation). Nevertheless, compared with the actual response, estimated response of synthesized circuit offers acceptable results.

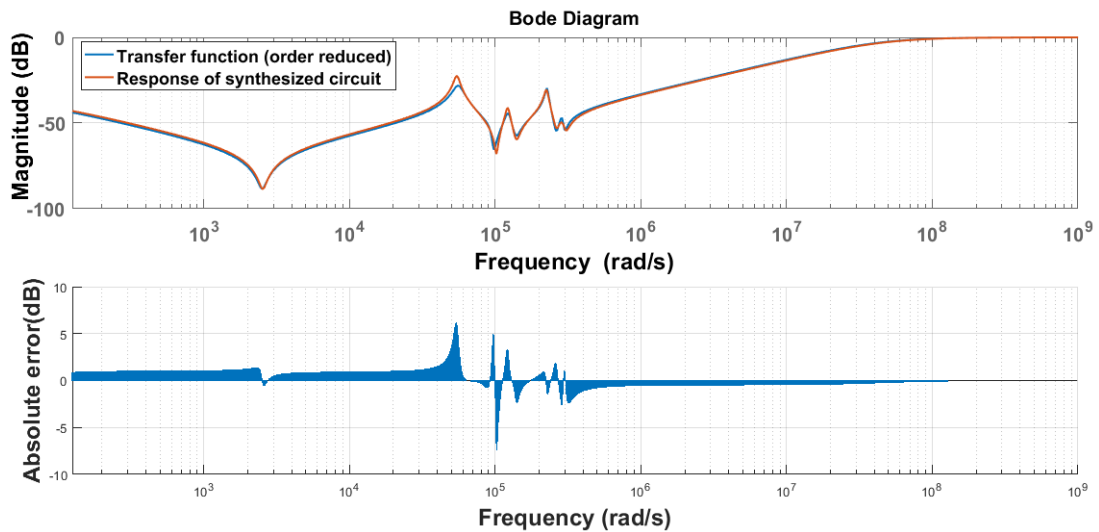


Figure 4.14: Magnitude plots of order reduced transfer function and synthesized network with Absolute error graph

4.5.2 Method validation: comparison with a faulty transformer frequency response

To validate model practically, recorded faults of an actual transformer can be

used. Figure 4.15 shows pre-fault and post-fault SFRA signature curves of actual transformer measured using omicron analyser. The fault was identified as a core issue by the on-field visual inspection of transformer .

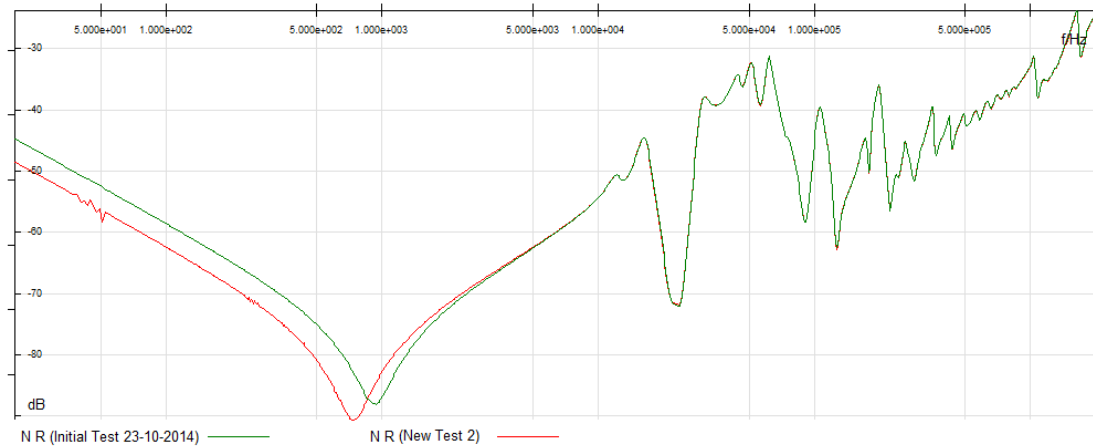


Figure 4.15: pre-fault and post-fault SFRA curves of Biyagama 83.3 MVA 3phase transformer (Phase Y, open circuit response)

To recreate this fault, parameter values of section 5 are altered by +5% as in Figure 4.16. (The 5th section of the obtained lumped parameter network has a large resistance and inductance values that corresponds to the transformer core as explained in the case study)

Comparing Figure 4.15 and Figure 4.16, the same trend can be observed where initial frequencies deviate in the same manner while the middle and high frequency response remains identical. Since the core effects dominate this low frequency region [4, 18, 53, 54], the shift of resonance point at low frequency can be attributed to an increase of capacitive behaviour in the transformer. This proves that the model can accurately represent the structure and the behaviour of actual power transformer.

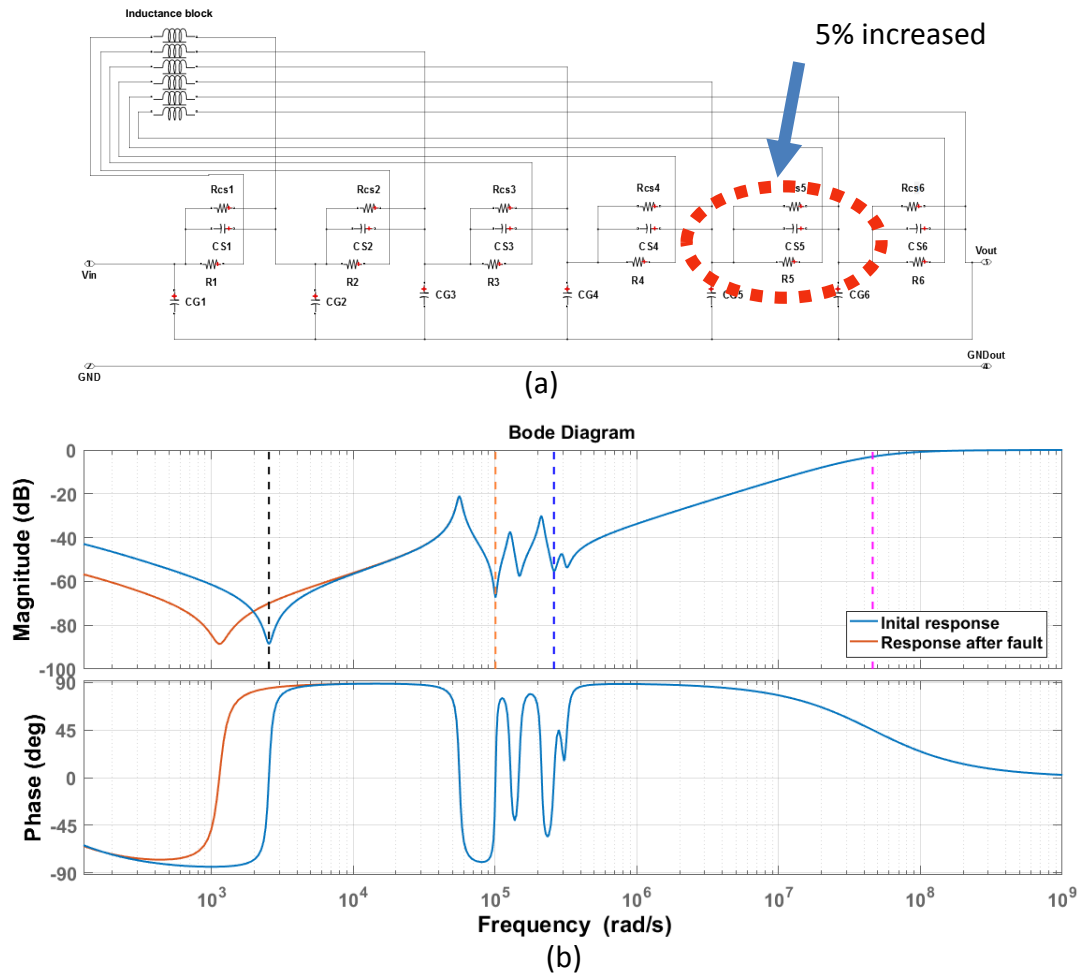


Figure 4.16: (a) Altered parameters of lumped parameter network (b) Frequency response before and after alteration

4.6 Results of other phases and different tests

Using the same sample transformer, variations of SFRA according to phases and test types can be shown.

4.6.1 Modelling of side phases (phase R/B for open circuit test)

Figure 4.17 depicts open circuit frequency response of all three phases performed to a selected power transformer where the middle phase is indicated as “phase Y” and side phases as “phase R” and “phase B”. As this figure illustrates, responses of side phases are different from the middle phase in the low and middle frequency region. This is caused by the effect of transformer core which is different in middle and side phases.

In fact, both the side phases are almost identical and have a different response from the middle phase. In particular, between $10^3 - 10^4 \text{ rad/s}$ where core dominates, two resonances can be observed in side phases compared with the middle phase that contains only one. Main reason for this single resonance in middle phase is, symmetrically surrounded transformer middle limb that makes the flux distribution symmetrical around its vertical axis. Unbalanced flux at side phases due to the asymmetrical transformer geometry around their limbs, result a couple of resonances which also have asymmetrical nature in the SFRA response.

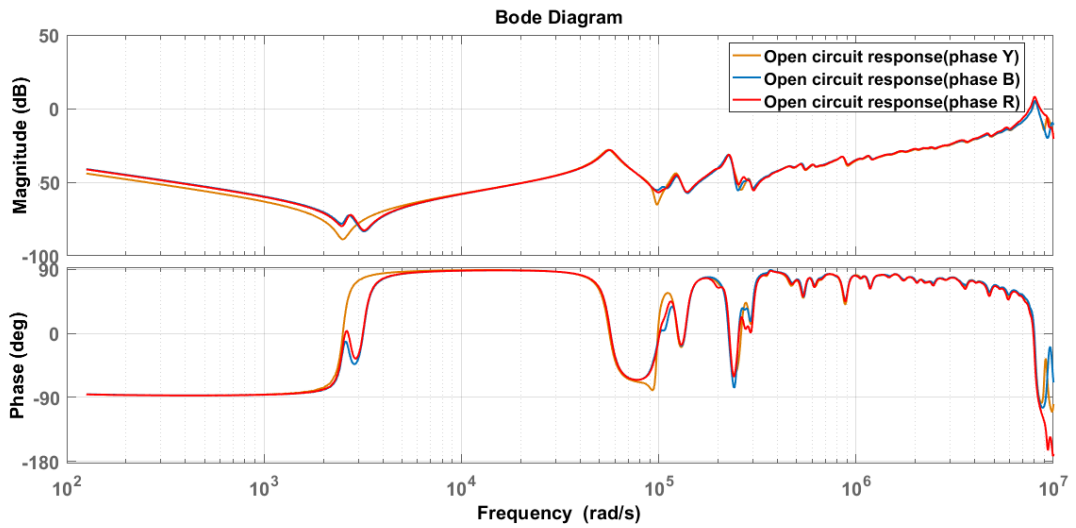


Figure 4.17: Original open circuit SFRA of 132/33 kV, 31.5 MVA Pauwels transformer (Phase R, Y and B)

This results the order reduced transfer function of side phases to be a relatively larger one compared with the middle phase. Since side phases are identical in nature, one of them is randomly selected for the modelling (Phase B is selected).

As described under Chapter 3, an order reduced transfer function is derived. Resultant transfer function has 14 order numerator and 14 order denominator satisfying Routh-Hurwitz criterion. Note that, due to the inclusion of double pole type resonance at low frequency, the order of estimated transfer function of side phases has increased by two.

Number of sections of the lumped parameter network used to model is 7 (= $14/2$). Estimated parameter values with the order reduced transfer function and the

output response are shown below.

$$\begin{aligned}
 & \text{Order reduced transfer function} = \\
 & \frac{3.315e48 s^{14} + 2.741e53 s^{13} + 6.569e59 s^{12} + 4.157e64 s^{11} + 4.295e70 s^{10} + 1.946e75 s^9 + 1.101e81 s^8 + 3.256e85 s^7 + 1.179e91 s^6 + 1.762e95 s^5 + 4.416e100 s^4 + 3.296e103 s^3 + 7.339e107 s^2 + 2.539e110 s + 2.847e114}{3.315e48 s^{14} + 1.557e56 s^{13} + 1.438e61 s^{12} + 2.568e67 s^{11} + 1.635e72 s^{10} + 1.343e78 s^9 + 5.726e82 s^8 + 2.577e88 s^7 + 6.716e92 s^6 + 1.866e98 s^5 + 2.15e102 s^4 + 3.689e107 s^3 + 1.349e110 s^2 + 2.791e114 s + 3.851e115}
 \end{aligned} \tag{4.9}$$

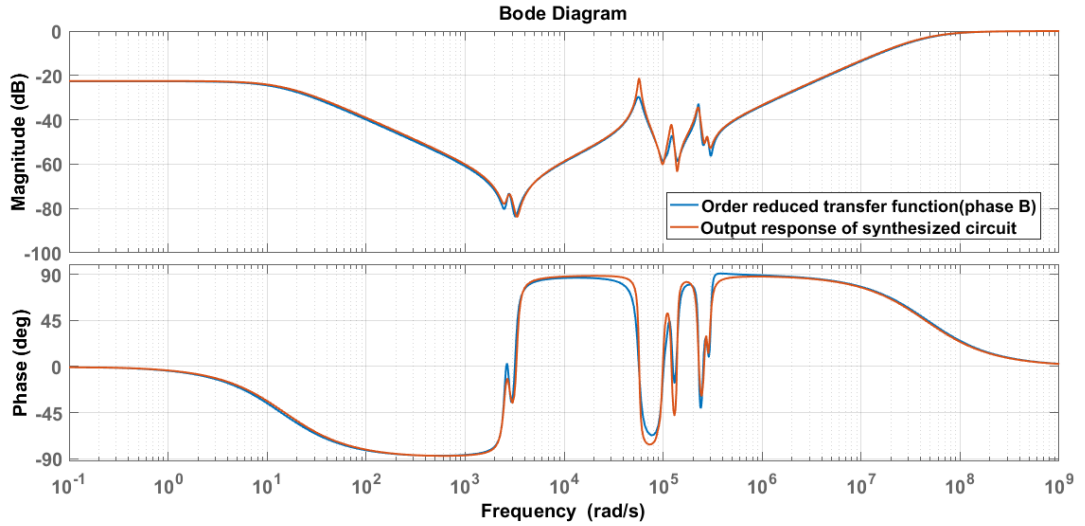


Figure 4.18: Frequency response of final synthesized circuit (red) with respect to the response of order reduced transfer function of phase B (blue)

Table 4.7: Final estimated parameter values for lumped parameter network of phase B (open circuit test)

	$R_i(\Omega)$	$L_i(H)$	$CS_i(F)$	$CG_i(F)$	$RCS_i(\Omega)$
Section 1	12.0885	0.0413	2.30E-09	1.47E-10	4.15E+04
Section 2	27.0303	0.0288	2.32E-10	1.68E-10	8.46E+04
Section 3	22.7906	0.0497	1.14E-10	6.54E-10	2.21E+05
Section 4	6.3537	0.0159	1.10E-09	9.71E-11	3.91E+04
Section 5	440.9081	38.3243	1.11E-09	4.00E-10	1.32E+06
Section 6	49.0663	5.8304	1.09E-08	1.35E-08	8.92E+04
Section 7	58.1778	0.0096	2.18E-09	4.94E-09	1.10E+05

$$M = \begin{bmatrix} 4.13E-02 & 1.66E-03 & 2.44E-04 & 6.67E-07 & 0 & 0 & 0 \\ 1.66E-03 & 2.88E-02 & 1.09E-03 & 3.11E-04 & 1.24E-09 & 0 & 0 \\ 2.44E-04 & 1.09E-03 & 4.97E-02 & 2.15E-03 & 4.67E-08 & 0 & 0 \\ 6.67E-07 & 3.11E-04 & 2.15E-03 & 1.59E-02 & 3.93E-05 & 1.25E-08 & 0 \\ 0 & 1.24E-09 & 4.67E-08 & 3.93E-05 & 3.83E+01 & 5.85E-04 & 2.79E-07 \\ 0 & 0 & 0 & 1.25E-08 & 5.85E-04 & 5.83E+00 & 9.69E-05 \\ 0 & 0 & 0 & 0 & 2.79E-07 & 9.69E-05 & 9.55E-03 \end{bmatrix}$$

Fifth, sixth and seventh sections demonstrate transformer core behaviour as components to the right resembles the transformer core structure. In fact, the 5th section of phase Y (the response considered previously) that corresponds to transformer core has effectively split into two section in this side phase responses.

Mutual inductance values between sections that far apart from each other, for an example, the mutual inductance between first and fifth sections (M_{15} and M_{51}), has negligible values compared with other inductances and estimated as zero.

4.6.2 Modelling of windings (phase R, Y & B for short circuit test)

Short circuit response curves of the same 31.5 MVA Pauwels transformer is shown in Figure 4.19. All these figures show similar responses for each windings irrespective of the core configuration. This is because, when the short circuit test is performed by short-circuiting unused windings, a relatively large current flows through each and every winding compared to the current taken by the power transformer core (for transformer core magnetization and core losses). Therefore the transformer core effects in low frequency region are neutralized. As depicted by the figure, no resonance point is present in the low frequency region where the transformer core effects dominate.

A few variations can be observed in mid frequency region that is influenced by both core and windings (around 10^5 rad/s). The reason for the core influence effect seen in the mid frequency range is, the transformer core losses increase with the frequency (hysteresis losses are proportional to the frequency and eddy current losses

are proportional to the square of frequency [55]). Therefore the core effects have a certain impact on the SFRA response in the mid frequencies (It should be noted that at high frequencies, series capacitances of windings are the most dominant influence. Hence the core effects are suppressed in high frequencies). In brief, even though short circuit response neutralize core effect of power transformer, still some variation can be seen between three phases in their mid-frequency range.

Phase Y (middle phase) response is randomly selected for the modelling. According to the proposed method in Chapter 3, order-reduced transfer function is derived for the middle phase (Phase Y), shown in (4.10).

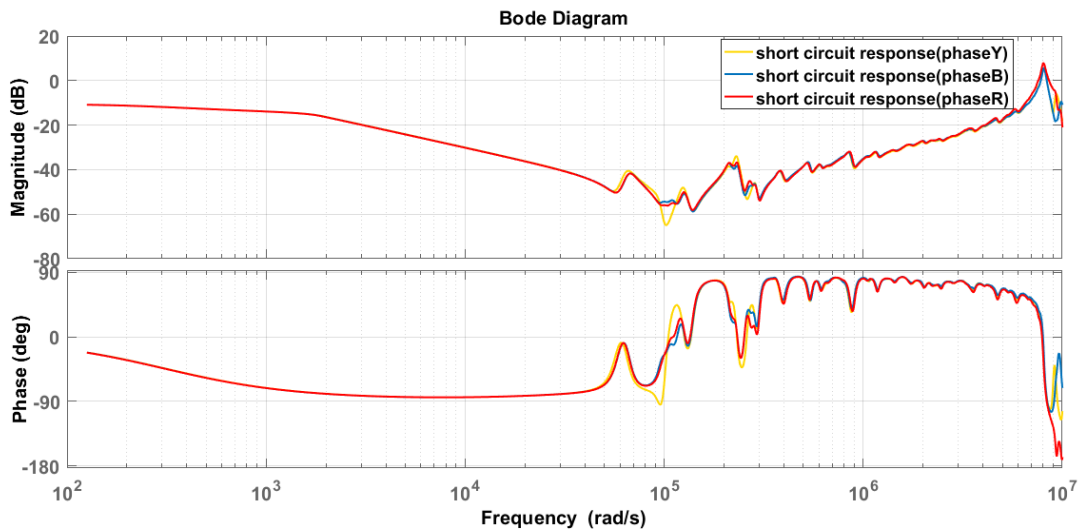


Figure 4.19: Original short circuit SFRA of 132/33kV, 31.5MVA Pauwels transformer (Phase R, Y and B)

$$\begin{aligned}
 & \text{Order reduced transfer function} = \\
 & \frac{2.197e15 s^{12} + 1.927e20 s^{11} + 4.47e26 s^{10} + 3.15e31 s^9 + 3.051e37 s^8 + 1.644e42 s^7 + 8.375e47 s^6 + 3.252e52 s^5 + 1.024e58 s^4 + 2.548e62 s^3 + 5.399e67 s^2 + 6.381e71 s + 9.175e76}{2.197e15 s^{12} + 8.915e22 s^{11} + 6.594e27 s^{10} + 1.491e34 s^9 + 8.121e38 s^8 + 7.833e44 s^7 + 3.008e49 s^6 + 1.477e55 s^5 + 3.648e59 s^4 + 1.056e65 s^3 + 1.277e69 s^2 + 2.321e74 s + 1.865e77}
 \end{aligned} \tag{4.10}$$

Number of sections of lumped parameter network used to model is 6 ($= 12/2$). Response for estimated lumped parameter network with order reduced transfer function is shown below.

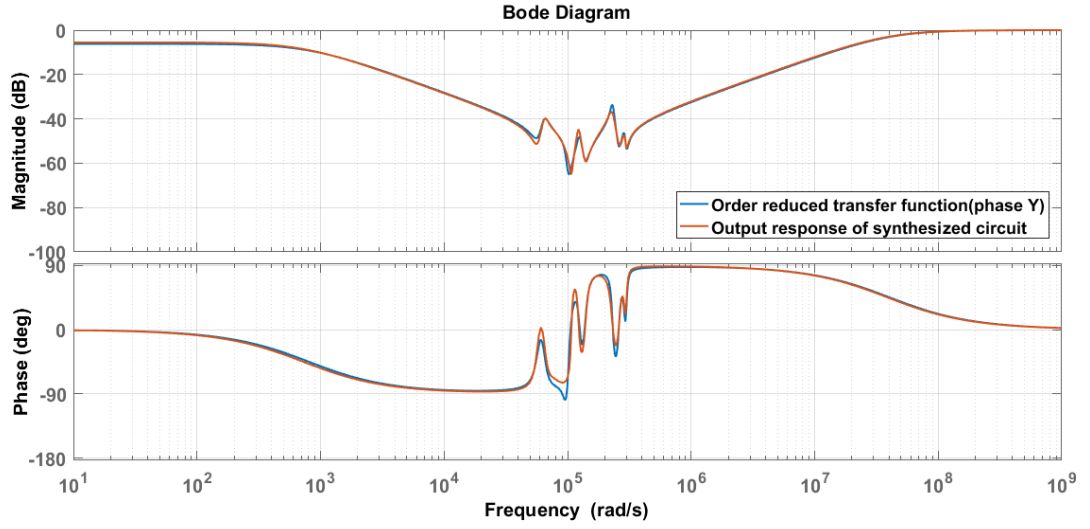


Figure 4.20: Frequency response of final synthesized circuit (red) with respect to the response of order reduced transfer function of phase Y (blue)

Final estimated parameter values for the corresponding lumped parameter equivalent network is shown in Table 4.8 and Mutual inductance matrix M .

Table 4.8: Final estimated parameter values for Lumped parameter network of phase Y (short circuit test)

	$R_i(\Omega)$	$L_i(H)$	$CS_i(F)$	$CG_i(F)$	$RCS_i(\Omega)$
Section 1	3.6808	0.0290	2.78E-09	1.86E-10	6.31E+04
Section 2	9.9959	0.0160	5.98E-10	4.48E-11	1.10E+05
Section 3	9.9229	0.0272	2.43E-10	5.30E-10	2.00E+05
Section 4	6.1409	0.0240	9.02E-10	9.27E-11	2.75E+04
Section 5	8.9341	0.0106	1.50E-08	1.44E-09	2.29E+03
Section 6	5.5730	0.0203	3.65E-09	8.46E-09	9.12E+03

$$M = \begin{bmatrix} 2.90E-02 & 1.34E-06 & 1.00E-06 & 5.68E-07 & 0 & 0 \\ 1.34E-06 & 1.60E-02 & 5.14E-04 & 3.07E-04 & 1.23E-06 & 0 \\ 1.00E-06 & 5.14E-04 & 2.72E-02 & 3.09E-04 & 6.32E-06 & 8.64E-07 \\ 5.68E-07 & 3.07E-04 & 3.09E-04 & 2.40E-02 & 1.12E-06 & 2.64E-06 \\ 0 & 1.23E-06 & 6.32E-06 & 1.12E-06 & 1.06E-02 & 1.51E-04 \\ 0 & 0 & 8.64E-07 & 2.64E-06 & 1.51E-04 & 2.03E-02 \end{bmatrix}$$

Unlike previous cases (i.e. open circuit responses), each section has similar parameter values especially winding resistance and inductances. Large parameter values correspond to the power transformer core cannot be seen in end sections of the network. This proves the fact that the core effects of power transformer are cancelled out in the short circuit responses.

4.7 Conclusions

This chapter presents an integrated method of ANN and GA to synthesise the transfer function of power transformer into lumped parameter equivalent circuit. Effect of the test type and phase to the resultant equivalent circuit has also been investigated in this chapter.

The number of sections of the modelled lumped parameter network depends on the estimated order-reduced transfer function. Therefore, other than using different sections in the circuit model used by GA, several ANN have to be trained by changing the number of sections in the circuit model. The training process of ANN can be performed in advance, which is useful in reducing the total time spent for the synthesis process.

Open-circuit and short-circuit tests are the test types considered in this thesis for the modelling as the response of a single winding is given by these two tests. The results show that the initial frequency region that depicts transformer core influence is different from each other. Parameters of rightmost windings of the modelled circuit for the open circuit response are relatively large compared to the circuit modelled for the short circuit response implying the effect of core elements. By comparing these two circuits modelled for open circuit and short circuit scenarios, core responses embedded in the open circuit response can be separated.

An order reduction by means of eliminating resonances that do not result in zero crossing points in phase response has been employed as the initial step of synthesis process. Eliminating resonances in this manner will give a more accurate transformer model while reducing its complexity. However, the high frequency

resonances eliminated during the order reduction step can be minor winding variations of the transformer, measurement noise of the frequency response analyser or external disturbances and interactions of setup connection. Therefore, a way to utilize this high frequency range by separating minor winding variations from the others is required to be investigated further.

Synthesis of lumped parameter equivalent circuit can be automated as each step of the proposed method can be implemented in terms of MATLAB coding. The results can be derived more accurately by using a dedicated computer with high processing power.

Chapter 5

REFERENCE CURVES OF POWER TRANSFORMER FAULTS

5.1 Introduction

An important aspect assessed during condition monitoring process is the mechanical integrity of the power transformer. Any deformation identified that exceeds their safety levels has to be fixed immediately. Even though the transformer can operate with minor winding damages, it is not recommended as it may be developed into a permanent transformer damage [56]. The main reason for the changes of power transformer's structure is the mechanical stresses build-up inside the asset during its operation. Heavy Electromagnetic forces caused by high fault currents result these mechanical stresses that can lead to winding movements or core displacements. These high currents may be resulted by power system fault such as line-to-earth fault of conductor wire, external sources such as lightning or even by inappropriate design and workmanship [56, 57]. Apart from these main reasons, vibrations due to re-location and transportation, insulation deterioration and loosening clamping pressure due to ageing can also cause mechanical deformations in power transformers.

These can lead to various types of faults inside a transformer, such as

- Shorted turns (Inter turn fault, Turn-to-turn fault)
- Winding displacement
- Conductor tilting
- Axial bending
- Winding buckling

The frequency response of power transformer will differ from its pre-fault response as these faults alter the internal structure. The sensitivity of regions of SFRA is different depending on the fault type [9]: Personnel who perform this test should possess enough experience and comprehensive knowledge to analyse these responses and interpret results. Knowing the behaviour of frequency response curves with regard

to different transformer parameters is an essential requirement in fault interpretation using SFRA. Thus reference signature curves for numerous potential faults are generated in this chapter using modelled transformer lumped parameter network. These can be incorporated with SFRA to interpret faults of transformers with a greater accuracy.

Section 5.2 explains a method to separate regions of SFRA and fault interpretation rules used in the industry. These rules can be used to check whether simulated fault reference curves in section 5.3 are accurate.

5.2 Fault interpreting using frequency ranges of SFRA

A method of separating frequency ranges of the frequency response is shown in this section. Fault interpretation is performed on the basis of variations in each section and presented as a set of rules.

5.2.1 Frequency ranges of SFRA

Transformer parameters have dissimilar influences on the different ranges of its frequency response [45, 57]. Generally, these parameter changes are the consequences of faults inside the transformer. Entire frequency region can be divided into three major frequency ranges: low frequency range (LF), medium frequency range (MF) and high frequency range (HF) [9].

The low frequency range can be further divided into two: very low frequency region (LF1) and low frequency region (LF2). In very low frequencies (LF1), magnetization inductance (L_m) govern the frequency behavior, representing the linear behaviour of transformer core whereas subsequent low frequency region (LF2) is influenced by shunt capacitances of windings (or ground capacitances Cg_i) in addition to magnetization inductance.

Medium frequency region where most of the resonances in frequency response exist, is the outcome of entire winding (self and mutual winding inductances (L_i and M_{ij}), series and ground capacitances (Cs_i and Cg_i)). Larger number of capacitive

and inductive interactions created by the winding sections result a group of resonances in this region.

Furthermore, the high frequency range can be categorized into two: high frequency region (HF1) and very high frequency region (HF2). The Capacitive behaviour of windings majorly series capacitances (Cs_i) dominate this high frequency (HF1) region. Very high frequency region, which is more than 1 MHz shows external influences such as measurement connectors and ground leads. In fact, this is the reason to ignore very high frequency variations during obtaining order reduced transfer function of proposed method in subsection 4.4.

Typical frequency ranges of these regions are: low frequency range (LF1/LF2 - 20 Hz to 2 kHz), medium frequency range (MF- 2 kHz to 50 kHz) and high frequency range (HF1/HF2- 50 kHz to 2 MHz) [18]. But these ranges are not identical for every transformer as frequency response depends on its design, and structure. Therefore dynamic range determination method used in [9] is used to separate regions, as shown in Figure 5.1.

This method separates frequency regions by means of inductive-capacitive zero crossing points, or in other words troughs in the amplitude plot. Whenever a trough exits in the amplitude response, corresponding phase response has a zero crossing point (at the same frequency). These troughs are resulted by “poles” of the transfer function. Initially, frequencies of all the inductive-capacitive zero crossing points are necessary to determine using the transfer function by equating its denominator to zero (referred to as F_{ZC} in Figure 5.1). Since the typical frequency response of middle phase has a single resonance compared to two resonances in side phases, two schemes have defined. Outputs of this step are frequency values denoted by A, B, C & D. For the middle phase the first and second values of F_{ZC} are selected as A and B whereas lateral phases frequency at which magnitude of the amplitude plot starts to decrease is taken as the reference to determine A and B. In both occasions, C is the final zero crossing point (m^{th} point of F_{ZC}) and D is the frequency at which

magnitude of amplitude become zero. $LF1_{up}$, $LF2_{up}$, MF_{up} and HF_{up} refer to upper frequency limits of considered regions which are determined using calculated A,B,C and D values.

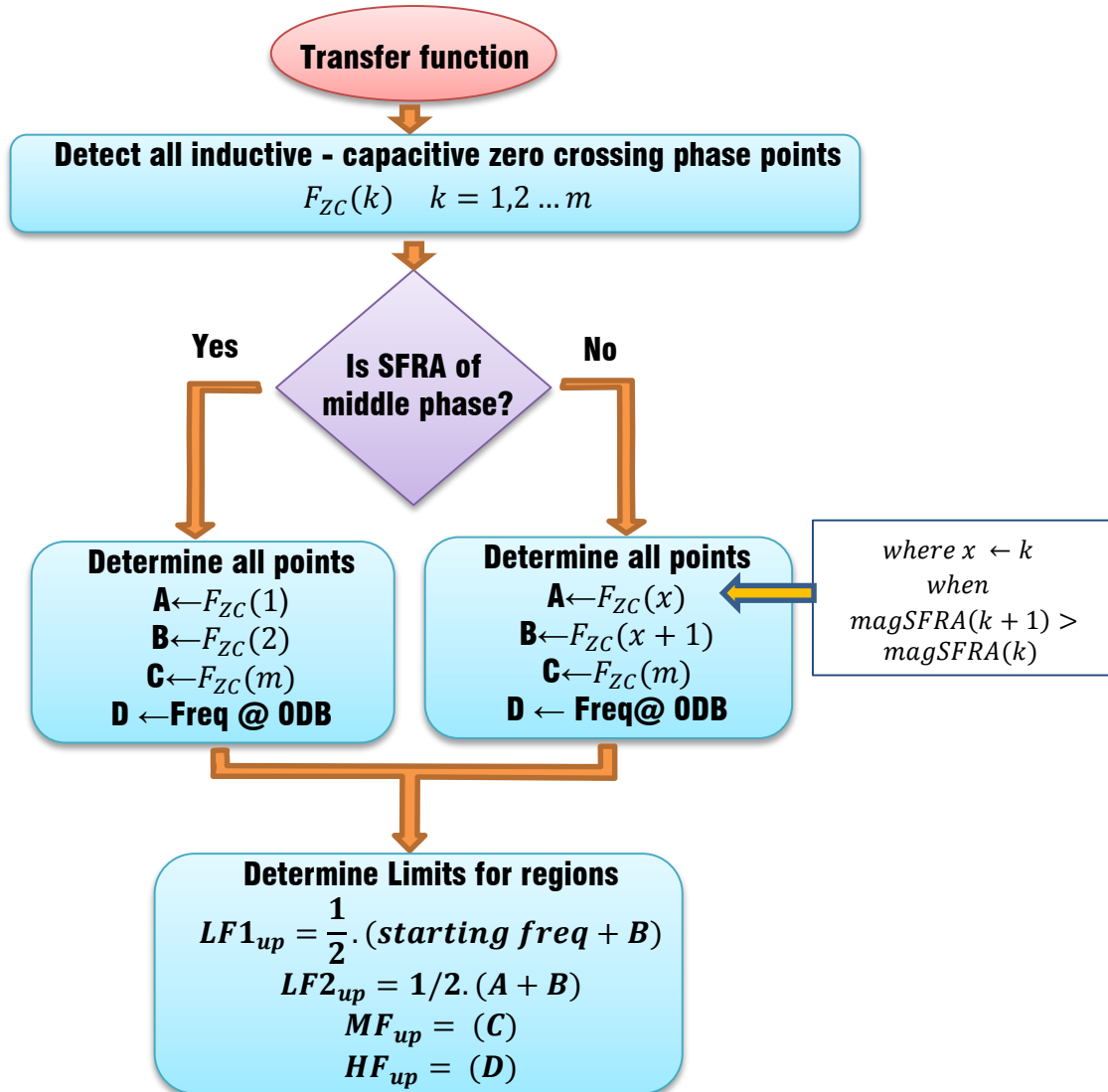


Figure 5.1: Method of region determination of SFRA

It should be noted that all major variations including zero crossing points are retained during the order reduction process of transfer function. Hence this method for region determination is applicable to the order-reduced transfer function derived in the previous chapter. Additionally, the very high frequency region that does not depict transformer variations is intentionally ignored in the process. Therefore the high frequency region determined by this method is same as $HF1$. Corresponding MATLAB code is shown in APPENDIX D.

5.2.2 Fault interpretation rules

Fault identification criteria used in the industry can be summarized as follows [18]. Following Table 5.1 shows deviations of frequency response regions with their possible parameter variations. Referring to this table, generated reference curves of various fault types can be validated.

Table 5.1: Fault interpretation rules

Region	Variation and cause
Low frequencies (LF1, LF2)	<ul style="list-style-type: none">• Pole shift higher freq.-core problem or SC between winding turns• Pole shift lower freq.- SC to ground or winding buckling
Mid frequencies (MF)	<ul style="list-style-type: none">• Pole shift higher freq.- SC between winding turns or winding compression• Pole shift lower freq.- Winding buckling, tilt of conductors or axial collapse
High frequency (HF)	<ul style="list-style-type: none">• Pole shift lower freq.- failures such as tilt of conductors or axial collapse

5.3 Generated reference curves

Availability of reference SFRA signature curves for a fault type is an added advantage in fault detection using SFRA as such reference curves can be integrated into the interpretation of responses. Simply, comparing post-fault response with a set of reference curves would reveal exact failure inside the power transformer. Even though reference curves can be formed by mechanically deforming a similar transformer, it is not suitable owing to the huge cost incurred for power transformers. Derivation of reference curves by means of simulations is the easiest and most economical way. Therefore synthesized equivalent circuit prepared by the proposed method is used to generate reference curves.

As a case study, 132/33 kV, 31.5 MVA Pauwels transformer (Phase Y) is selected. The same procedure can be applied to other transformers. Reference curves for some of the common fault types produced by simulations are presented as follows.

5.3.1 Inter-turn faults

Inter turn faults occur in a single winding section of transformer due to a short circuit between adjacent coils. Starting with few turns, these faults can grow up to complete short-circuiting between winding sections. Differential current protection schemes and dissolved gas analysis (DGA) are some of the methods used to detect inter-turn faults [58]. Reference SFRA response curves for inter-turn fault at its incipient stage can be derived by reducing the resistance value of windings, or by short-circuiting windings at its matured stage. As an example, reference SFRA curve for inter-turn fault at third section is simulated by short-circuiting third section (resistance and inductance blocks) as shown in Figure 5.2.

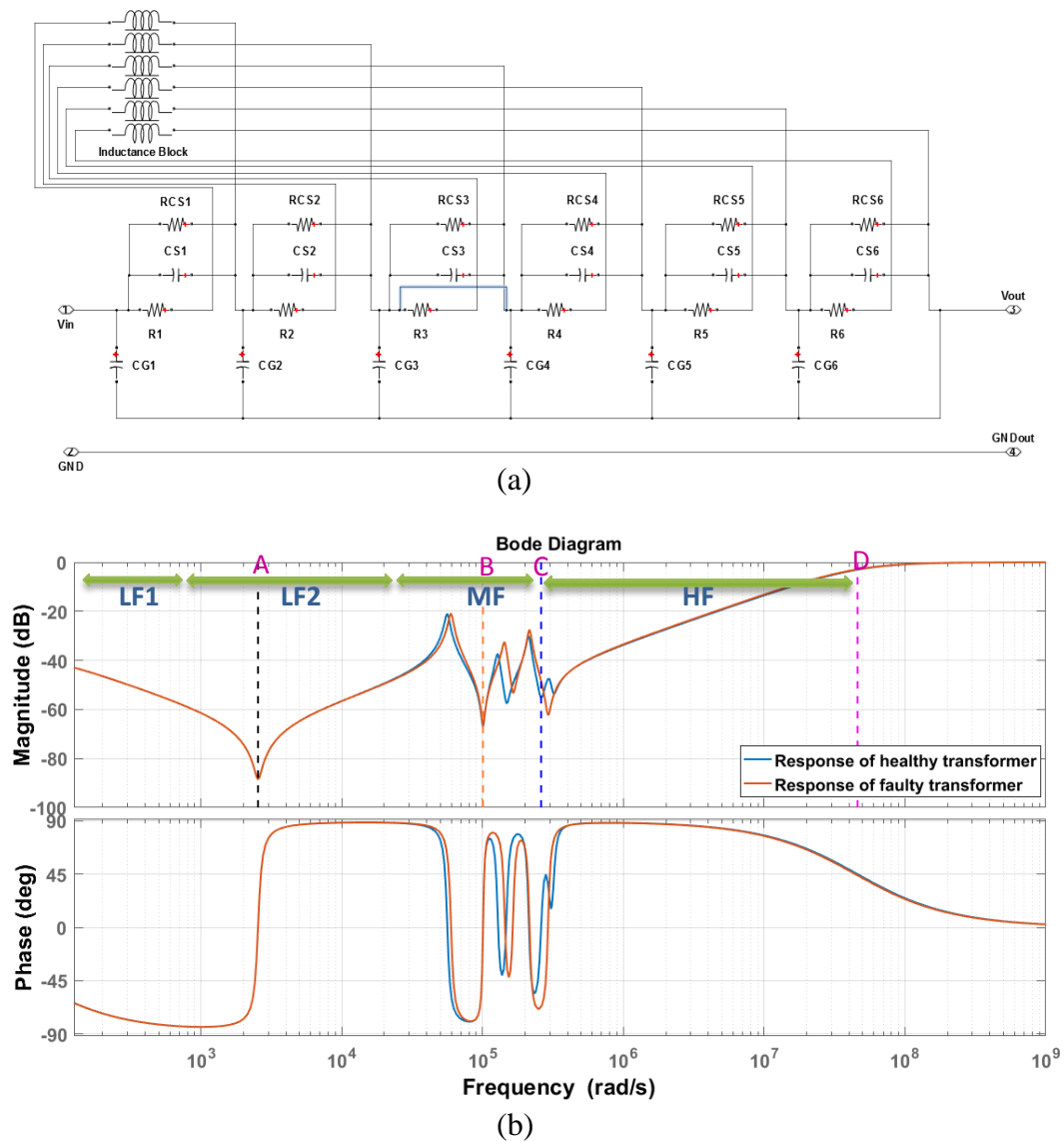


Figure 5.2: (a) Simulating an inter-turn fault by short circuiting section-3 (b) Pre fault and post fault Frequency response

Very few variations can be seen in the low frequency region and high frequency regions whereas the majority of variations are in medium frequency region (MF). Compared with the healthy transformer response (blue coloured graph), resonances of MF region in faulty transformer (red coloured graph) have shifted towards higher frequencies, indicating inductive behaviour. Referring to the rules given in Table 5.1, the fault can be confirmed as “SC between winding turns” or short circuit fault.

Moreover, actual inter-turn fault recorded at transformer is shown in Figure 5.3. This graph validates the model having the similar variations as estimated inter-turn fault curve (Resonances of mid frequency range have shifted towards higher frequencies).

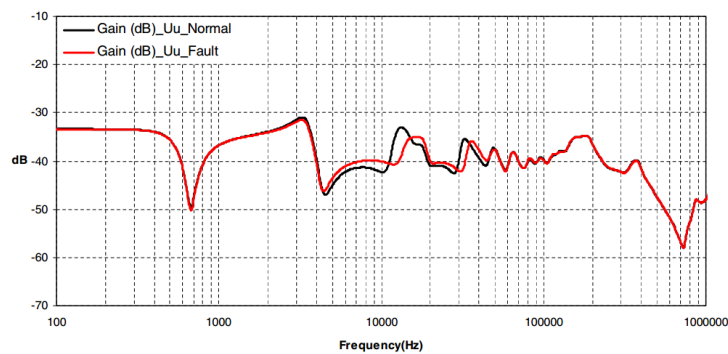


Figure 5.3: Frequency response of phase ‘Y’ of the transformers before and after inter-turn fault occurrence on phase ‘Y’ of the HV winding (logarithmic frequency scale from 100 Hz to 1 MHz) [16]

Accordingly, reference curves of other sections are generated by short-circuiting corresponding winding sections and illustrated in Figure 5.4.

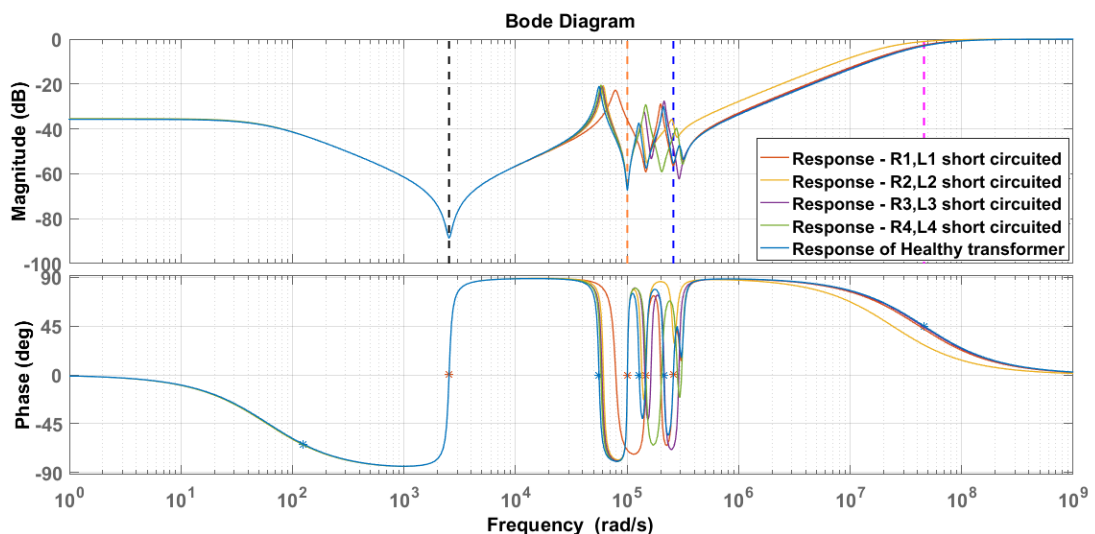


Figure 5.4: Reference frequency responses of inter-turn fault (for each winding section)

5.3.2 Transformer core faults

Generally, Buchholz relay is used to detect core faults of oil cored power transformers [59]. However, by performing SFRA, core issues can be analysed as its low frequency region is sensitive to the condition of transformer core [4, 18, 53, 60].

Core faults can be simulated by modifying end sectional parameters of the lumped equivalent circuit as those correspond to transformer core, explained under section 4.5. As a case study, reference SFRA curve for a core fault is simulated by reducing fifth section inductance (corresponds to magnetizing inductance) by 50 %. The reason to decrease magnetizing inductance is, if any undesirable mechanical deformation is present inside the transformer core, it will degrade transformer core characteristics that will increase the current drawn from the supply for its energizing. Healthy transformer response and the simulated faulty transformer response are shown in Figure 5.5.

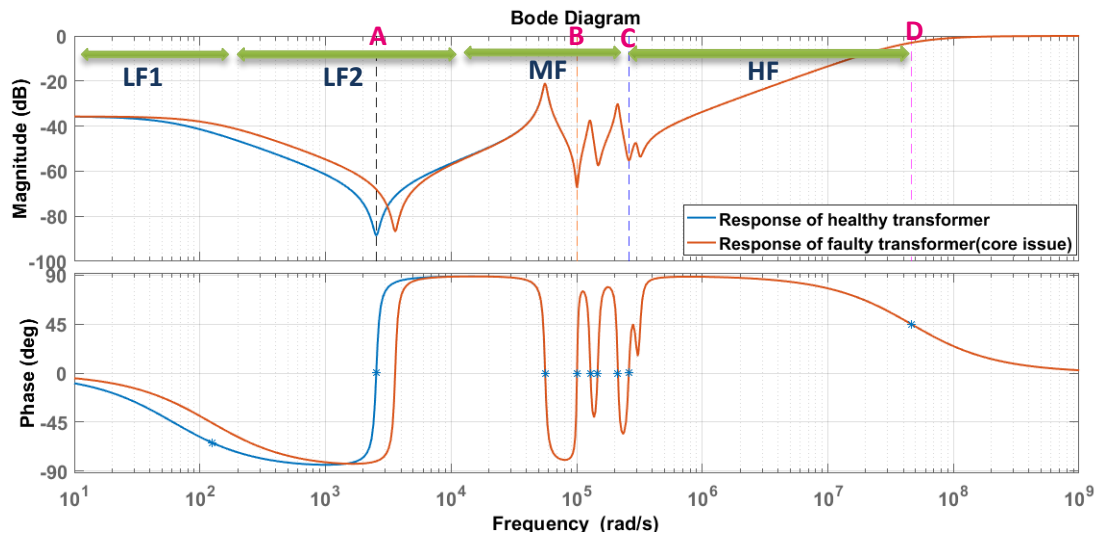


Figure 5.5: pre-fault and post-fault (core fault) Frequency response

In High frequency and medium frequency regions, no variations are present. The only variation that can be seen is the shift of the resonance point in low frequency region (between $10^3 - 10^4 \text{ rad/s}$) to a higher frequency. Referring to the Table 5.1, the fault can be confirmed as “core problem”.

Again, the simulated reference curve is validated by actual response shown in

Figure 5.6. The fault was diagnosed as core issue by visual inspection. This validates the reference curve generated from simulation by having a similar variation of post-fault and pre-fault responses. By deriving reference curves changing the percentage deviation of magnetizing inductance and comparing with post-fault curves, severity of the core issue can be determined.

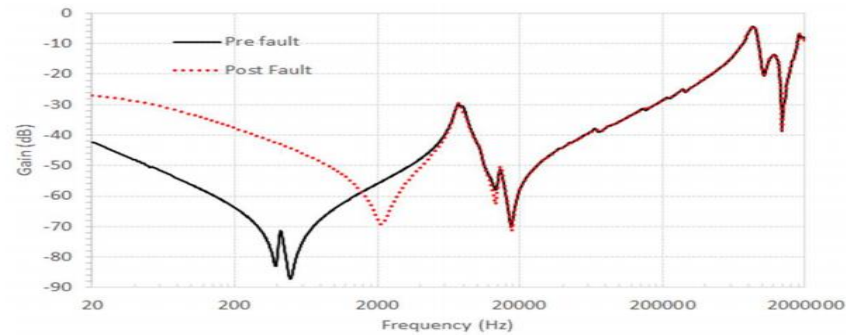


Figure 5.6: Comparison of Pre-fault and post-fault, HV, B phase, SFRA [60]

5.3.3 Earth faults

During winding earth fault, part of the source current deviates to the earth due to the reduction of ground resistance. Inter-turn faults pertaining for a long time and insulation ageing are the two main sources of earth faults of power transformers. Occasionally, moving parts like tap changer, connecting cables also result in earth faults. Residual ground fault protection, zero sequence sensors and placement of current transformer on grounded neutral (with relay) are major earth fault detection schemes of transformers [61]. Even though earth faults are not clearly distinguishable in its response, SFRA can be used to detect these faults with a profound analysis.

Earth fault can be simulated by short-circuiting the windings and ground through a resistor. As a case study, earth fault is simulated by connecting a resistor of 5000Ω in parallel with CG_3 as shown in Figure 5.7(a). Corresponding frequency response is shown in Figure 5.7(b). Compared with variations in low frequency regions (LF1 and LF2), few deviations can be observed in high and medium frequency ranges. Change in the ground resistance has made the curve to be flat at low frequency region. Apart from this decline in resonance magnitude, it has produced a phase shift towards low frequencies. Referring to the Table 5.1, the fault can be confirmed as “SC to

ground”.

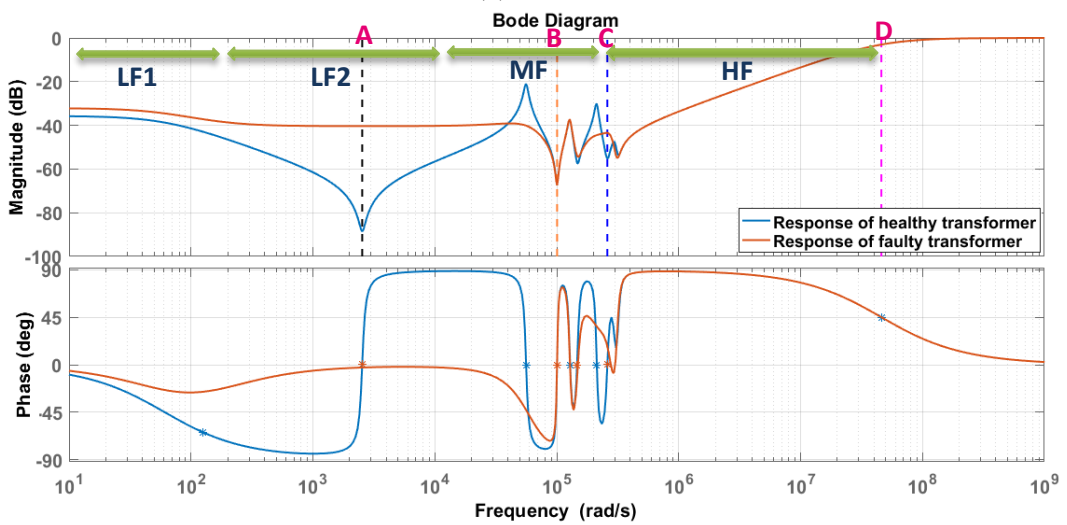
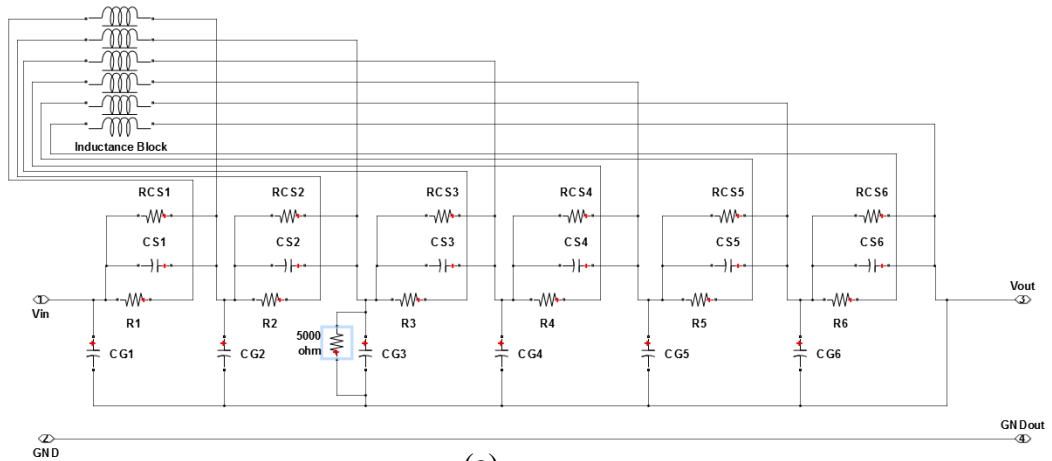


Figure 5.7: (a) simulating earth fault by adding parallel resistance (b) pre fault and post fault Frequency response

Figure 5.8 shows an actual response, measured from Doble M5100 Sweep Frequency Response Analyser, of a 5 MVA transformer diagnosed with ground fault and it validates simulated results. The ground fault current has affected both Y and B phases as both of them have flatter responses in low frequency region. This constant frequency range in which no resonance point is observable provides a better way of identifying ground faults than the shift of resonances (because resonance points are not observable even if they exist).

By changing the ground resistance and its location, set of reference curves can

be developed. Such curves can be used to isolate the ground fault location and determine its severity

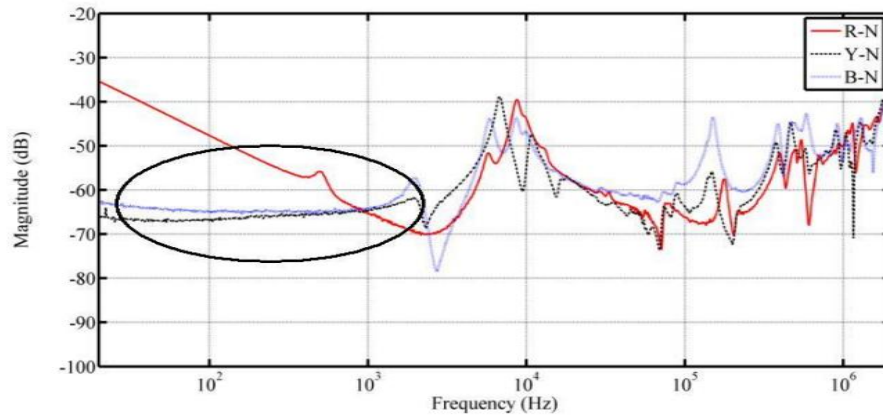


Figure 5.8: Comparison of Pre-fault and post-fault responses of 5 MVA, 3 phase transformer [66]

5.3.4 Conductor tilting/ winding buckling

Usually, internal short circuit conditions of transformer impact on its solid insulation system (paper/pressboard) while the external through-fault short circuit conditions impact on transformer by exerting electro-dynamic forces on windings [62]. These forces result in radial winding movements (generated forces in external windings act from within and act on internal windings inwardly) [63] causing winding buckling and tilting. Currently, SFRA is considered as best option to detect these mechanical faults.

Structural variations due to these faults can be attributed to variations of its ground capacitances. In fact, tilting and buckling reduce the effective distance from winding to earth (or to transformer core) resulting respective capacitance created by oil and paper/pressboard insulation to be more than their normal condition values (equivalent capacitance at a given node is the parallel equivalent value of all the capacitances around the conductor. When capacitance at one side reduces due to tilting, it's opposite side capacitance will increase as the distance from the node to core increases. But, the equivalent capacitive value increases as capacitances are in parallel). The difference of tilting and buckling is tilting effects winding as a whole and buckling is moreover a localized effect that impacts on a single or few sections of

transformer winding. Therefore to simulate tilting, every ground capacitance value can be increased and a single ground capacitance can be increased to simulate buckling.

As a case study, reference SFRA curve for tilting is generated by increasing all ground capacitances of the model by two times (200%), as shown in Figure 5.9.

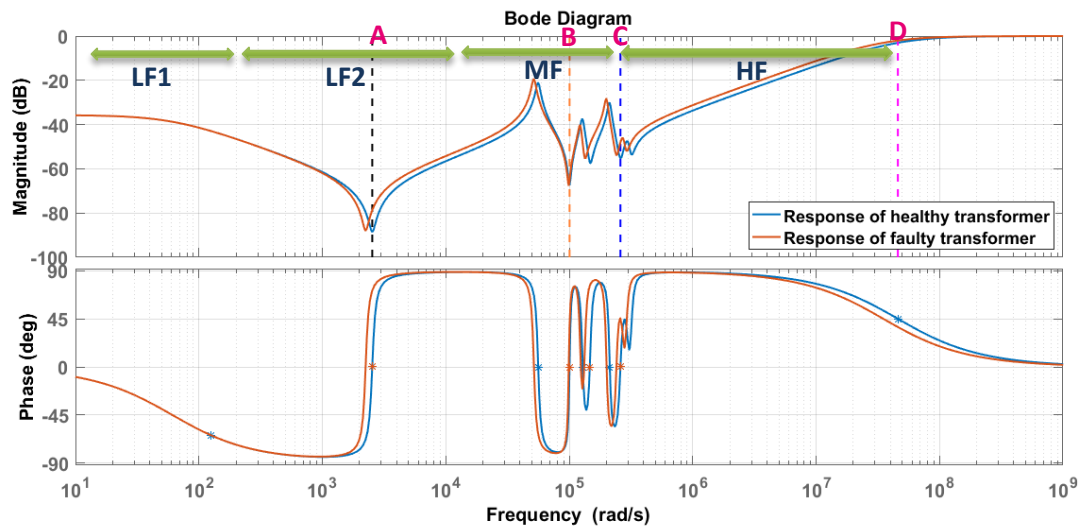


Figure 5.9: Simulating conductor tilting by increasing the ground capacitances

In all three frequency ranges, a shift of resonances to the lower frequency can be observed. Referring to Table 5.1, the fault can be confirmed as “conductor tilting”. To validate this, an actual frequency response of a transformer in which the fault was diagnosed as conductor tilting, is presented in Figure 5.10. Same as the simulated response, resonances are shifted towards lower frequency.

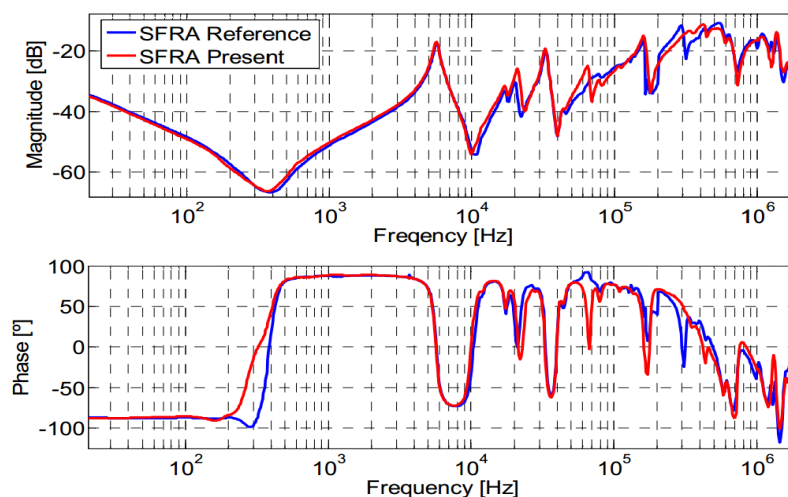


Figure 5.10: Frequency response of 230kV transformer before and after conductor tilting [9]

Multiple curves can be generated by varying its capacitance value as Figure 5.11 which can be used to infer its fault severity level.

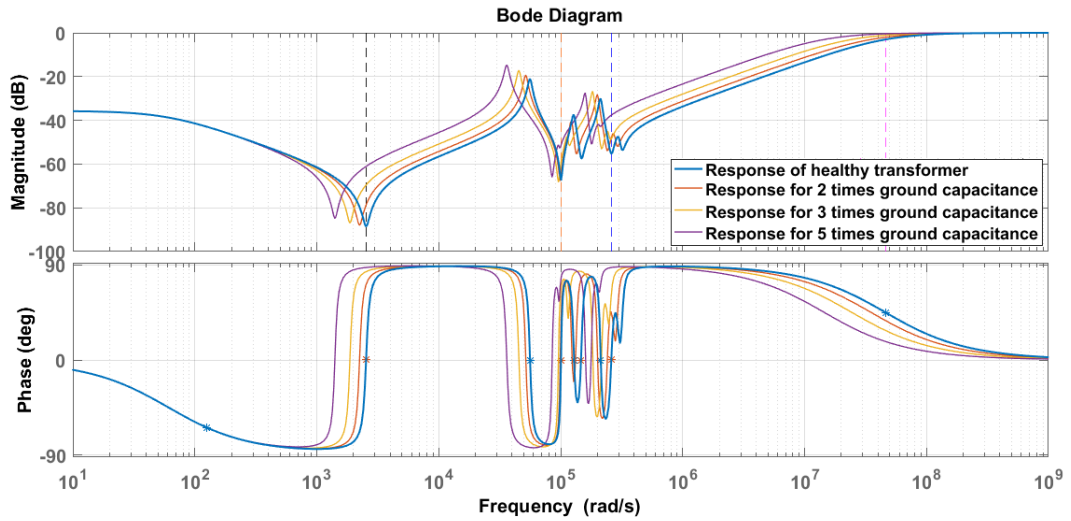


Figure 5.11: Reference frequency responses of tilting/buckling (for different severity levels)

5.3.5 Insulation ageing

Even though this is not considered as a fault, the quality of insulation is a very important factor of transformer condition as bad quality insulation causes numerous other faults such as inter-turn faults [64]. Normally, the power transformer's insulation system is made of organic materials (Insulation paper/pressboard are made of cellulose and insulation oil used for most of the transformers are mineral oil). Therefore, the quality of insulation system reduces over time with the degradation of cellulosic materials due to pyrolysis, hydrolysis and oxidation [65]. In electrical terms, ageing of insulation reduces effective permittivity of the medium that in turn results in lower capacitance.

Therefore insulation ageing is replicated by reducing capacitances of every capacitor inside the model as shown in Figure 5.12. For this case, capacitance values have been reduced by half.

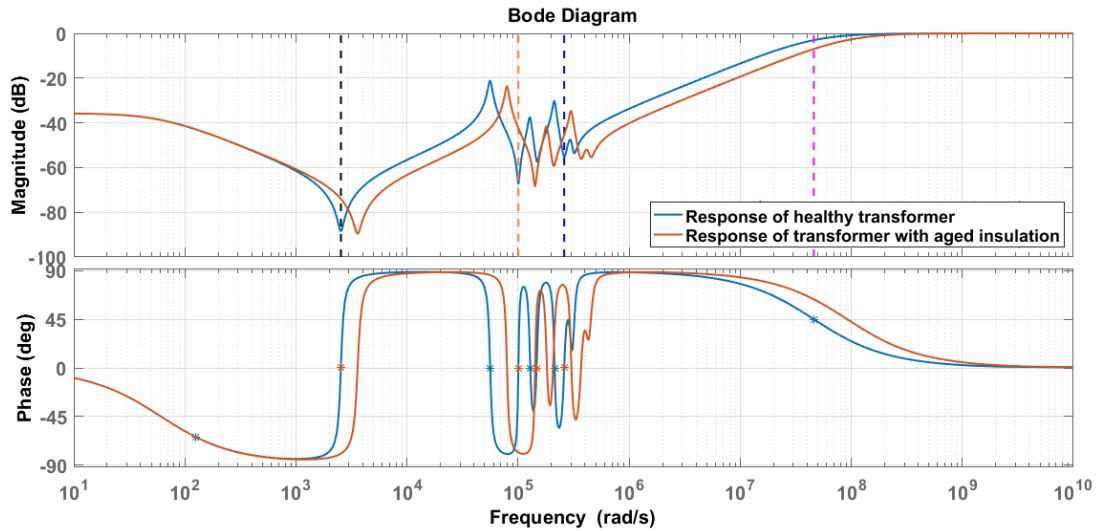


Figure 5.12: Simulating insulation ageing by reducing capacitances

To confirm this reference curve, the frequency response of transformer with and without oil can be used as illustrated in Figure 5.13. As depicted by the figure, adding insulation oil which has a higher permittivity than air, replaces capacitances of the equivalent circuit with relatively higher values. This causes the entire response to shift towards lower frequencies with the shape being almost identical.

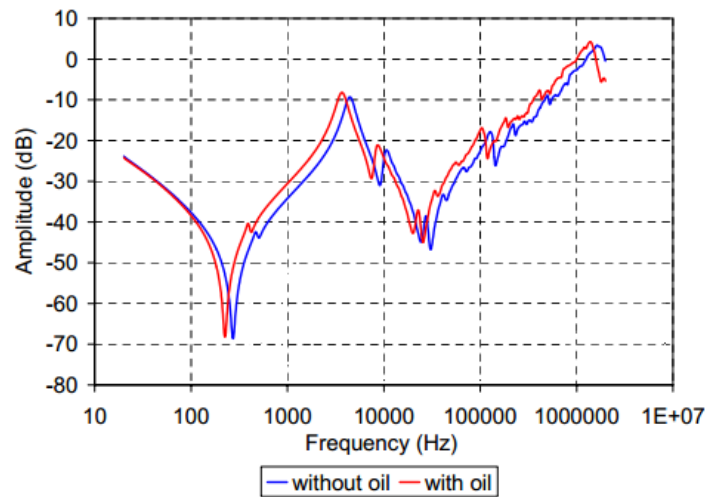


Figure 5.13: Frequency response of 400MVA transformer with and without insulation oil [67]

In other words, the decrease of capacitance values should shift the curve towards higher frequencies. This validates the generated reference curve as the reduction of capacitances due to ageing has shifted the curve (in Figure 5.12) towards

higher frequencies

If this method is utilised to check the insulation paper quality, SFRA test has to be performed and results should be compared after its oil filtration. Otherwise, it will lead to miscalculations of insulation paper quality. Moreover, the relation between the amount of shift and effective age can be investigated by performing an accelerated ageing test for the transformer in a laboratory.

5.4 Conclusions

This chapter presents the derivation of reference curves for transformer fault types and ageing. Generated reference curves for the faults are validated using SFRA responses of faulty transformers and fault interpretation rules used in the industry.

A fault (or incipient fault) changes the mechanical structure of a transformer or the characteristics of transformer elements such as tensile strength of insulation paper and permittivity of transformer oil. This is used as the argument in developing reference curves. In other words, the reference curves are derived by changing the circuit structure or changing the parameter values. Amount of variation of parameters is attributed to the fault severity whereas the location of the changed parameter is attributed to fault location. Therefore, deriving curves by changing parameters at different levels with different locations, fault severity determination and fault localisation can be achieved.

Results can be validated with the help of prototypes of transformers. For an example, the effect of ageing can be examined by an accelerated ageing test. Modelling of the lumped parameter equivalent circuit before and after this artificial ageing will reveal the real effect of ageing to the parameter values. An advanced investigation regarding fault severity and fault location has to be performed before the generated reference curves are used in fault detection process.

Chapter 6

CONCLUSION AND FUTURE WORK

The power transformer is one of the most expensive and vital component in electrical power networks. Most of these devices have been in operation for many years are approaching their expected lifetime. These equipment undergo various electrical and mechanical stresses during their operation that can cause structural deformations resulting major breakdowns of transformers. Not only the capital losses but also economic losses are enormous in case of accidental transformer outages. Also these outages adversely impact on the stability and reliability of power grids. Therefore condition monitoring of power transformers has become an essential aspect that maintains the quality and the reliability of a power supply.

Types of transformer failures can be categorized into two, as electrical failures and mechanical failures. There are various techniques to detect these two categories, but most of them are capable of diagnosing a single fault type. With the advancement of power electronics, the area of condition monitoring has enhanced with the introduction of new techniques with more capabilities and higher accuracy. Sweep frequency response analysis (SFRA) is one such technique that is capable of identifying a range of failures including both electrical and mechanical defects. The response of a transformer to a sweep signal is measured in this test in which the results are presented in terms of amplitude and phase plots called “Bode plots”. Comparing with a reference plot, the results obtained from the tests are analysed and interpreted as the variations of graphs are attributed to parameter changes of the transformer structure. The major drawback of this method is that the process should be handled by an expert in the subject. As a solution, usage of transformer models derived from SFRA is suggested in this thesis, where fault detection is performed using the degree of model’s parameter value variations instead of comparing two graphs.

This thesis presents a novel approach to model the equivalent circuit of power

transformers using SFRA. The proposed method consists of two steps: The transfer function estimation and synthesis of equivalent circuit. A novel algorithm based on Levy and Sanathanan-Koerner methods has been proposed to convert SFRA into transfer functions which are synthesised by an integrated approach of ANN and GA. As the proposed method accurately and efficiently estimates the equivalent circuits of power transformers, resultant models can be incorporated in condition monitoring of power transformers using SFRA.

An outline of this thesis is given below.

1. A novel algorithm to estimate the transfer of power transformers is proposed that can be used to estimate the entire transfer function of a power transformer with high accuracy. Mathematical relations used by two constituent methods (Levy and Sanathanan-Koerner methods) are investigated in detail. Application of proposed algorithm was demonstrated using a case study of actual transformer under operating condition in Sri Lanka.
2. A new approach based on ANN and GA is proposed to derive the lumped parameter equivalent circuit of power transformers. A detailed study was carried out to assess the usability of these two methods in parameter estimation. Optimum options of ANN and GA, objective function of GA, fitting function of GA were derived to achieve the best results in an efficient manner. Effects of the results due to test types and transformer phases were also studied.
3. A detailed investigation was carried out to discover the factors affecting SFRA of power transformers. Reference curves of common fault types were simulated by changing parameter values attributed to the factors identified. Resultant reference curves were validated using actual SFRA responses of power transformers.

6.1 Conclusions

In this thesis, the lumped parameter network modelling approach, one of the Gray-box modelling methods has been used for the modelling transformer equivalent

circuit. Comparing with other modelling approaches, the main advantage of these type of models is the ability to physically interpret resultant model components with respect to the components inside the transformer. This feature is a necessary aspect for the models that are used to interpret actual transformer faults.

It is required to transform gathered graphical data from frequency response analysers into a numerical quantity before equivalent circuit modelling. The transfer function in Laplace domain is the best candidate for this purpose as these Bode plots are also in the same frequency domain. Even though there are well-established techniques available in the literature, they cannot be directly used in this conversion due to the complexity of transformer frequency response. Therefore, a novel algorithm based on Levy and Sanathanan-Koerner method has been proposed in this thesis which can be used to estimate the entire transfer function of a power transformer. Estimation of transfer function as a single quantity was one of the challenges in modelling power transformers and that was well addressed by this novel algorithm.

Modelling lumped parameter network has been performed using two techniques: Artificial neural network (ANN) and Genetic algorithm (GA). Each of these methods has individual pros and cons but as a combined method, they offer accurate results. The novel approach of utilizing both these methods to estimate parameters of the equivalent circuit has been presented as a method with 3 major steps. In fact, ANN is used to derive an initial approximation for the GA method. Due to the exclusion of parallel resistances (R_{cs_i}) and mutual inductances (M_{ij}) in the ANN, estimated response in the first step is different from the actual values which is rectified by reducing winding resistance values in the middle step. In the last step, the final lumped parameter network is estimated by GA incorporating all the excluded parameters in previous steps. If ANN or GA is used alone without this sort of integration, processing time would be relatively very large other than large errors in the estimation. Especially, it requires dedicated digital computers with high processing power and data handling capacities which brings up a large additional cost if such method is implemented in the industry.

Reference curves for common fault types are also presented in this thesis. These can be incorporated in the fault detection process to detect faults more accurately. There are two key benefits of these reference curves, those are the fault severity determination and fault localization. Reference curves for different severity levels can be derived by changing the values of parameters whereas changing values of different model parameters give a set of reference curves that can be used to isolate the exact locations of faults (localize). Basic variations of curves depending on the fault types are simulated and validated using fault interpretation rules and actual responses.

The general equivalent circuit that has been used for a long time can be replaced by the lumped parameter equivalent circuit modelled using the proposed method. During the design stage of power networks, these models can be used for the power transformer that will result in better simulation outputs. In addition, the usage of lumped parameter network model opens a whole new chapter in transient analysis. By replacing general equivalent circuit with the proposed model, the accuracy of transient analysis results can be significantly enhanced owing to the fact that high frequency behaviour that couldn't be properly represented is simulated perfectly with the help of lumped parameter network. Since every step of the proposed method, from performing SFRA to deriving lumped parameter network, has been implemented in terms of coding in MATLAB software, the method can be automated. This enables the method to be used in on-site fault diagnosis.

6.2 Future works

Even though the model can estimate the transformer behaviour with a high accuracy, further improvements can be done before the method is going to be implemented in the power system for the condition monitoring of power transformers.

1. Effect of high frequency resonances to the final model that were excluded during order-reduction process should be investigated.
2. During the derivation of equivalent circuit, basic ANN structure has been used where number of hidden layers and its hidden neurons has to be defined by the

user. Using a dedicated computer with high processing power, this process can be automated to find the best combination.

3. The results can be confirmed using actual prototypes of transformers under laboratory conditions.

References

- [1] A. P. Kaur, A. Helwig and N. Das, "SFRA transformer reliability engineering modelling for undergraduates," in *2016 Australasian Universities Power Engineering Conference (AUPEC)*, Brisbane, 2016.
- [2] Cigre Working Group A2.37, Transformer Reliability Survey, *Electra*, no. 261, p. 48-49.
- [3] A. Kraetge, M. Krüger, J. L. Velásquez, M. Heindl, and S. Tenbohlen, "Experiences with practical application of Sweep Frequency Response Analysis (SFRA) on power transformers," in *Proc. of the 16th International Symposium on High Voltage Engineering © 2009 SAIEE*, Johannesburg, 2009.
- [4] *IEEE Guide for the Application and Interpretation of Frequency Response Analysis for Oil-Immersed Transformers*, IEEE Std C57.149, 2012.
- [5] F. Predl, "Interpretation of Sweep Frequency Response Analysis (SFRA) Measurement Results," in *Techcon Asia-Pacific 2016*, Sydney, 2016.
- [6] D. K. Xu, C. Z. Fu and Y. M. Li, "Application of artificial neural network to the detection of the transformer winding deformation," in *1999 Eleventh International Symposium on High Voltage Engineering*, London, 1999.
- [7] A. Contin, G. Rabach, J. Borghetto, M. D. Nigris, R. Passaglia and G. Rizzi, "Frequency-response analysis of power transformers by means of fuzzy tools," *IEEE Transactions on Dielectrics and Electrical Insulation*, vol. 18, no. 3, pp. 900-909, June 2011.
- [8] P. M. Joshi and S. V. Kulkarni, "Transformer winding diagnostics using deformation coefficient," in *2008 IEEE Power and Energy Society General Meeting - Conversion and Delivery of Electrical Energy in the 21st Century*, Pittsburgh, 2008.
- [9] J. C. Gonzales and E. E. Mombello, "Automatic detection of frequency ranges of power transformer transfer functions for evaluation by mathematical indicators," in *2012 Sixth IEEE/PES Transmission and Distribution: Latin*

America Conference and Exposition (T&D-LA), Montevideo, 2012.

- [10] P. Vaessen, "Transformer model for high frequencies," *IEEE Trans. Power Del.*, vol. 3, no. 4, p. 1761–1768, Oct. 1988.
- [11] A. Morched, L. Marti, and J. Ottewangers, "A high frequency transformer model for the EMTP," *IEEE Trans. Power Del.*, vol. 8, no. 3, p. 1615–1626, Jul. 1993.
- [12] K. Ragavan and L. Satish, "Construction of Physically Realizable Driving-Point Function From Measured Frequency Response Data on a Model Winding," *IEEE Transactions on Power Delivery*, vol. 23, no. 2, pp. 760-767, April 2008.
- [13] V. Rashtchi, E. Rahimpour and E.M. Rezapour, "Using a genetic algorithm for parameter identification of transformer R-L-C-M model," *Electrical Engineering*, vol. 88, no. 5, pp. 417-422, 2006.
- [14] G. B. Gharehpetian, H. Mohseni, and K. Moller, "Hybrid modeling of inhomogeneous transformer windings for very fast transient overvoltage studies," *IEEE Transactions on Power Delivery*, vol. 13, no. 1, p. 157–163, Jan. 1998.
- [15] *Measurement of frequency response*, IEC 60076-18, 2012.
- [16] V Behjat, A Vahedi, A Setayeshmehr, H Borsi and E Gockenbach, "Identification of the most sensitive frequency response measurement technique for diagnosis of interturn faults in power transformers," *Meas. Sci. Technol.* 21, vol. 21:1–14, 2010.
- [17] S. Tenbohlen and S. A. Ryder, "Making frequency response analysis measurements: a comparison of the swept frequency and low voltage impulse methods," in *XIIIth International Symposium on High Voltage Engineering*, Netherlands, 2003.
- [18] J. C. Gonzales and E. E. Mombello, "Fault Interpretation Algorithm Using Frequency-Response Analysis of Power Transformers," *IEEE Transactions on Power Delivery*, vol. 31, no. 3, pp. 1034-1042, June 2016.
- [19] A. A. ElFaraskoury, "Experiences of Sweep Frequency Response Analyser for

- the Diagnosis of Transformer Winding Damage,” in *17th International Middle-East Power System Conference (MEPCON'15) Mansoura University, Egypt*, 2015.
- [20] R. D. Jiwane, “Detection Of Mechanical Faults On Transformer Winding,” in *International conference on computing, communication and energy systems*, India, 2016.
- [21] E. Dick and C. Erven, “Transformer Diagnostic Testing by Frequency Response Analysis,” *IEEE Transactions on Power Apparatus and Systems*, Vols. PAS-97, no. 6, pp. 2144-2153, 1978.
- [22] K. P. Badgujar, M. Maoyafikuddin and S. V. Kulkarni, “Alternative statistical techniques for aiding SFRA diagnostics in transformers,” *IET Generation, Transmission & Distribution*, vol. 6, no. 3, pp. 189-198, March 2012.
- [23] Y. Shibuya, S. Fujita and N. Hosokawa, “Analysis of very fast transient overvoltage in transformer winding,” *IEE Proceedings - Generation, Transmission and Distribution*, vol. 144, no. 5, pp. 461-468, Sept. 1997.
- [24] K. Ragavan and L. Satish, “Localization of Changes in a Model Winding Based on Terminal Measurements: Experimental Study,” *IEEE Transactions on Power Delivery*, vol. 22, no. 3, pp. 1557-1565, July 2007.
- [25] G. Joginadham, H. A. Mangalvedekar and A. Venkatasami, “Development of networks for SFRA data using circuit synthesis,” in *2008 International Conference on Condition Monitoring and Diagnosis*, Beijing, 2008.
- [26] D. M. Sofian, Z. D. Wang and P. Jarman, “Interpretation of transformer FRA measurement results using winding equivalent circuit modelling technique,” in *CEIDP '05. 2005 Annual Report Conference on Electrical Insulation and Dielectric Phenomena*, Nashville, TN, USA, 2005.
- [27] S. P. Ang, J. Li, Z. Wang and P. Jarman, “FRA low frequency characteristic study using duality transformer core modeling,” in *2008 International Conference on Condition Monitoring and Diagnosis*, Beijing, 2008.
- [28] M.R. Barzegaran, M. Mirzaie, A. S. Akmal, “Frequency Response Analysis in Power Transformer for Detection of Winding Short-circuit using Quasi-static

- Finite Element and Circuit-based Method,” *World Applied Sciences Journal*, vol. 7, no. 8, pp. 1006-1015, 2009.
- [29] P. Mukherjee and L. Satish, “Construction of Equivalent Circuit of a Single and Isolated Transformer Winding From FRA Data Using the ABC Algorithm,” *IEEE Transactions on Power Delivery*, vol. 27, no. 2, pp. 963-970, April 2012.
- [30] M. Bigdeli, D. .Azizian, H Bakhshi and E. Rahimpour, “Identification of Transient Model Parameters of Transformer Using Genetic Algorithm,” in *2010 International Conference on Power System Technology*, Hangzhou, China, 2010.
- [31] M. S. Chaouche, H. Houassine, S. Moulahoum and I. Colak, “BA to construction of equivalent circuit of a transformer winding from frequency response analysis measurement,” *IET Electric Power Applications*, vol. 12, no. 5, pp. 728-736, 2018.
- [32] A. Shintemirov, W.J. Tang, W.H. Tang and Q.H. Wu, “Improved modelling of power transformer winding using bacterial swarming algorithm and frequency response analysis,” *Electric Power Systems Research*, vol. 80, no. 9, pp. 1111-1120, 2010.
- [33] M. A. Eldery, E. F. El-Saadany and M. M. A. Salama, “Parameters Identification of Sectional Winding High Frequency Transformer Model Using Neural Network,” in *2003 46th Midwest Symposium on Circuits and Systems*, Cairo, 2003.
- [34] G. M. V. Zambrano, A. C. Ferreira and L. P. Caloba, “Power transformer equivalent circuit identification by artificial neural network using frequency response analysis,” in *2006 IEEE Power Engineering Society General Meeting*, Montreal, Que., 2006.
- [35] D. L. Alvarez, J. A. Rosero and E. E. Mombello, “Circuit model of transformers windings using vector fitting, for frequency response analysis (FRA),” in *2013 Workshop on Power Electronics and Power Quality Applications (PEPQA)*, , Bogota, 2013.
- [36] K. F. Man, K. S. Tang and S. Kwong,, “Genetic Algorithms: Concepts and

- Applications,” *IEEE Transactions on Industrial Electronics*, vol. 43, no. 5, pp. 519-534, Oct. 1996.
- [37] “MATLAB User’s Guide,” The Mathworks, 2018.
- [38] E. C. Levy, “Complex-curve fitting,” *IRE Transactions on Automatic Control*, Vols. AC-4, no. 1, pp. 37-43, May 1959.
- [39] A. O. Soysal and A. Semlyen, “Practical transfer function estimation and its application to wide frequency range representation of transformers,” *IEEE Transactions on Power Delivery*, vol. 8, no. 3, pp. 1627-1637, July 1993.
- [40] C. Sanathanan and J. Koerner, “Transfer function synthesis as a ratio of two complex polynomials,” *IEEE Transactions on Automatic Control*, vol. 8, no. 1, pp. 56-58, January, 1963.
- [41] P. Payne, “An improved technique for transfer function synthesis from frequency response data,” *IEEE Transactions on Automatic Control*, vol. 154, no. 4, pp. 480-483, Aug 1970.
- [42] A. K. Kamath et al., “Modeling of transformer characteristics using fractional order transfer functions,” in *2009 IEEE International Conference on Control and Automation*, Christchurch, 2009 .
- [43] K. L. I. M. Pramod B. Jayarathna, W. E. P. Sampath Ediriweera, J. R. Lucas and R. Samarasinghe, “Modelling Transfer Function of Power Transformers Using Sweep Frequency Response Analysis,” in *2018 Moratuwa Engineering Research Conference (MERCOn)*, Moratuwa, 2018.
- [44] D. Valrio and J. S Da Costa, “Levy’s identification method extended to commensurate fractional order transfer functions,” in *Fifth EUROMECHNonlinear Dynamics conference*, Eindhoven, 2005.
- [45] U.A.Bakshi and S.C.Goyal, *Principles of Control Systems*, India: Technical Publications, 2008.
- [46] E. Bjerkan, "High frequency modeling of power transformers: Stresses and Diagnostics", Ph.D. Dissertation, Norwegian university of science and technology, May 2005.
- [47] K. R. Gandhi and K. P. Badgajar, “Artificial neural network based

- identification of deviation in frequency response of power transformer windings,” in *2014 Annual International Conference on Emerging Research Areas: Magnetics, Machines and Drives (AICERA/iCMMMD)*, Kottayam, 2014.
- [48] “MATLAB ANN toolbox,” MATLAB®, Mathwork Ltd., [Online]. Available: <https://www.mathworks.com/discovery/neural-network.html>.
- [49] “Genetic Algorithm,” MATLAB®, Mathwork Ltd.. [Online].
- [50] S. Bagheri , R. Efftejad and A. Salami , “ Transformer Winding Parameter Identification based on Frequency Response Analysis using Hybrid Wavelet Transform (WT) and Simulated Annealing Algorithm (SA) and Compare with Genetic Algorithm (GA),” *Indian Journal of Science and Technology*, vol. 7, no. 5, pp. 614-621, May, 2014.
- [51] U. Sharma, S. Chatterjee and K. Bhuyan, “Development of reference SFRA plot of transformer at design stage using high frequency modelling,” in *2012 1st International Conference on Power and Energy in NERIST (ICPEN)*, Nirjuli, 2012.
- [52] “MATLAB GA Toolbox,” MATLAB®, Mathwork Ltd., [Online]. Available: <https://www.mathworks.com/help/gads/genetic-algorithm.html>.
- [53] V. Behjat, A. Vahedi, A.Setayeshmehr, H. Borsi and Ernst Gockenbach, “Sweep frequency response analysis for diagnosis of low level short circuit faults on the windings of power transformers: An experimental study,” *International Journal of Electrical Power & Energy Systems*, vol. 42, no. 1, pp. 78-90, November 2012.
- [54] S. Alsuhaibani, Y. Khan, Beroual, M. Abderrahmane and N. Hussain, “A review of frequency response analysis methods for power transformer diagnostics,” *Energies*, vol. 9, no. 11, pp. 1-17, Nov 2016.
- [55] J. C. Olivares-Galvan, R. Escarela-Perez, E. Campero-Littlewood, F. de Leon and C. A. Cruz, “Separation of core losses in distribution transformers using experimental methods,” *Canadian Journal of Electrical and Computer Engineering*, vol. 35, no. 1, pp. 33-39, Winter 2010.
- [56] M. F. Bin Mohd Yousof, "*Frequency Response Analysis for Transformer*

- Winding Condition Monitoring*", Ph.D. Dissertation, School of Information Technology and Electrical Engineering, University of Queensland, 2015.
- [57] T. Mariprasath and V. Kirubakaran, "Power Transformer Faults Identification using SFRA," *International Journal of Scientific & Engineering Research*, vol. 5, no. 5, pp. 581-587, May, 2014.
- [58] R. S. Bhide, M. S. S. Srinivas and I. Voloh, "Detection of inter-turn fault in transformers at incipient level," in *2014 International Conference on Electrical Machines (ICEM)*, Berlin, 2014.
- [59] R. Prudhvi Raj, "Transformer Core Fault Detection and Control," *Advances in Electronic and Electric Engineering*, vol. 3, no. 4, pp. 485-490, 2013.
- [60] G. A. T. N. Aravinda, K. Bandara, G. A. Jayantha, J. R. S. S. Kumara and M. A. R. M. Fernando, "Application of SFRA techniques to discriminate short circuit faults of transformer winding," in *2017 IEEE International Conference on Industrial and Information Systems (ICIIS)*, Peradeniya, 2017.
- [61] G. Energy, "geindustrial," [Online]. Available: <http://apps.geindustrial.com/publibrary/checkout/LAPL0084?TNR=Articles%7CLAPL0084%7CPDF&filename=LAPL0084.pdf>. [Accessed 4 oct 2018].
- [62] M. Bagheri, M.S. Naderi, T Blackburn and T. Phung, "Case study on FRA capability in detection of mechanical defects within a 400MVA transformer," *CIGRE, Paris, France*, pp. 1-9, 2012.
- [63] M. Florkowski and J. Furgał, "Transformer winding defects identification based on a high frequency method," *Measurement Science and Technology*, vol. 18, no. 9, p. 1986–1992, July, 2007.
- [64] M. Bagheri, B. Stojcevski and B. T. Phung, "Frequency response technique to recognize turn-to-turn insulation deterioration in transformer winding," in *016 IEEE International Conference on Power and Renewable Energy (ICPRE)*, Shanghai, 2016.
- [65] D. Allan, C. Jones and B. Sharp, "Studies of the condition of insulation in aged power transformers. 1. Insulation condition and remnant life assessments for in-service units," in *3rd International Conference on Properties and*

Applications of Dielectric Materials, tokyo, 1991.

- [66] S. Rai and N.P. Gupta, "SFRA, Detect Of Winding Deformation in Power Transformer," *IOSR Journal of Electrical and Electronics Engineering (IOSR-JEEE)*, vol. 9, no. 6, pp. 53-57, dec, 2014.
- [67] C. W. G. A2.26, *Mechanical Condition Assessment of Transformer Windings Using Frequency Response Analysis (FRA)*, paris: Brochure, 2008.

Appendix A: MATLAB code of Levy method estimation

```
for nnn=1:25
    for ppp=1:25
load('mahoNY_NR-NB_data.mat');
load('max_min_and_middle_points');

pause(1);

%select R,Y or B phase
Freq_selected=freq_NY4;
mag_selected=mag_NY4;
phase_selected=phase_NY4;

s=tf('s');;% select pole zero comination
num_pz_numer=ppp
num_pz_den=nnn;

a=125;b=midpoint_array_in_radians(5); % select region limits

index_bw_given_values=find( Freq_selected>= a/(2*pi) & Freq_selected
<= b/(2*pi));
gain=power(10,(mag_selected(index_bw_given_values)/20));
response =
gain.*exp(1j*phase_selected(index_bw_given_values)*pi/180);
data = frd(response,Freq_selected(index_bw_given_values).*(2*pi));
mag1111=gain;
phase1111=phase_selected(index_bw_given_values(1:end));
w1111_inrad = Freq_selected.*(2*pi);
w1111=w1111_inrad(index_bw_given_values(1:end));
F=mag1111.*(cos(phase1111*pi/180) + sin(phase1111*pi/180)*i);
R1=real(F);
I1=imag(F);
R=R1 ; I=I1;

L_da =[];
S     =[];
T     =[];
U     =[];

A =zeros(num_pz_numer+1,1);
B =zeros(num_pz_den+1,1);
B(1)=1;% because, B0 is taken as 1
C =zeros(num_pz_numer+num_pz_den+1,1);
N=zeros(num_pz_numer+num_pz_den+1,1);

for cc= 0:2:(2*(num_pz_numer+num_pz_den))
L_da(cc+1,1)=sum(w1111.^cc);
end
for cc= 0:2:(2*(num_pz_numer+num_pz_den))
S(cc+1,1)=sum(w1111.^cc.*R) ;
end
```

```

for cc= 1:2:(2*(num_pz_numer+num_pz_den))
T(cc+1,1)=sum(w1111.^cc.*I);
end
for cc= 2:2:(2*(num_pz_numer+num_pz_den))
U(cc+1,1)=sum(w1111.^cc.*(R.^2+I.^2));
end

M1=zeros(num_pz_numer+1,num_pz_numer+1);
M2=zeros(num_pz_numer+1,num_pz_den);
M3=zeros(num_pz_den,num_pz_numer+1);
M4=zeros(num_pz_den,num_pz_den);

for aa=0:1:num_pz_numer
    for bb=0:1:num_pz_numer
        if mod((aa+1-3),4)==0 || mod((aa+1),4)==0
            M1(bb+1,aa+1)=-L_da(bb+1+aa);
        else
            M1(bb+1,aa+1)=L_da(bb+1+aa);
        end
    end
end

for aa=0:1:num_pz_den-1
    for bb=0:2:num_pz_numer
        if mod((aa+1-1),4)==0
            M2(bb+1,aa+1)=T(bb+2+aa);
            if bb==num_pz_numer
                break;
            end
            M2(bb+2,aa+1)=-S(bb+3+aa);
        elseif mod((aa+1-2),4)==0
            M2(bb+1,aa+1)=S(bb+2+aa);
            if bb==num_pz_numer
                break;
            end
            M2(bb+2,aa+1)=T(bb+3+aa);
        elseif mod((aa+1-3),4)==0
            M2(bb+1,aa+1)=-T(bb+2+aa);
            if bb==num_pz_numer
                break;
            end
            M2(bb+2,aa+1)=S(bb+3+aa);
        else mod((aa+1-4),4)==0
            M2(bb+1,aa+1)=-S(bb+2+aa);
            if bb==num_pz_numer
                break;
            end
            M2(bb+2,aa+1)=-T(bb+3+aa);
        end
    end
end

for aa=0:1:num_pz_numer
    for bb=0:2:num_pz_den
        if mod((aa+1-1),4)==0
            if bb==num_pz_den
                break;
            end
        end
    end
end

```

```

        M3(bb+1,aa+1)=T(bb+2+aa);
        if bb==num_pz_den-1
            break;
        end
        M3(bb+2,aa+1)=S(bb+3+aa);
elseif mod((aa+1-2),4)==0
    if bb==num_pz_den
        break;
    end
    M3(bb+1,aa+1)=-S(bb+2+aa);
    if bb==num_pz_den-1
        break;
    end
    M3(bb+2,aa+1)=T(bb+3+aa);
elseif mod((aa+1-3),4)==0
    if bb==num_pz_den
        break;
    end
    M3(bb+1,aa+1)=-T(bb+2+aa);
    if bb==num_pz_den-1
        break;
    end
    M3(bb+2,aa+1)=-S(bb+3+aa);
else mod((aa+1-4),4)==0
    if bb==num_pz_den
        break;
    end
    M3(bb+1,aa+1)=S(bb+2+aa);
    if bb==num_pz_den-1
        break;
    end
    M3(bb+2,aa+1)=-T(bb+3+aa);
end
end
end

for aa=0:1:num_pz_den-1
    for bb=0:1:num_pz_den-1
        if mod((aa+1-3),4)==0 || mod((aa+1),4)==0
            M4(bb+1,aa+1)=-U(bb+3+aa);
        else
            M4(bb+1,aa+1)=U(bb+3+aa);
        end
    end
end

M1_2 = horzcat(M1,M2);
M3_4 = horzcat(M3,M4);
M_final=vertcat(M1_2,M3_4);

for aa=0:1:num_pz_numer
    if mod(aa,2)==0
        C(aa+1)=S(aa+1);
    else
        C(aa+1)=T(aa+1);
    end
end
end

```

```

for aa=0:1:num_pz_den-1
    C(num_pz_numer+2+aa)=U(aa+2);
end
N=inv(M_final)*C

Numerator=fliplr(N(1:num_pz_numer+1)')
Denominator=fliplr(horzcat([1],N(num_pz_den+2:end)'))
TF_Found=tf(Numerator,Denominator); % Transfer function before
removing high frequency poles and zeros

[mag_found1,phase_found1,w_found1111] = bode(TF_Found);
mag_found1111=squeeze(mag_found1(1,1,:));
phase_found1111=squeeze(phase_found1(1,1,:));

%draw graphs
cla;
opts = bodeoptions('cstprefs');
opts.PhaseWrapping = 'on';

index_to_to_drawgraph=find( Freq_selected>= (a-1e5)/(2*pi) &
Freq_selected <= (b+1e5)/(2*pi));
opts.Xlim=[w1111_inrad(index_to_to_drawgraph(1)),w1111_inrad(index_t
o_to_to_drawgraph(end))];

hhh=bodeplot(TF_Found,opts);
hold on ;
grid on;
legend('show','location','southwest');

plot(w1111_inrad(index_bw_given_values(end)),phase_selected(index_bw_
given_values(end)),'r*');
plot(w1111_inrad(index_bw_given_values(1)),phase_selected(index_bw_g
iven_values(1)),'b*');
gain111=power(10,(mag_selected/20));
response111 = gain111.*exp(1j*phase_selected*pi/180);
data111 = frd(response111,Freq_selected.*(2*pi));
bodeplot(data111);

%find resonance frequencies
syms x;
p_num = poly2sym(Numerator);
p_den=poly2sym(Denominator);
num_factorized=factor(p_num , 'FactorMode', 'real')
den_factorized=factor(p_den , 'FactorMode', 'real')

clear zero_values
clear pole_values

for uu=1:length(num_factorized)
    pp= sym2poly(num_factorized(uu));
    if length(pp)==1
        zero_values(uu).resonantpoint=pp;
        zero_values(uu).type='constant-num';
        zero_values(uu).num_or_den='N';
        zero_values(uu).number_ofthe_poleorzero=uu;
    end
    if length(pp)==2

```

```

        zero_values(uu).resonantpoint=pp(end);
        zero_values(uu).type='single zero-up';
        zero_values(uu).num_or_den='N';
        zero_values(uu).number_ofthe_poleorzero=uu;
    end
    if length(pp)==3
        zero_values(uu).resonantpoint=sqrt(pp(end));
        zero_values(uu).type='double zero-trough';
        zero_values(uu).num_or_den='N';
        zero_values(uu).number_ofthe_poleorzero=uu;
    end
end
end

for uu=1:length(den_factorized)
    pp= sym2poly(den_factorized(uu));
    if length(pp)==1
        pole_values(uu).resonantpoint=pp;
        pole_values(uu).type='constant-den';
        pole_values(uu).num_or_den='D';
        pole_values(uu).number_ofthe_poleorzero=uu;
    end
    if length(pp)==2
        pole_values(uu).resonantpoint=pp(end);
        pole_values(uu).type='single pole-down';
        pole_values(uu).num_or_den='D';
        pole_values(uu).number_ofthe_poleorzero=uu;
    end
    if length(pp)==3
        pole_values(uu).resonantpoint=sqrt(pp(end));
        pole_values(uu).type='double zero-peak';
        pole_values(uu).num_or_den='D';
        pole_values(uu).number_ofthe_poleorzero=uu;
    end
end
end

%sort arrays according to frequency
clear array_to_sorted;
array_to_sorted(:,1)=[zero_values(:).resonantpoint];
array_to_sorted(:,2)=[1:length(zero_values)];
sorted_array= sortrows(array_to_sorted,1);
zero_values_sorted=zeros_values(sorted_array(:,2));

clear array_to_sorted;
array_to_sorted(:,1)=[pole_values(:).resonantpoint];
array_to_sorted(:,2)=[1:length(pole_values)];
sorted_array= sortrows(array_to_sorted,1);
pole_values_sorted=pole_values(sorted_array(:,2));

Allresonance_freq_rad=[zero_values,pole_values];
clear array_to_sorted;
array_to_sorted(:,1)=[Allresonance_freq_rad(:).resonantpoint];
array_to_sorted(:,2)=[1:length(Allresonance_freq_rad)];
sorted_array= sortrows(array_to_sorted,1);

Allresonance_freq_rad_sorted=Allresonance_freq_rad(sorted_array(:,2)
);

```

```

%create transfer function removing high frequency poles and zeros
clear Numer_pz
if index_bw_given_values(1)==1
    [ind,~] = find( [zero_values_sorted(1:end).resonantpoint]' >= 0
& [zero_values_sorted(1:end).resonantpoint]' < b);
else
    [ind,~] = find( [zero_values_sorted(1:end).resonantpoint]' >= a
& [zero_values_sorted(1:end).resonantpoint]' < b);
end

check_cons=find(cellfun('length',regexp({zero_values_sorted(:).type}
,'constant-num')) == 1)

if isempty(ind)==1 ||
strcmp(zero_values_sorted(check_cons).type,'constant-num')==1 &&
ind(1)~=check_cons;
    ind=vertcat(check_cons,ind);
end
Numer_pz(:,1)=[zero_values_sorted(ind).number_ofthe_poleorzero];
unused_pz =
setdiff([zero_values_sorted(:).number_ofthe_poleorzero],Numer_pz');

factor_ofconstant_num=1;
for uu=1:length(unused_pz)
    pp=sym2poly(num_factorized(unused_pz(uu)));
    if length(sym2poly(num_factorized(unused_pz(uu))))==2
        factor_ofconstant_num=factor_ofconstant_num*polyval(pp,1);
    end
    if length(sym2poly(num_factorized(unused_pz(uu))))==3
        factor_ofconstant_num=factor_ofconstant_num*polyval(pp,1);
    end
end

    Numerator_aftr_rmved_othrfeq=num_factorized(Numer_pz);

Numerator_aftr_rmved_othrfeq(1)=poly2sym(sym2poly(Numerator_aftr_rmve
ed_othrfeq(1))*factor_ofconstant_num);

clear den_pz

if index_bw_given_values(1)==1
    [ind,~] = find( [pole_values_sorted(1:end).resonantpoint]' >= 0
& [pole_values_sorted(1:end).resonantpoint]' < b);
else
    [ind,~] = find( [pole_values_sorted(1:end).resonantpoint]' >=
a & [pole_values_sorted(1:end).resonantpoint]' < b);
end

check_cons=find(cellfun('length',regexp({pole_values_sorted(:).type}
,'constant-den')) == 1)

if isempty(ind)==1
||strcmp(pole_values_sorted(check_cons).type,'constant-den')==1 &&
ind(1)~=check_cons;
    ind=vertcat(check_cons,ind);
end

```

```

den_pz(:,1)=[pole_values_sorted(ind).number_ofthe_poleorzero];
unused_pz =
setdiff([pole_values_sorted(:).number_ofthe_poleorzero],den_pz');

factor_ofconstant_den=1;
for uu=1:length(unused_pz)
    pp=sym2poly(den_factorized(unused_pz(uu)));
    if length(sym2poly(den_factorized(unused_pz(uu))))==2
        factor_ofconstant_den=factor_ofconstant_den*polyval(pp,1);
    end
    if length(sym2poly(den_factorized(unused_pz(uu))))==3
        factor_ofconstant_den=factor_ofconstant_den*polyval(pp,1);
    end
end
Denominator_aftr_rmved_othrfreq=den_factorized(den_pz);

Denominator_aftr_rmved_othrfreq(1)=poly2sym(sym2poly(Denominator_aftr_
_rmved_othrfreq(1))*factor_ofconstant_den);

bodeplot(tf(sym2poly(prod(Numerator_aftr_rmved_othrfreq)),sym2poly(pr
od(Denominator_aftr_rmved_othrfreq))));

mytf1=
tf(sym2poly(prod(Numerator_aftr_rmved_othrfreq)),sym2poly(prod(Denomi
nator_aftr_rmved_othrfeq)));
save('Maho_tr02_mytf1.mat','mytf1');

%RMS error
Resultant_responce=freqresp(mytf1,wl111);
Resultant_responce=squeeze(Resultant_responce(1,1,:));
RMS_error=1/(length(mag1111))*abs(F-Resultant_responce);
RMS_error=sum(RMS_error)
% relative error
Relative_error=abs(F-Resultant_responce)./abs(F);
Relative_error=sum(Relative_error)

if exist('array_of_errors_mytf1')== 0
    array_of_errors_mytf1=[];
end

vv(1,1)=num_pz_numer;
vv(1,2)=num_pz_den;
vv(1,3)=RMS_error;
vv(1,4)=Relative_error;

array_of_errors_mytf1=[array_of_errors_mytf1;vv];

end
end

```

Appendix B: MATLAB code of constraint function used in GA (“*constraint_fcn*”)

```
function [c,ceq]=myconstraint_6section(x)

global Hdiff_constr
global Hdiff_constr11

%Nonlinear inequality constraints have the form c(x) <=0, where c is
a vector of constraints,one component for each constraint.
Similarly, nonlinear equality constraints are of the form ceq(x)= 0.

c(1)=x(25)-min(x(19),x(20)); %Constraints for inductances and
c(2)=x(30)-min(x(20),x(21)); %mutual inductances
c(3)=x(34)-min(x(21),x(22));
c(4)=x(37)-min(x(22),x(23));
c(5)=x(39)-min(x(23),x(24));
c(6)=x(26)-min(x(25),x(30));
c(7)=x(31)-min(x(30),x(34));
c(8)=x(35)-min(x(34),x(37));
c(9)=x(38)-min(x(37),x(39));
c(10)=x(27)-min(x(26),x(31));
c(11)=x(32)-min(x(31),x(35));
c(12)=x(36)-min(x(35),x(38));
c(13)=x(28)-min(x(27),x(32));
c(14)=x(33)-min(x(32),x(36));
c(15)=x(29)-min(x(28),x(33));

trns_fcn %Load estimated transfer function of proposed algorithm
tfnummm=trns_fcn.Numerator{1,1};
tfdennn=trns_fcn.Denominator{1,1};
trns_fcn.Numerator{1,1}=trns_fcn.Numerator{1,1}/tfnummm(1);
trns_fcn.Denominator{1,1}=trns_fcn.Denominator{1,1}/tfdennn(1);

%Assign paramtere values for Simulink model
assignin('base','CG1',CG1);
assignin('base','CG2',CG2);
assignin('base','CG3',CG3);
assignin('base','CG4',CG4);
assignin('base','CG5',CG5);
assignin('base','CG6',CG6);

assignin('base','CS1',CS1);
assignin('base','CS3',CS3);
assignin('base','CS4',CS4);
assignin('base','CS5',CS5);
assignin('base','CS6',CS6);

assignin('base','R1',R1);
assignin('base','R2',R2);
assignin('base','R3',R3);
```



```

assignin('base','R4',R4);
assignin('base','R5',R5);
assignin('base','R6',R6);

assignin('base','L1',L1);
assignin('base','L2',L2);
assignin('base','L3',L3);
assignin('base','L4',L4);
assignin('base','L5',L5);
assignin('base','L6',L6);

assignin('base','L12',L12);
assignin('base','L13',L13);
assignin('base','L14',L14);
assignin('base','L15',L15);
assignin('base','L16',L16);

assignin('base','L23',L23);
assignin('base','L24',L24);
assignin('base','L25',L25);
assignin('base','L26',L26);

assignin('base','L34',L34);
assignin('base','L35',L35);
assignin('base','L36',L36);

assignin('base','L45',L45);
assignin('base','L46',L46);

assignin('base','L56',L56);

assignin('base','Rcs1',Rcs1);
assignin('base','Rcs2',Rcs2);
assignin('base','Rcs3',Rcs3);
assignin('base','Rcs4',Rcs4);
assignin('base','Rcs5',Rcs5);
assignin('base','Rcs6',Rcs6);

% reu simunk model and measure frequ3ency response
sps =
power_analyze('mycct11_for6sections_modified_withmutual_ind__powergu
i','structure');
[nnn,ddd]=ss2tf(sps.A,sps.B,sps.C(1,:),sps.D(1,:));
H=tf(nnn,ddd);

%second constrainet-check the order of numerator and denominator
ceq(1) = length(H.numerator{1,1})-
length(trns_fcn.numerator{1,1}); %since it order is 12 in numerator
ceq(2) = length(H.denominator{1,1})-
length(trns_fcn.denominator{1,1});

end

```

Appendix C: MATLAB code of fitness function used in GA (“fit_fcn”)

```
function F=my6sections_3(x)

global Hdiff_constr
global Hdiff_constr11

%Nonlinear inequality constraints have the form c(x) <=0, where c is
a vector of constraints,one component for each constraint.
Similarly, nonlinear equality constraints are of the form ceq(x)= 0.

c(1)=x(25)-min(x(19),x(20)); %Constraints for inductances and
c(2)=x(30)-min(x(20),x(21)); %mutual inductances
c(3)=x(34)-min(x(21),x(22));
c(4)=x(37)-min(x(22),x(23));
c(5)=x(39)-min(x(23),x(24));
c(6)=x(26)-min(x(25),x(30));
c(7)=x(31)-min(x(30),x(34));
c(8)=x(35)-min(x(34),x(37));
c(9)=x(38)-min(x(37),x(39));
c(10)=x(27)-min(x(26),x(31));
c(11)=x(32)-min(x(31),x(35));
c(12)=x(36)-min(x(35),x(38));
c(13)=x(28)-min(x(27),x(32));
c(14)=x(33)-min(x(32),x(36));
c(15)=x(29)-min(x(28),x(33));

trns_fcn %Load estimated transfer function of proposed algorithm
tfnummm=trns_fcn.Numerator{1,1};
tfdennn=trns_fcn.Denominator{1,1};
trns_fcn.Numerator{1,1}=trns_fcn.Numerator{1,1}/tfnummm(1);
trns_fcn.Denominator{1,1}=trns_fcn.Denominator{1,1}/tfdennn(1);

%Assign paramtere values for Simulink model
assignin('base','CG1',CG1);
assignin('base','CG2',CG2);
assignin('base','CG3',CG3);
assignin('base','CG4',CG4);
assignin('base','CG5',CG5);
assignin('base','CG6',CG6);

assignin('base','CS1',CS1);
assignin('base','CS3',CS3);
assignin('base','CS4',CS4);
assignin('base','CS5',CS5);
assignin('base','CS6',CS6);

assignin('base','R1',R1);
assignin('base','R2',R2);
assignin('base','R3',R3);
```

```

assignin('base','R4',R4);
assignin('base','R5',R5);
assignin('base','R6',R6);

assignin('base','L1',L1);
assignin('base','L2',L2);
assignin('base','L3',L3);
assignin('base','L4',L4);
assignin('base','L5',L5);
assignin('base','L6',L6);

assignin('base','L12',L12);
assignin('base','L13',L13);
assignin('base','L14',L14);
assignin('base','L15',L15);
assignin('base','L16',L16);

assignin('base','L23',L23);
assignin('base','L24',L24);
assignin('base','L25',L25);
assignin('base','L26',L26);

assignin('base','L34',L34);
assignin('base','L35',L35);
assignin('base','L36',L36);

assignin('base','L45',L45);
assignin('base','L46',L46);

assignin('base','L56',L56);

assignin('base','Rcs1',Rcs1);
assignin('base','Rcs2',Rcs2);
assignin('base','Rcs3',Rcs3);
assignin('base','Rcs4',Rcs4);
assignin('base','Rcs5',Rcs5);
assignin('base','Rcs6',Rcs6);

% reu simunk model and measure frequ3ency respone
sps =
power_analyze('mycct11_for6sections_modified_withmutual_ind__powergu
i','structure');
[nnn,ddd]=ss2tf(sps.A,sps.B,sps.C(1,:),sps.D(1,:));
H=tf(nnn,ddd);

freq_Seperation_vec=logspace(log10(125),log10(2+06),1000);

[mag_trns_fcn,phase_trns_fcn,wout_trns_fcn] =
bode(trns_fcn,freq_Seperation_vec);

mag_trns_fcn=reshape(mag_trns_fcn,size(mag_trns_fcn,1)*size(mag_trns
_fcn,2),size(mag_trns_fcn,3));
phase_trns_fcn=squeeze(phase_trns_fcn);

[mag_H,phase_H,wout_H] = bode(H,freq_Seperation_vec);

```

```

mag_H=reshape(mag_H, size(mag_H,1)*size(mag_H,2), size(mag_H,3));
phase_H=squeeze(phase_H);

Hdiff=abs(20*log10(mag_H)-20*log10(mag_trns_fcn));
Hdiff_constr =Hdiff;

F(1)= sum(Hdiff); %sumatino of abs error

c(1)=x(25)-min(x(19),x(20));
c(2)=x(30)-min(x(20),x(21));
c(3)=x(34)-min(x(21),x(22));
c(4)=x(37)-min(x(22),x(23));
c(5)=x(39)-min(x(23),x(24));
c(6)=x(26)-min(x(25),x(30));
c(7)=x(31)-min(x(30),x(34));
c(8)=x(35)-min(x(34),x(37));
c(9)=x(38)-min(x(37),x(39));
c(10)=x(27)-min(x(26),x(31));
c(11)=x(32)-min(x(31),x(35));
c(12)=x(36)-min(x(35),x(38));
c(13)=x(28)-min(x(27),x(32));
c(14)=x(33)-min(x(32),x(36));
c(15)=x(29)-min(x(28),x(33));

%%% if any Constrinst don not satisfy, assign large value
if any(c>0)==1
    F(1)=1e20;
end

end

```

Appendix D: MATLAB code to determine regions

```
variables_original % run the variable defining variables
sps = power_analyze('mycct11_for6sections_ori','structure'); % run
                                                                    simulink

[nnn,ddd]=ss2tf(sps.A,sps.B,sps.C(1,:),sps.D(1,:));
H=tf(nnn,ddd);
newmytf=H;

%select the phase
prompt = {'Give middle phase or side phases (M/S)'};
title = 'Check for the phase';
num_lines = 1;
defaultans = {'M'};
answer = inputdlg(prompt,title,num_lines,defaultans);

w=logspace(-1,10,10000);

bode(newmytf)
hold on;
grid on;

f1=@(w) angle(polyval(newmytf.Numerator{1,
1},(j*w)))/polyval(newmytf.Denominator{1, 1},(j*w))*180/pi;
f2=@(x) 0*ones(size(w));

f1a= angle(polyval(newmytf.Numerator{1,
1},(j*w)))/polyval(newmytf.Denominator{1, 1},(j*w))*180/pi;
f2a= 0*ones(size(w));

x1=w; y1=f1a;
x2=w; y2=f2a;
P = findcrossings([x1;y1],[x2;y2]);

points=horzcat([125],P(1,:))
[Wn_num,zeta_num,P_num] = damp(newmytf)
points=horzcat(points,Wn_num(end))
plot(points,f1(points),'*')

VCI=points([2:2:length(points)-1])
plot(VCI,f1(VCI),'*')

if strcmp('M',answer)
AA=VCI(1);
BB=VCI(2);
CC=VCI(end);
DD=points(end)

h=get(findall(get(gcf,'Children'),'String','Magnitude
(dB)'),'Parent'); % select mag curve
axes(h);

line([AA AA],get(h,'YLim'),'Color','Black','LineStyle','--')
line([BB BB],get(h,'YLim'),'Color',[1 0.5 0.2],'LineStyle','--')
```

```

line([CC CC],get(h,'YLim'),'Color','Blue','LineStyle','--')
line([DD DD],get(h,'YLim'),'Color','Magenta','LineStyle','--')

end

x=[];
if strcmp('S',answer)
    for i=1:length(VCI)
        [mag1,phase1,wout1] = bode(newmytf,VCI(i));
        [mag2,phase2,wout2] = bode(newmytf,VCI(i+1));
        if mag2>mag1
            x=i
            break
        end
        if mag2<mag1 && i~=1
            x=i-1;
            break
        end
    end

    end
AA=VCI(x);
BB=VCI(x+1);
CC=VCI(end);
DD=points(end)

h=get(findall(get(gcf,'Children'),'String','Magnitude
(dB)'),'Parent'); % select mag curve
axes(h);

line([AA AA],get(h,'YLim'),'Color','Black','LineStyle','--')
line([BB BB],get(h,'YLim'),'Color',[1 0.5 0.2],'LineStyle','--')
line([CC CC],get(h,'YLim'),'Color','Blue','LineStyle','--')
line([DD DD],get(h,'YLim'),'Color','Magenta','LineStyle','--')

end

```